UNIVERSITÀ DEGLI STUDI DI PALERMO
Dottorato di Ricerca in Fisica
Dipartimento di Fisica e Chimica
FIS/07

Aggregation processes of intrinsically disordered proteins: influence of the environment

IL DOTTORE
Maria Giovanna Di Carlo

IL COORDINATORE
Prof. Antonio Cupane

IL TUTOR
Prof. Maurizio Leone

CICLO XXV
2015

UNIVERSITÀ DEGLI STUDI DI PALERMO

To the six people I love the most

Contents

List of acronyms

Aβ: Beta amyloid peptide

α**SN**: α-synuclein

AD: Alzheimer's disease

CD: Circular dichroism

FRAP: Fluorescence recovery after photobleaching

IPDs: Intrinsically disordered proteins

MD: Molecular dynamics

PD: Parkinsons' disease

SAXS: Small angle x-ray scattering

TEM: Transmission electron microscopy

TFE: 2,2,2-Trifluoroethanol

ThT: Thioflavin T

2-PM: Two photons excitation microscopy

Introduction

Neurodegenerative diseases afflict millions of elder people in the world, with a very high social and economic cost. These diseases are usually identified as amyloidosis, proteopathies, protein conformational disorders or protein misfolding diseases. Among them, Alzheimer's disease (AD) and Parkinson's disease (PD) are dramatically frequent [1, 2]. AD is a neurodegenerative disorder characterized by an accumulation of aberrant folded tau protein and beta-amyloid peptides in brain [3, 4]. To date, there are no effective therapies for AD and its cellular and molecular mechanisms are not well understood yet. PD is a neurodegenerative movement disorder of the central nervous system, characterized by the accumulation of misfolded α-synuclein protein in the brain [5, 6]. Nowadays, it is well established that misfolding, misfunction and aggregation processes of proteins are involved in the aetiology of neurodegenerative diseases, such as AD and PD, but their specific role in the observed symptoms is still unclear [1, 2, 7]. As a consequence, protein misfolding and aggregation are a focal area in current scientific research, with an interest spanning from biophysics and biochemistry to medical sciences. In particular, the analysis of aggregation processes is a key topic in soft matter and biophysics aimed at discovering common principles which regulate supramolecular assembly. Indeed, supramolecular aggregation is considered a general pathway in the inter-protein free energy landscape, leading to a deep minimum assigned to fibrillar status [8]. Amyloid fibrils are ordered elongated aggregates, characterized by a common highly organized cross-β structure [9]. Their formation is a complex hierarchical process, determined by the interconnection and modulation of multiple mechanisms appearing at different times and length scales. These mechanisms potentially lead to a pronounced polymorphism of intermediate and final structures [9–11], with different biological effects [12, 13]. Depending on environmental conditions, multiple intermediates can be formed during amyloid fibril growth. These species may exhibit peculiar biological activity often associated to toxic effects [12–15]. The nature and the role of toxic species are still highly debated, although the scientific community nowadays tends to consider oligomeric species the actual effectors of cytotoxicity [13, 16].

One of the main goals is to rationalize how the balance among different interactions regulates the differences in structure, morphology and toxicity of both fibrils and intermediate species. In this regard, the understanding of molecular mechanisms at the basis of the aggregation processes is of utmost importance. Indeed, the detailed comprehension of amyloid formation phenomena will bring to the rational control of

them, potentially leading to the development of new pharmacological strategies against amyloid related pathologies. In this context, the modulation of protein environmental conditions and, in turn, protein-protein interactions, by the presence of small molecules, represents a suitable route for designing potential inhibition/control strategies of their *in vivo* aggregation processes.

The work described in this thesis was developed within the framework of the research activities of Molecular Biophysics research group of the Dept. of Physics and Chemistry of the Palermo University. In the last decades, the experimental research has been focused on the study of *in vitro* aggregation processes of different proteins. The overall scientific approach mixes studies on aggregation processes of model proteins and proteins directly involved in neurodegenerative diseases. The first are studied to select experimental conditions allowing elucidating specific features of aggregation processes. This is important, in particular, in order to individuate common principles and driving forces regulating supramolecular assembly. The experimental work described in this thesis was focused on the molecular mechanisms involved in *in vitro* aggregation of Amyloid β peptide (Aβ) and α-synuclein (αSN), proteins directly implicated in the AD and PD neurodegenerative pathologies [2, 3, 5]. In physiological conditions, these two proteins are intrinsically disordered proteins (IDPs) and, in general, their conformation and aggregation propensity is strongly affected by their environment [17, 18]. Different protein conformations are available at the equilibrium for a single polypeptide chain, giving to the reactive groups the possibility of being exposed and of interacting with specific groups of small molecules. In particular, the presence of specific molecules in solution may alter the energy landscape profile, trapping specific conformational substates and consequently altering the balance of multiple species in solution [19].

In the first part of the thesis it is shown how aggregation propensity of Aβ(1-40) is strongly affected by the presence of the dye Thioflavin T (ThT) in solution. In particular, this molecule was found to trigger fibril formation in conditions where the supramolecular assembly would not occur in the absence of the dye. In literature, this small molecule is widely used to analyze *in situ* formation of amyloid fibrils, under the hypothesis that its presence does not affect the whole evolution of the process [20–22]. Using both experiments and molecular dynamics simulations it was found that, as a consequence of the ThT presence, a rigid Aβ(1-40) conformation occurs. It was highlighted that steric and chemical properties of this small molecule are able to modulate peptide conformation and aggregation propensity. An analogous effect was also observed for αSN. As a consequence, the results suggest a thermodynamic drive toward the formation of partially folded states, in natively unfolded proteins, by interaction of exposed residues with ThT specific groups. Indeed, it is nowadays believed that the earliest stage of fibrillation of IDPs is their partial folding [23]. This result could be really significant since ThT may favour the conversion of possible toxic oligomers into less reactive amyloid fibrils. Indeed, mature fibrils are nowadays considered as reservoirs of oligomeric species. In this regard, a recent study showed that ThT decreases paralysis in worm models of

Alzheimer's disease [24]. This is an example of implications of ThT in the evolution of amyloid related aging processes in living organisms. Importantly, the result presented here constitutes a fundamental warning for experiments where ThT is used as normal amyloid fluorescent probe with the assumed hypothesis of non interaction with the peptide.

Protein-solvent interaction modulated by small molecule not only affects aggregation kinetics but also conformation, structure and stability of aggregates [25]. In the second part of the thesis, using α-synuclein as a model, it is shown that not only fibrillation kinetics but also aggregates stability and morphology can be modulated by trifluoroethanol (TFE). The aggregation process was studied and fibril stability tested in its presence. This alcohol is known to modulate the protein secondary structure and stability on the basis of its concentration [26, 27]. It acts changing protein solvation properties, but also lowering the dielectric constant of the solution [25]. The experimental results draw the attention on the dependence of native αSN and amyloid aggregates stability on their environment. In particular, at moderate TFE concentration αSN aggregated species are formed. These structures represent an activated state for following fibril growth, which would not occur in the absence of TFE. The stability of the already formed αSN fibrillar structures was found to be dependent on TFE concentration, whose changes may lead to aggregates stabilization and clustering or to their complete dissolution. This aspect is really important to take into account since, as already said, nowadays fibrils are considered as reservoirs of actual cytotoxic species, which can be released if fibrils stability is modified [13].

This thesis is divided in four chapters, the first two are introductory chapters while the other two describe the experimental results. In Chapter 1, an overview on IPDs and the state of the art of the amyloid aggregation kinetics is given, particularly focusing on the literature dealing with Aβ(1-40) and αSN fibrillation. In Chapter 2, a short description of the theoretical background of the experimental techniques used in the thesis is given. In Chapter 3, experimental results obtained in studying the aggregation process of Aβ(1-40) in quiescent conditions and in the presence of ThT are reported. Experimental results are well supported by molecular dynamics simulations. In Chapter 4, the analysis of αSN fibrillation process and fibril stability in TFE water mixtures is presented. Finally, main results and future perspectives are discussed in Section. 4.2.

Chapter 1

State of the art

Proteins are the most abundant class of organic macromolecules in all living organisms. They consist of polypeptide chains of amino acids linked to each other by peptide bonds. These macromolecules are essential for all biological processes related to life, playing a key role in the structure and function of cellular processes such as enzymatic catalysis, transport and storage, immunization and differentiation. Moreover, it is nowadays established that their dysfunctions are often related to different degenerative pathologies, e.g. type-II diabetes, the transmissible prion disorders, Parkinson's, Alzheimer's and Huntington's disease, generally referred to as amyloidosis [8, 28]. These are characterized by extracellular or intracellular insoluble protein depositions, mainly composed by ordered protein aggregates known as amyloid fibrils.

Due to both their crucial role in living cells and their involvement in amyloidosis, proteins have become one of the most interesting and challenging topics in biophysical, biochemical and biomedical research. Numerous works in this area led, among the others, to the identification of a relatively new category of functional proteins lacking a 3-D structure, known as intrinsically disordered proteins (IDPs) [29–32]. To them belong the two proteins object of this study (the Aβ(1-40) peptide and αSN). Particular attention has been paid to the comprehension of mechanisms regulating their physiological functions [33–35] and their connections with the ones leading to amyloid fibril formation [36–40]. Several models for the mechanism of protein aggregation and, in particular, amyloid formation have been proposed [41–43], in this second case most of them are based on both homogeneous and heterogeneous nucleation-growth [36–38, 42, 44–47].

The first section reports an overview on IDPs with the aim of giving their main structural characteristics, highlighting the strong influence of the environment on their conformation and behavior. In the second section an overview on fibril formation processes, with particular regard to nucleated mechanisms, is given. Eventually, in the third and fourth sections the state of the art of Aβ(1-40) and the one of αSN are presented.

1.1 Overview on intrinsically disordered proteins (IDPs)

1.1.1 Historical introduction

To date, a lot of efforts have been addressed to understand the relation between protein conformation and functionality and the basic mechanisms leading to aggregation, and in particular to amyloidosis. In this landscape, the last century saw the emergence and the subsequent consolidation of the so-called *Structure-Function Paradigm* [48]. The key concept is that protein folding would be a *condicio sine qua non* for protein functionality. In other words, proteins would have to proceed from an highly disordered state to their 3D-structure, or native state, in order to accomplish their physiological function. For this role in functionality, protein folding has been widely investigated with the intent to understand its regulating mechanisms [49–53]. Firstly, it was proposed that proteins find their way to functional structure randomly searching among the enormous number of possible configuration. This hypothesis led to the *Levinthal's Paradox* [54], which states that it would take an almost infinite time for a protein to reach its native state, while proteins frequently fold in less than 1 second. To explain how a polypeptide chain can fold in a finite time, in 1973 Anfinsen suggested that "it is necessary to postulate the existence of a limited number of allowable initiating events in the folding process" [55]. Starting from this consideration, the apparent paradox was definitively overcame in 1980s and 1990s with the introduction of a statistical approach to the energetics of protein conformation landscape [56–58]. On the basis of this view, the different conformations, which a protein can assume, are not all equally likely, but the probability of a polypeptide chain to explore the different conformational states on the energetic landscape surface depends on its amino acidic sequence [57]. The native state of a protein is reached through kinetic pathways on a *funnelled energy landscape* of intramolecular contacts (see Fig. 1.1-Left) [59–62]. Such pathways drive the proteins trough relative minima, in such a way that the protein explores a reduced number of conformations. On the basis of this picture, protein aggregation and consequently protein misfolding diseases, would be caused by abnormal folding, or misfolding, as well as unfolding, which lead proteins to experience partially folded states [1, 8]. Indeed, the correct folding towards the native state relegates the most hydrophobic amino acids into the core, hiding them from the solvent. As a consequence, an incorrect folding or a partially unfolding, leading to the exposure of such amino acids, enhances protein aggregation propensity.

Despite the large amount of experimental and computational works confirming the picture drawn above, in the last two decades, the scientific community had to reappraise the relationship between proteins in disordered states and amyloidosis and completely dismiss the concept of *Structure-Function Paradigm* as a general rule [17, 31, 63]. Indeed, it has been demonstrated that not only several globular proteins possess disordered regions necessary for their function [64, 65], but also that biologically active proteins lacking of a 3D-structure along the whole chain are actually very common in nature [18, 33, 65, 66]. In a recent review Dunker et al. [67] identified the expression Intrinsically

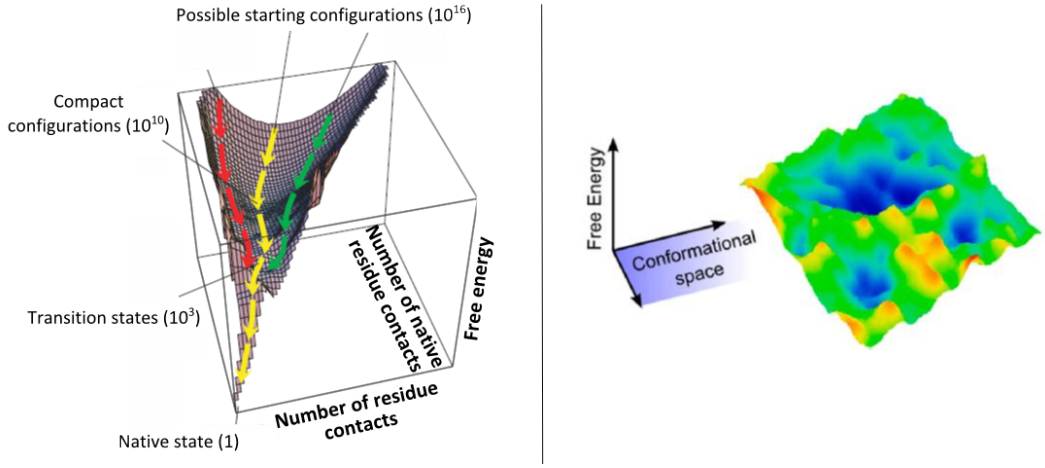

Figure 1.1: Left: an example of funnelled energy landscape describing the process of folding for a globular protein containing 27 residues. Rows indicate the average path (in yellow) and a range of two standard deviations around it (in red and green). Adapted from the original paper [61]. Right: an example of IDPs energy landscape showing multiple shallow local minima corresponding to the comparable more stable conformations. Adapted from the original paper [32].

Disordered Proteins (IDPs) as the most meaningful to indicate proteins from this second group.

1.1.2 Structural and conformational fingerprints of IDPs

The choose of the name IDPs to indicate proteins without a well folded conformation in physiological conditions derives from two characteristics that distinguish them. Indeed, the word "disordered" indicates the major characteristic common to all the IDPs: the almost completely, or even completely, lack of a rigid tertiary structure, typical of globular proteins [29]. The word "intrinsically" indicates that the conformational disorder represents an inherent property of these proteins, which is encoded in their amino acidic sequence [30, 65, 68].

More in detail, in 2002 Uversky demonstrated that hydrodynamic volumes of IDPs show comparable values to that of globular proteins with the same chain length in their premolten globule or denatured conformational states [18]. Moreover, several works shown that IDPs are characterized by a great flexibility and a low content in secondary structure [69–71]. For example, it has been established that the High-Mobility-Group Chromosomal Protein HMG 17 almost completely lacks secondary structure [69]; bone sialoprotein (BSP) and osteopontin (OPN) explore an ensemble of conformations, both being completely unstructured in solution [70]; the NAC region of αSN (residues 61-95) has a larger hydrodynamic radius than globular protein of similar molecular weight and it is characterized by the absence of significant secondary structure content [72]. In summary, *in vitro* and in physiological conditions, IDPs are mainly characterized

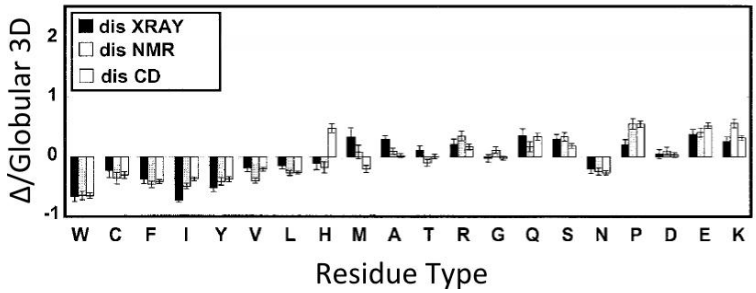

Figure 1.2: Comparisons of amino acid compositions for disordered (a) and globular (b) proteins. For each residue the amino acid mole fractions $(R_i^a - R_i^b)/R_i^b$ are reported as determined by X-ray diffraction, NMR and CD measurements. Adapted from the original paper [30].

by i) a large hydrodynamic radius [18, 72, 73], ii) a low content of ordered secondary structure [69–72] and iii) an high intramolecular flexibility [29, 70, 71].

To give an example of what is meant by "encoded in the amino acid sequence", the amino acid composition of different protein segments, identified as disordered by x-ray diffraction, nuclear magnetic resonance or circular dichroism, respect to the one of ordered proteins is reported in Fig. 1.2 [30]. The amino acid mole fractions $(R_i^a - R_i^b)/R_i^b$, which compare pairs of disordered (a) and globular (b) proteins sets, are reported for each amino acid i. As shown, IDPs are depleted in aromatic (Trp, Tyr, Phe) and hydrophobic (Iso, Val) residues, and enriched in structure-breaking (Pro ang Gly) and charged residues (Lys, Glu). In particular, a combination of low overall hydrophobicity and large net charge represent a unique structural feature of IDPs [29, 30]. This is evident from the charge-hydrophobicity phase space shown in Fig.3, where IDPs are localized in a specific region, aside the one for globular proteins. Only α-synuclein and other two proteins (green, yellow and white circles in Fig.3) do not fit the general trend shown by the other 88 analysed IDPs [29].

These IDPs structural characteristics are really important to consider in order to establish if a protein belongs to IDPs. Indeed, when recombinant proteins are used, the question could arise if the lack of rigid melted tertiary structure observed *in vitro*, in physiological conditions, is an artifact due to protein purification, or if it is indeed a viable reproduction of their *in vivo* behavior. In this regard, computational approaches looking over the amino acidic sequence represent valuable tools [74]. Indeed, strictly speaking, in the absence of direct *in vivo* evidences, assignment of a protein to the family of IDPs can only be done when its sequence (see Fig. 1.2) and physico-chemical properties (see Fig. 1.3) both converge to show that protein is intrinsically disordered in physiological conditions [74]. Obviously, this is only a general rule, which can be applied in the absence of *in vivo* observations. For example, in the case α-synuclein, although it is localized outside the IDPs region in Fig. 1.3, in-cell NMR measurements demonstrated that in E. coli cytosol α-synuclein presents the same characteristics as the disordered monomeric form observed *in vitro* in aqueous solutions [17] (see also

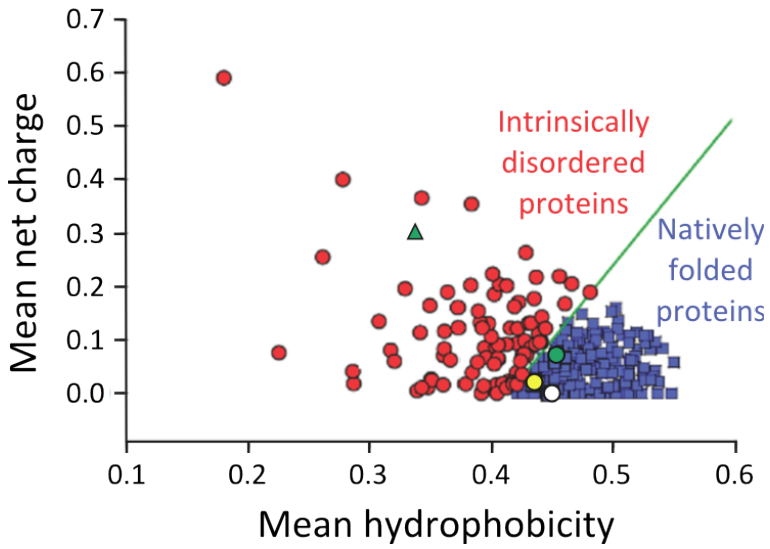

Figure 1.3: Mean net charge as a function of mean hydrophobicity for 275 monomeric ordered proteins (blue squares) and 88 disordered proteins (red circles). Green, yellow and white circles refer to α-synuclein, negative factor (NEF) and helix destabilizing protein, respectively. The green triangle refers to the last 44 residues in the C-terminal region of α-synuclein (see Section 1.4). Adapted from the original paper [29].

Section 1.4). Beside these structural fingerprints, IDPs are also characterized by a dynamic conformation. Indeed, in the last two decades, different experimental techniques [e.g. nuclear magnetic resonance (NMR), small angle scattering (SAS), gel-filtration, dynamic light scattering (DLS), circular dichroism (CD)], revealed that IDPs do not represent a homogeneous class, but an ensemble of different conformations [70, 75, 76]. Indeed, in contrast to globular proteins, *in vitro* and in physiological conditions, they exhibit a relatively flat energy landscape (see Fig. 1.1-Right), enabling them to sample a variety of conformations [32, 77]. In particular, IDPs can be found in any of these three conformations: molten globule (MG), premolten globule (PMG) and random-coil-like (RC-like) structures [17, 78, 79]. With respect to their globular state, proteins in the MG state retain almost all the secondary structure, while their hydrodynamic volume increases of about 1.5 times, also accompanied by a considerable increasing of affinity to hydrophobic fluorescent probes (e.g. 8-anilinonaphthalene-1-sulfonate, ANS). In the case of PMG state the secondary structure is reduced to about 50%, the hydrodynamic volume increases of about three times and the affinity to hydrophobic dyes is still higher, although lower than in the MG state. IDPs in the random coil state are devoid of any secondary structure and they completely lose the affinity to hydrophobic probes, while the hydrodynamic volume becomes even twelve times larger [29].

The observation that in IDPs biological function can arise from any of the three states MG, PMG, RC-like, or from transitions between them [79, 80], led to the replacement of

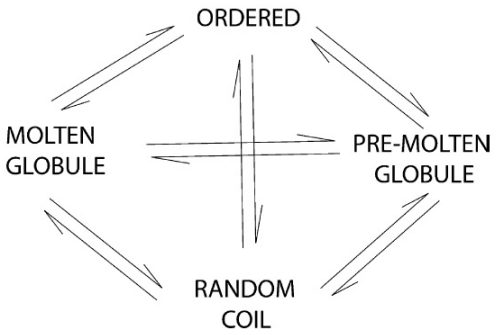

Figure 1.4: Schematic representation of *Protein quartet model*: protein function can arise from any of the four indicated states or from the transition between two of them. Adapted from the original paper [17].

the above cited *Structure-Function Paradigm* with *The Protein Quartet Model* reported in Fig. 1.4 [17, 29]. According to this model, protein function can arise from globular proteins as well as from IDPs and, in particular, from any of the four states globular, MG, PMG or RC-like, or as result of a transition between two of them. For example, it has been shown that the High-Mobility-Group Chromosomal Protein HMG 17 [69] and heat shock transcription factors of Kluyveromyces lactis and Saccharomyces cerevisiae [81] partially fold upon interaction with DNA, their N- terminal regions remaining disordered; 4E binding proteins fold only in their central region upon interaction with limiting, proto-oncogenic initiation factor eIF4E, the remaining being in its disordered state [82].

1.1.3 Influence of the environment on IDPs conformation

It has been established that IDPs perform several specific functions that can be divided in molecular assembly and recognition, protein modification and entropic chain activities. In order to accomplish these functions, IDPs often undergo *in vivo* disorder-to-order transitions as sketched in Fig.4, although sometimes they remain in their disordered conformation [17, 29, 79, 80]. Indeed, the main peculiarity of these proteins is their huge plasticity. IDPs are able to interact with different partners, modulating their conformation on the basis of the particular function. Several observations reveal IDPs folding before, during or after interaction with partners. This is often only a partial folding, involving only part of the IDPs chain [69, 81, 82].

To date, different scientists have posed the question if the induction of folding in *in vivo* environment is essentially a process driven by an excluded volume effect due to crowding, or if it is a more complex process, due to specific interactions and to environmental factors such as, for example, pH, ionic strength or temperature. To answer this question *in vitro* experimental studies have been carried out using concentrated solutions of model "crowding agents", such as polyethylene glycol, dextran, Ficoll or inert proteins [83, 84]. Not all these works revealed significant conformational change

attributable to crowding [84–87]. Based on these observations it has been concluded that molecular crowding effects are not necessarily sufficient to induce ordered structure in IDPs [17, 84].

In this landscape, other *in vitro* studies showed that IDPs conformations are strongly influenced by the environment. For example, the disorder-to-order, partial or total, transitions upon binding to metal ions [88–93], upon interaction with membranes or liposoms [94–97] or for the addition of co-solvents to the solution [26, 27, 98, 99] have been observed [17, 18]. In this regard, it has been shown that binding of metal ions Cd^{2+} and Zn^{2+} induces metallothioneins folding [90]; the peptide R2, derived from tau protein (residues 287-304) (showing a CD spectrum typical of partially disordered secondary structures in aqueous solutions), assumes a monomeric α-helical conformation upon binding with Cu^{2+} [91]; binding of the metal ion Zn^{2+} leads the unstructured peptide Aβ(1-16) to assume a compact conformation [92]; α-synuclein assumes a molten-globule conformation upon binding of copper or iron, resulting in an enhanced fibrillation propensity [88, 89]. Moreover, it folds in α-helical conformations upon interaction with membranes and it is able to modulate its secondary structure in the presence of simple and fluorinates alcohols [26, 27]; one of the tate embryogenesis abundant (LEA) proteins, the protein LEA18, partially folds in β-sheet structures in the presence of negatively charged liposomes [97]. The intrinsically disordered protein Methyl CpG binding protein 2 (MeCP2) undergoes a partially coil-to-helix transition in the presence of trifluoroethanol [98]. Moreover, interaction of IDPs with small molecules has resulted in a modified functionality or aggregation propensity [100]. This is the case, for example, of the oncoprotein c-Myc whose transcriptional activity can be inhibited upon interaction with the small molecule 10058-F4 [101]; while the inositol stereoisomers epi- and shyllo-inositol stabilize Aβ(1-42) oligomers with a β-sheet structure Aβ peptides [102].

Solution conditions as temperature, pH, ionic strength or dielectric constant have to be taken into account. Indeed, changing these factors can lead to a partial or total folding, or a variation in the secondary structure content [26, 27, 103, 104]. This is due to the fact that, on increasing temperature, the strength of hydrophobic interactions can increase [105]. In contrast, variations in pH change the large net charge present at neutral pH and consequently modify the charge/charge intramolecular repulsion, thus possibly shifting the conformational ensemble toward more compact states [77]. For example, a temperature-induced folding was found for caldesmon 636-771 fragments [31], α_S-casein [106], and several other IDPs [74, 77]. In 2010 Kjaergaard and coworkers showed that the tree IDPs ACTR, NHE1, and Spd1 change their secondary structure as a function of temperature [103]. In 2001 Uversky and coworkers showed that either a decrease in pH or an increase in temperature induce αSN partial folding, with a significant amount of secondary structure [104]. Besides αSN, several other IDPs show structural parameters depending on pH, such as protymosin α, pig calpastatin domain I, histidine rich protein II [74]. All the peculiarities above reported, reveal a strong IDPs dependence on their environment, highlighting a really complex scenario. This is reflected in IDPs energetic landscapes describing intramolecular interactions, which are rough surfaces lacking of

a deep global minimum typical of globular proteins (see Fig. 1.1-Right). This shallow roughness reflects the high conformational dynamics and flexibility typical of IDPs, and also provide a clear description of how an IDP can specifically interact with many ligands of different nature and fold differently as a result of these interactions. Indeed, this type of energy landscape is exceptionally sensitive to local environment, much more than the relatively robust funnel-like energy landscape of an ordered protein [77]. Free energy minima can be made deeper or barriers higher by modifying some environmental factors, explaining the ability of an IDP to fold differently depending on the environmental conditions. Moreover, it is also necessary to keep in mind that IDPs are heterogeneous systems which, in general, can not be described by only one landscape as the one reported in Fig. 1.1-Right. To be more precise, a single protein might be described by a set of these landscapes one for each different part, each replying to the environmental changes in its own way, which can be dependent, semi-dependent or independent on the others [77]. This heterogeneity of the energy landscape defines the ability of IDPs to form fuzzy complexes, where significant part of a protein preserves its intrinsically disordered state even in the bound conformation [77].

1.2 Amyloid fibrils

Protein dysfunctions are related with several human diseases, such as cancer, cardiovascular diseases, neurodegenerative diseases and diabetes. Often these pathologies are characterized by extracellular or intracellular amyloid fibrils deposition, which accumulate in a variety of organs and tissues. These are insoluble protein aggregates characterized by an high ordered β-sheet structure [9]. More than 20 proteins are known to be involved in these human diseases referred as amyloidoses [7]. These include, for example, immunoglobulins in primary systemic amyloidosis and multiple myeloma, amylin in the diabetic pancreas, α-synuclein in Parkinson's disease and small soluble peptide such as the amyloid β-peptide (Aβ) in Alzheimer's disease. However it is nowadays believed that the propensity to aggregate forming amyloid fibrils is a general property of all the amino acidic chains [7]. Indeed, a great number of not-amyloidogenic proteins have been shown to form amyloid fibrils.

During the last decades, several works showed that amyloidosis are related to globular proteins as well as IDPs dysfunctions. However, molecular mechanisms of fibrillation of IDPs and of ordered proteins are different. Contrary to what found for globular proteins, in order to populate disordered conformations to accomplish their functions, IDPs are poorer in hydrophobic amino acids content [17, 29, 30]. The exposure to the solvent of any amino acids, being the native functional condition of IDPs, does not lead to aggregation. In this case the cause for an increased aggregation propensity is the formation of non-native more compact conformations. In other words, if for ordered proteins the first critical step in fibrillogenesis is the partial unfolding [8], the earliest stage of fibrillation of IDPs is their partial folding [23].

Fibrillation and, more in general, protein aggregation are complex processes involving protein-protein interactions mediated by the solvent. They depend on environmental condition such as pH, temperature, ionic strength, cosolvents, presence of metals [26, 40, 41, 107]. In general, aggregation processes are characterized by multiple interconnected mechanisms. Among them, the appearance of oligomers, on-pathways or off-pathways for fibril formation, is of particular interest. Until the end of 1990s data available and genetics of amyloid diseases supported a quite general consensus that amyloid fibrils are the basic toxic species in amyloid plaques. However, at the end of the 1990s the attention shifted to the cytotoxicity of amyloid fibril precursors, notably amyloid oligomers and protofibrils [108]. Data also started to appear indicating that neuronal synapses were the main target of cytotoxicity [109]. Soon after, in 2002, data were reported suggesting for the first time that cytotoxicity is a generic property of amyloid oligomers [110] associated with a shared "toxic" fold [111]. The detrimental role of oligomers is presently supported by a large number of data on many *in vivo* and *in vitro* amyloidogenic proteins indicating a direct cytotoxic effect of amyloid aggregates [1]. The cytotoxicity of pre-fibrillar amyloid assemblies has been confirmed for all proteins and peptides associated with amyloid diseases, including Aβ peptides, α-synuclein, amylin, β2-microglobulin, transthyretin and others [112, 113]. At the present, the pivotal role of amyloid oligomers as key players of amyloid cytotoxicity is widely recognized. Nowadays, fibrils are considered as reservoirs of oligomeric species. As a consequence, to date most of the efforts of the scientific community have been addressed to the comprehension of mechanisms regulating amyloid fibril formation [37, 47, 114, 115], and to the detection of possible intermediate species and interconnected aggregation pathways leading to fibril production [22, 116]. Indeed, a deep understanding of such processes is fundamental in order to develop effective therapeutic strategies. In particular, several efforts have been addressed to the formulation of aggregation models able to describe fibrillation processes at a molecular level [14, 41–43, 117].

In general, supra-molecular association leading to fibril formation involves conformational changes, which drive the protein from its native conformation (globular or disordered) to ordered fibril structures. These conformational changes can take place before or during supramolecular assembly [40, 118, 119]. Although some proteins seem to assemble through entirely non-nucleated processes [40, 116, 120], the fibrillation mechanisms of most proteins can be well described by means of models based on nucleation-growth, both homogeneous and heterogeneous [37, 38, 44, 121].They can include initial micelle formation [122], changes in protein conformation [28, 104, 123], and filament-filament association [124]. In particular Aβ peptides and αSN, objects of this study, are reported to form amyloid fibrils by means of nucleated processes [41, 104, 125, 126]. A brief description of such aggregation mechanisms is reported in the following.

1.2.1 Nucleation mechanisms of aggregation

Nucleation processes are first-order phase transitions including crystallization, self-organization of ferroelectric domains and nanofilms, formation of micellar solutions, formation and growth of diamonds from vitreous carbon, and, as already said, of amyloid fibril from monomers or oligomers [127]. These processes can be divided in two categories: primary nucleation (or homogeneous nucleation) and secondary nucleation [37, 38, 127]. Fig. 1.5 shows a schematic representation illustrating the microscopic mechanisms of nucleated mechanisms for the particular case of polymerization, to which this section refers. Homogeneous nucleation is characterized by two main steps, a nucleation phase and a growth phase. During the nucleation phase the system is in a metastable state, the unfavorable formation of oligomeric species proceeds with the same probability of critical nucleus formation in any given volume or surface element (see Fig. 1.5-A) [37, 47, 127]. All oligomers shorter than a critical size, defining the so called nucleus n_c, are unstable. The growth phase only starts when the population of nuclei is enriched. After this step, unit addition to the ends of polymers takes place contemporary with the first phase. This step is characterized by dissociation constants much smaller than association ones [37, 128]. Together with homogeneous nucleation processes, secondary nucleation mechanisms can be identified, either heterogeneous nucleation or fragmentation or branching [37, 47], indicated by C), D) and E) in Fig. 1.5, respectively. Heterogeneous nucleation consists in the formation of aggregation nuclei directly on the polymer surface (surface-catalysed nucleation) [37, 47]; fragmentation consists in breaking of polymeric chains with the subsequent formation of new ends available for the addition of monomers; branching is the addition of a unit or an oligomer on filament surface leading to polymeric elongation from it. The three mechanisms lead to a great enhancement of the aggregation rate in comparison to the one characterizing primary nucleation.

Different models have been formulated to describe such processes. The classical theory of nucleated polymerization, formulated by Oosawa and coworkers in the 1960s, describes the growth of filamentous structures formed through homogeneous nucleation [129]. It predicts a quadratic time dependence of mass concentration of polymers, for $t \longrightarrow 0$. This model applies to the case of nuclei in thermodynamic equilibrium with monomeric population (see Fig. 1.5-A), and was successful in describing a variety of characteristics of the polymerisation of actin and tubulin. When nuclei are formed by subsequently monomer addition, in the so called *downhill polymerization* model, the mass concentration of polymers, for $t \longrightarrow 0$, shows a power behaviour (see Fig. 1.5-B) [130]. This is characterized by a biphasic behavior: a first phase during which polymer mass does not apparently increase, known as lag-phase, followed by an abrupt growth. In 1980s the Oosawa's theory has been generalized by Eaton and Ferrone to include secondary nucleation processes, such as surface-catalyzed nucleation [36, 37] (see Fig. 1.5-C), and by Wegner in order to include fragmentation processes into the growth model for actin filaments (see Fig. 1.5-D) [131]. In these cases an exponential behavior is found for $t \longrightarrow 0$ [38], leading to the observation of biphasic behavior: a lag-phase and a growth phase. Recently, a more

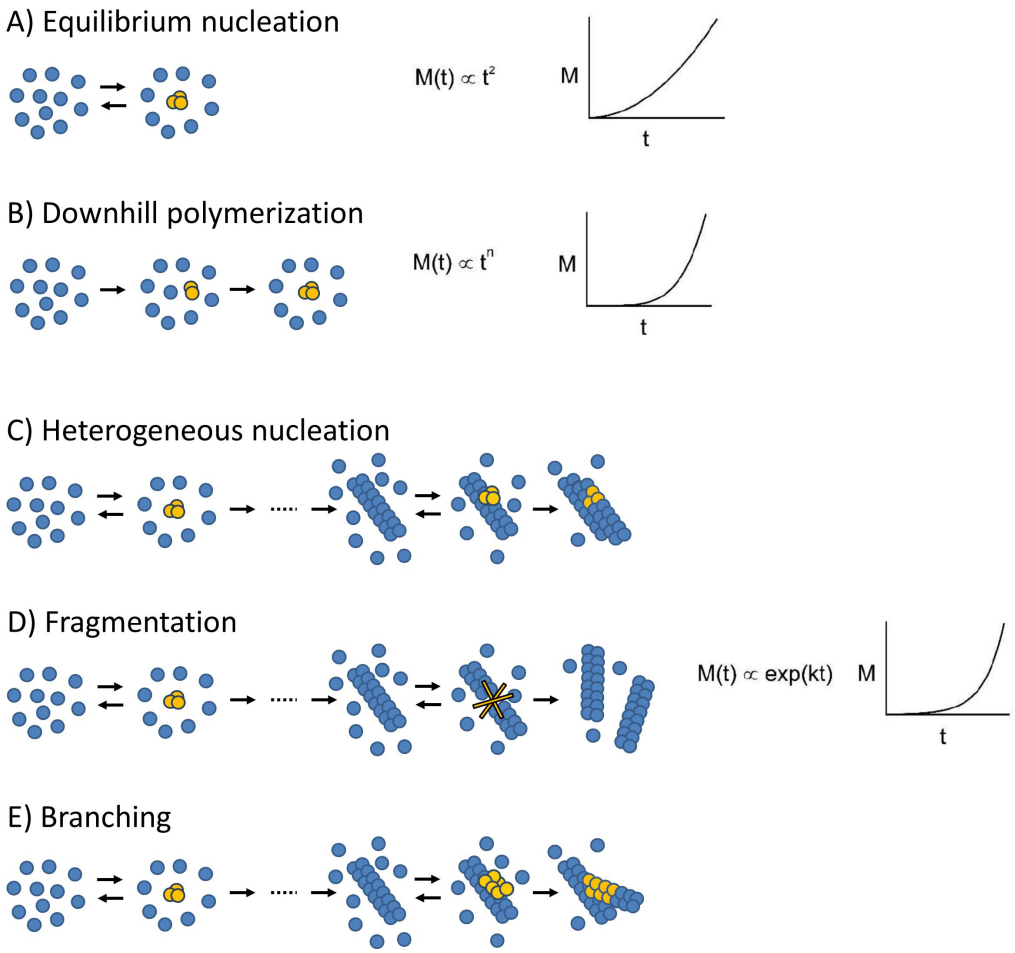

Figure 1.5: Schematic representation illustrating the microscopic mechanisms of nucleation processes. Homogeneous nucleation during its first phase (sketched on the left sides of A and B) leads to the creation of nuclei of length n_c from soluble units. Nuclei can be in thermodynamic (very unfavorable) equilibrium with the units (A), or created by subsequently unit addition. From them, filaments growth from both ends. Secondary nucleation mechanisms (sketched on the left sides of C, D and E) lead to the creation of new fibril ends from pre-existing polymers, through nucleation on their surfaces (C), fragmentation (D) or branching (E). Graphs on the right sides show the polymer mass growth behavior during the early times of the kinetics ($t \longrightarrow 0$). Equilibrium nucleation shows a quadratic time dependence [129]; downhill polymerization a power low [130]; secondary nucleation mechanisms an exponential behavior [37]. Adapted from the original paper [38].

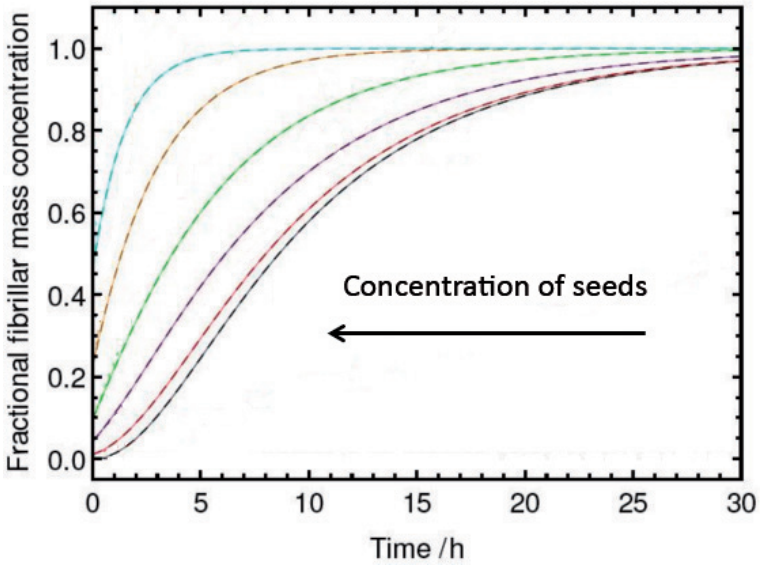

Figure 1.6: Nucleated polymerisation in the presence of an increasing quantity of seed material of a fixed average length (5000 monomers per seed) added at the beginning of the reaction. The seed concentrations given as a fraction of the total concentration of monomer present are: 0, 0.01, 0.04, 0.1, 0.2, 0.5 (right to left). Adapted from the original paper [134].

complete description theory of nucleation processes, including primary and heterogeneous nucleation and fragmentation , has been reported by Knoweles' research group in a set of exhaustive works [47], [132], [133], [134]. All the models just mentioned describe the process of nucleation from a kinetic point of view, taking the moves from the master equations. Besides these, it is worth to mention that, more recently, Di Michele and coworkers published a notable work in which they develop a theoretical model for fibril formation [115]. This model is based on the mathematical description of protein-protein interactions, from a physical point of view. It is able to reproduce the exponential growth due to self-catalytic conversion of monomers towards aggregation-prone conformations in the presence of pre-existing aggregates.

In *in vitro* experiments, during fibril formation starting from soluble monomers, primary and secondary nucleated mechanisms often coexist. Aggregation processes controlled by secondary mechanisms are intrinsically unrepeatable. They are characterized by stochasticity, which is experimentally revealed in a random duration of the lag-phase [46, 125, 135]. Its average value and standard deviation are function of protein concentration, both lowering as protein concentration increases [45, 46, 125, 126, 135].

Interestingly, in certain cases, in these processes the prevalence of a mechanism rather than another can be inferred by the qualitative behavior of kinetics curves. A remarkable example is given by the case in which the aggregation process takes place in the presence of preformed aggregates, usually referred as seeds. If the process is

essentially governed by homogeneous nucleation and elongation from ends, secondary nucleation mechanisms being negligible, the lag-phase reduces as seeds concentration is raised (see Fig. 1.6) [42, 134, 136]. The extreme case is represented by the concave growth in Fig. 1.6 (cyan dashed line), where no lag-phase is observed. The reaction kinetics is characterized by an exponential approach to equilibrium [42, 134]. In this case the polymeric mass only increases for the addition of monomers to polymer ends, and the number of polymers remain constant along the whole reaction since no nucleation occurs [42, 134]. This observation will be taken into account in Chapter 3. Indeed, the ThT fluorescence signal as a function of time of Aβ(1-40) kinetics presents a concave behaviour similar to that shown by the cyan dashed line in Fig. 1.6, without a lag-phase. This is compatible with a pre-seeded nucleation process with the elongation from ends more effective than primary nucleation [134].

1.2.2 Amyloid fibril structure

Mature amyloid fibrils are ordered protein aggregates which are made by a variable number of protofilaments (see Fig. 1.7). These are characterized by a well defined structure, usually referred as *cross-β*, whose main features are independent of the amino acidic chain from which fibrils originate. Fig. 1.8) shows a schematic representation of a protofilament. It consists in the repetition of fundamental units extending along a preferential direction, the fibril axis. These units are β-strands arranged at a distance (*main chain spacing*) of approximately 10 $\mathring{A}$, bounded together by means of hydrogen bonds in such a way that they form β-sheets. The cross-β structure protofilament consists in two juxtaposed β-sheets, at a distance varying in the range 8.8-14.6 $\mathring{A}$, usually indicated with the term *side chain spacing*, depending on the particular fibril [9].

In general, mature fibrils can differ for side chain spacing, number and arrangement of protofilaments and in the arrangement of the side chain within the cross-β structure (see Fig. 1.7) [9, 137, 138]. Such variable arrangement is usually indicated with *polymorphism* or *microscopic polymorphism*. Polymorphism is not only related to fibrils grown from different amino acidic chains, but it can also arise from the same protein, in samples differing in chemico-physical parameters as well as in the same sample [9]. Interestingly, structures with different morphologies can show different degree of cytotoxicity [10]. In this regard, a notable study has been published in 2005 by Petkova et al. The authors studied two identical samples of Aβ(1-40), incubating them in quiescent conditions or in the presence of mechanical agitation. They found that fibrils fibrils from these two samples show different molecular and/or secondary structures, and morphologies, has been shown to propagate from mother to daughter samples in seeded experiments [10, 139]. Recent studies have point out that, beside microscopic fibril polymorphism, *macroscopic polymorphism* also exist. Indeed, fibrils can be arranged in different 3D packing structures called *superstructures*, although maintaining their cross-β structure. In a recent and generalized work Foderá et al. demonstrated that the formation of any kind of aggregates superstructures, and in particular fibril superstructures, is driven

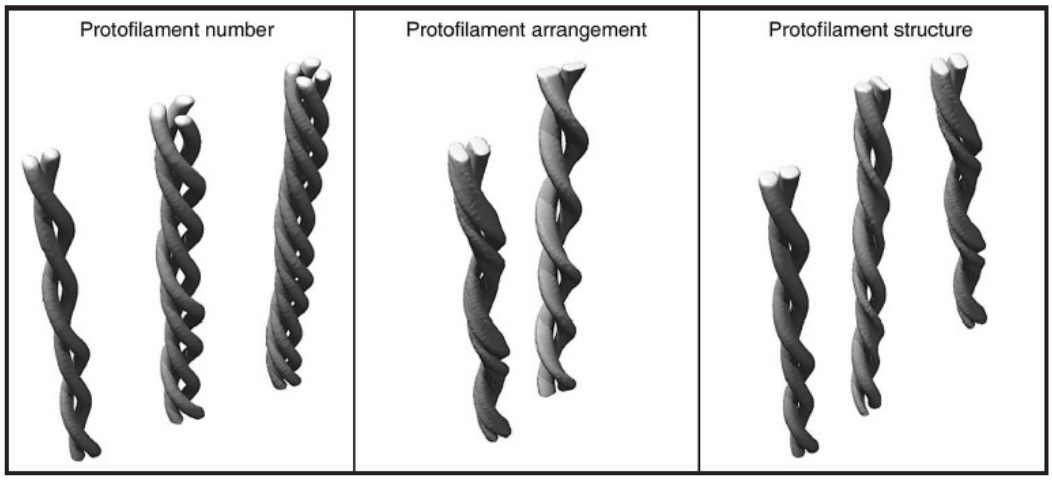

Figure 1.7: Schematic representation of different amyloid fibril morphologies which differ in the number, relative orientation or structure of the underlying protofilaments. Adapted from the original paper [9].

by electrostatic protein-protein interactions [114]. Branched, twisted or straight fibrils, bundles of fibrils, dense network of filaments and spherulites are all example of fibril superstructures, with characteristic sizes in the range of several micrometers [11]. Fig. 1.9 shows an environmental scanning electron microscopy imagine of a fractured spherulite, grown from an insulin sample at pH 1.8 [11]. These kind of structures consist in a dense

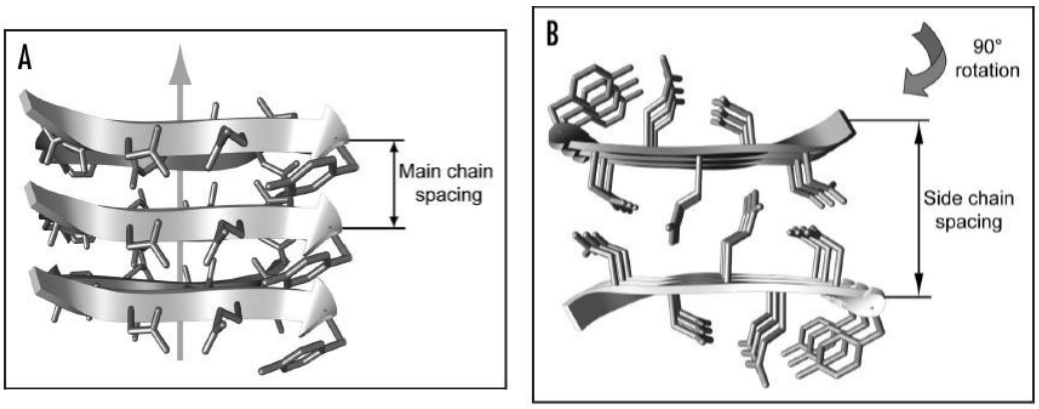

Figure 1.8: A: representation of the frontal view of a β-sheet, consisting of β-strands, whose mutual distance is usually referred as *main chain spacing*. The arrow indicate the direction of the fibril axis. B: representation of the top view of two juxtaposed β-sheets, whose distance is usually indicated with *side chain spacing*. Adapted from the original paper [9].

core, referred as *precursor*, and an external shell made of spherical arranged fibrils. Since they have been found to coexist in solution with free fibrils, it is still not clear if they

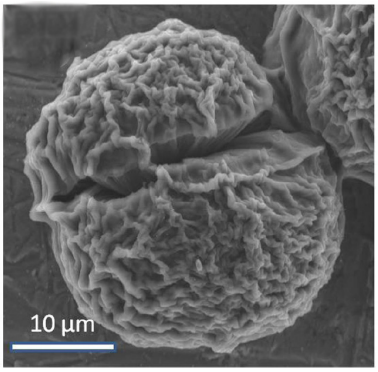

Figure 1.9: environmental scanning electron microscopy imagine of a spherulite grown from an insulin sample at pH 1.8. Adapted from the original paper [11].

form from monomers or from pre-formed fibrils, which subsequently arrange in a spherical shape around precursors [11]. Spherulites have been shown to form from several globular proteins, under destabilizing conditions, at low pH values, distant from the protein isoelectric point [11, 140, 141]. It is worth to mention that, in 2010 Exley et al. showed for the first time the *in vitro* formation of Aβ(1-40) spherulites in near-physiological conditions [142]. These kind of structures have been found *in vivo* within amyloid plaques of Alzheimer's disease. Besides, only recently, also αSN spherulites have been observed *in vivo* [143]. However, they have never been observed in *in vitro* aggregation processes.

1.3 β-Amyloid peptide 1-40

The self-assembly of beta amyloid peptide 1-40 into fibrillar structures is closely related to Alzheimer's disease development. The 40 residues peptide (Aβ(1-40)) is one of three peptides naturally occurring from the proteolitic cleavage of the amyloid precursor protein (APP) [35]. Two enzymes, β-secretase and γ-secretase, act in sequence cutting the transmembrane protein APP. On the basis of cleavage position along the polypeptide chain, three different peptides can be released in the extracellular space: the beta amyloid peptides 1-39, 1-40, 1-42. Although their physiological role has yet to be clarified, they seems involved in the regulation of synaptic activity [35]. Among these three peptides, the Aβ(1-40) is the most abundant species in human brain. Its primary structure of 40 amino acids is given by:

DAEFRHDSGYEVHHQKLVFFAEDVGSNKGAIIGLMVGGVV

Aβ(1-40) peptide belongs to IDPs; indeed, in solution at physiological pH it is unstructured, presenting a CD spectrum typical of random coil conformation with a deep minimum at about 198 nm [118]. It exists as an ensemble of rapidly converting, nearly isoenergetic, conformations whose population is dependent on the physico-chemical

properties of the solution.

Depending on solution conditions Aβ(1-40) can also form amlyloid fibrils in vitro, giving the opportunity for a more thorough investigation of the aggregation kinetics. Several reports indicate that the in vitro Aβ(1-40) aggregation process proceeds via nucleated mechanisms characterized by multiple pathways involving a number of intermediate species eventually leading to polymorphic structures [9]. These mechanism are characterized by a nucleation phase, followed by a growth phase, consisting in the addition of monomers to filament ends. Different studies suggest a "dock and lock" mechanism regulating the second phase. On the basis of this mechanism monomers initially bind to (or dock onto) the exposed regions of a fibril in a reversible manner. The docking step is then followed by an irreversible re-organization of the fibril surface, which generates the most optimal surface area for further fibril growth [115, 119].

It has been found that at low pH Aβ(1-40) fibrillation occurs by means of a nucleated process in which nuclei consist of peptide micelles and fibril elongation occurs by irreversible binding of Aβ monomers to the fibril ends [122, 144].

At physiological pH, in some experimental conditions, the formation of oligomeric transient α-helix species has been reported to represent a key step in the fibrillogenesis of 18 Aβ peptides, among which Aβ(1-40) [118, 145]. The most rapid formation of the partially helical intermediate occurs in the pH regime in which the β-carboxyl group of Asp23 is ionized and the imidazole ring of His13 is protonated, suggesting a significant role exerted by these two residues on the kinetics of Aβ fibrillogenesis. The formation of helical intermediates was also investigated by trifluoroethanol (TFE) addition to the solution. In particular, low concentrations of TFE, favouring the conversion to conformations containing a certain amount of α-helical secondary structure, enhance the fibrillation rate; while concentration higher than 20% v/v leads to α-helix stabilization hindering, as a consequence, fibril production [145]. However, the direct conversion from random coil to β-sheet structures has been observed as well [145].

It is worth to mention that, in very similar conditions to that employed in the experimental work of this thesis, the Aβ(1-40) peptide fibrillation process has been reported to occur by means of an heterogeneous nucleation [125]. The main difference between the experimental conditions employed in this study and those reported in this thesis consists in the different volumes of incubation. In particular, Hortschansky and co-workers employed volumes of about 200 μl, while in this work volumes of about 750 μl were used.

Different studies emphasize the importance of the dynamic interplay between Aβ monomer conformation and oligomerization state in controlling fibrillogenesis kinetics. In specific conditions, aggregation-prone conformations can be favored, also involving the appearance of oligomeric species in solution, causing the onset of supramolecular assembly that leads to fibril formation [118, 145]. In this regard, in a recent study, a chemical kinetic based approach was used in order to connect the measurements of macroscopic observables to microscopic mechanisms, in Aβ(1-42) amyloid fibril and oligomers formation [126]. Such an approach aimed at gaining some insights into the

multiple events involved in the formation of such supramolecular assembly. The authors of this work showed that cytotoxic oligomers form once a critical concentration of fibrils has reached. The formation of these species occurs by means of secondary nucleation mechanisms, in a fibril-catalysed manner [126].

1.4 α-Synuclein

Wild type α-synuclein (αSN) belongs to a family of proteins highly expressed in neurons usually indicated as synucleins. It is mainly localized at presynaptic nerve terminals and is almost absent from peripheral tissues [146]. It was first identified in 1993 as the precursor protein for the non-β amyloid component (NAC) found in Alzheimer's disease plaques. It has been associated with Parkinson's disease (PD) since 1997, when its mutation, A53T, was identified to cause early-onset autosomal dominant PD. αSN is the major component of Lewy bodies and Lewy neuritis [5, 6]. These consist of proteinaceous deposits, which are the hallmarks of PD [147]. Nowadays it is largely accepted that αSN aggregation and interaction with membranes are involved in the PD pathogenesis [148].

The primary sequence of the human αSN consists of 140 amino acids, which can be divided into three regions (see Fig. 1.10): the amphipathic repeat or N-terminal region; the non Aβ component (NAC) region; and the acidic or C-terminal region [149]. The first one, consisting of the first 60 amino acids that contain 4-11-residue imperfect repeats with a conserved KTKEGV motif, is characterized by a high inclination to form α-helix structures upon interaction with membranes. The NAC region is formed by residues 61-95 and is the second major component of amyloid plaques typical of Alzheimer's disease brains. It seems also to be directly involved in the pathologic aggregation of αSN. The last one (residues 96-140) is rich in acidic residues and prolines and is characterized by high net mean charge and low mean hydrophobicity (see the green triangle in Fig. 1.3), which induce a disordered structure in physiological conditions.

αSN is characterized by a disordered conformation *in vitro* and in physiological conditions. For example, in aqueous solutions at neutral pH, αSN leads to CD, FTIR and SAXS signals typical of a polypeptide chain lacking a tertiary structure and with low content of secondary structure [2]. However, it assumes a conformation slightly more compact than expected for a random coil [146].

It is nowadays well known that either a decrease in pH or an increase in temperature transforms the αSN ensemble of disordered native states in an ensemble containing a certain percentage of partially folded states, with a significant amount of secondary structure [2, 104].

Despite the great number of *in vitro* experimental works revealing a monomeric disordered structure, physicochemical properties of αSN differ from that of the other IDPs shown in Fig. 1.3. Indeed, it is characterized by lower mean net charge and higher hydrophobicity. As a consequence, according to what said previously (see 1.1), these evidences would not be sufficient to assign the protein to the class of IDPs. In this last years, this aspect has been investigate by several studies resulting in ambiguous evidences.

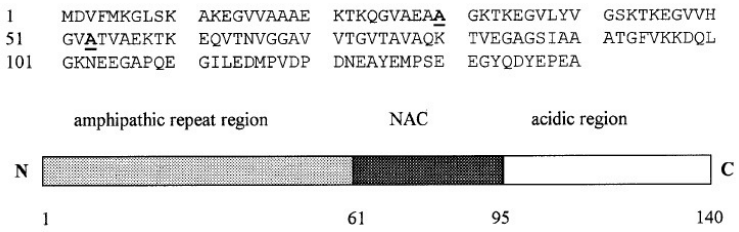

Figure 1.10: α-Synuclein primary sequence. Adapted from the original paper [149].

In 2011 it had been suggested that αSN could form a tetramer *in vivo* and that the disordered highlighted behaviour is not an intrinsic protein property but originates from employed purification protocols [150, 151]. However, this remains a minority position, contradicted by a vast literature on the properties of natively unfolded αSN. Among them, it has been recently demonstrated that, at least within *E. coli* cytosol, αSN populates a highly dynamic state, with the same characteristics as the monomeric form observed in aqueous solutions [152]. These contradictory findings, combined with the fact that αSN is extremely sensitive to its environment, have led to the emergence of the concept of the *protein chameleon*. According to it, αSN can modulate its structural behaviour on the basis of the surroundings. Its conformation can span from disordered monomeric species or a more compact state to soluble oligomers with different morphologies and cytotoxicity. In this landscape, α-helical tetramer is likely to be just one of many potential structures realized under the umbrella of the dynamic conformational ensemble [2], due, for example, to the interaction with biological membranes.

αSN fibril formation occurs by means of a nucleated processes, which are characterized by a rate-limiting step, usually called lag phase, due to the formation of nuclei, and a growth phase, during which fibrils elongate by means of monomer addition to the filament ends (see 1.2).

Being αSN an intrinsically disordered protein, its aggregation propensity is highly increased by the formation of partially folded conformations. This has been point out in 2001 by Uversky and coworkers who shown how a decrease in pH or an increase in temperature, leading to partially folded conformations, enhances αSN fibrillation propensity [104]. In this work the authors proposed the scheme reported in Fig. 1.11 for αSN fibrillation. On the basis of this model, the formation of αSN nuclei takes place starting from a population of αSN partially folded states. Polymer elongation could involve the addition to their ends of disordered monomers as well as of partially folded intermediates.

In the light of this study, in 2009 Morris et al. confirmed the model suggested by Uversky in 2001 demonstrating that αSN fibrillation can be described by means of the so called Finke-Watzky 2-step model of nucleation and autocatalytic growth.

Further confirming the role played by αSN folding in fibrillation, recently, it has been shown that αSN folding in dimeric species enhances the production of cytotoxic

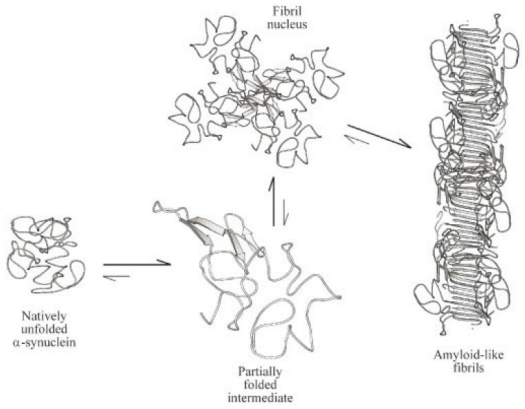

Figure 1.11: Representation of α-synuclein fibrillation model proposed by Uversky et al. in 2001. The nucleation process takes place from partially folded states, which lead to nuclei formation. Elongation of polymers could involve the addition to their ends of disordered monomers as well as of partially folded monomers. Adapted from the original paper [104].

oligomeric species and accelerates the formation of not cytotoxic fibrils [108]. This seems mainly due to the fact that dimerization of αSN increases surface hydrophobicity, as suggested by the observed increased affinity of ANS [108].

Since the intrinsically disordered nature of αSN manifests in its extraordinary capability to modulate its conformation in relation to the environment, changing chemico-physical parameters leads to changes in protein structure and, in the light of what said, strongly influences the αSN aggregation propensity. In this context, in addition to temperature and pH above mentioned, it is important also to consider the dielectric constant of the solution or solvation properties of αSN. In this regard, fluorinated alcohols, such as trifluoroethanol (TFE), are able to modulate this two parameters and, as a consequence, the fibrillation process of αSN.

Furthermore, interaction with membranes has to be taken into account. It is well established that αSN interaction with membranes results in protein folding with the formation of α-helices. The number and kind of helices seems to be regulated by lipid/protein ratio and membranes curvature radius [95]. For example, αSN shows an extended α11/3-helix (11 residues per 3 full turns) upon binding to unilamellar vesicles, both small (SUVs) and large (LUVs), or to SDS micelles at a lipid-to-protein ratio of 2000. Lowering this ratio to 400 leads to the population of a conformational state containing two canonical α-helices, coexisting with the other one just mentioned. In both cases, however, the the C-terminal region is not involved in the folding, remaining in its disordered state [95]. Recent evidences report that the N-terminal consisting of the first 25 residues interacts with membranes in a stronger manner than the remain residues [153, 154]. Moreover, in 2012 Zigoneanu et al. investigated the affinity of αSN for lipid vesicles with a composition similar to mitochondrial membranes, suggesting that

the protein destabilizes the inner membrane [154].

The interaction of aNS with membranes alters the kinetics and pathways of its aggregation in vitro. Both acceleration and inhibition of αSN aggregation have been observed in the presence of membranes [155, 156]. A detailed study of α-synuclein aggregation in the presence of phospholipid membranes found that the structures and heterogeneity of the aggregates strongly depended on the experimental conditions [157]. Moreover, it has been observed that the interaction of αSN oligomeric species with membranes results in membrane permeabilization [158, 159], suggesting a possible cause for oligomer cytotoxicity [160].

Chapter 2

Materials and experimental methods

Aim of this chapter is to describe the experimental approach employed in the study of the aggregation process of Aβ(1-40) peptide and αSN, object of this thesis. These are two intrinsically disordered proteins involved in the neurodegenerative diseases of Alzheimer and Parkinson, respectively.

Aggregation kinetics were monitored by means of Rayleigh scattering intensity measurements and ThT fluorescence intensity measurements, both acquired as a function of time. Besides these two techniques, circular dichroism (CD), small angle x-ray scattering (SAXS), two photon excitation microscopy (2-PhM) and transmission electron microscopy (TEM) measurements were employed to investigate protein and aggregate secondary structure, protein global 3D structure and aggregate morphology, respectively. Moreover, fluorescence recovery after photobleaching (FRAP) measurements were used to measure the average hydrodynamic radius of oligomeric species binding ThT in solution.

2.1 Experimental techniques

2.1.1 Rayleigh scattering and fluorescence spectroscopy

In this experimental work Rayleigh scattering intensity and ThT fluorescence signal were simultaneously acquired as a function of time to monitor the aggregation kinetics. Rayleigh scattering gives qualitative information about the average size of aggregates in solution; while ThT is a fluorescent dye widely employed to reveal the presence of fibrils both in *in vivo* and *in vitro*. As a consequence, the Rayleigh scattering signal, acquired as a function of time, gives information about the overall aggregation process, monitoring the kinetic of supramolecular assembly, independently of the type of aggregates. On the other hand, ThT fluorescence signal, acquired as a function of time, allows one to monitor the kinetics of only fibril formation. These two techniques simultaneously acquired allow one to individuate possible interconnected pathways of aggregation.

Fluorescence spectroscopy was widely employed also to perform both two photon excitation fluorescence microscopy measurements, and fluorescence recovery after photobleaching measurements. ThT was employed in these two techniques as a fluorescent dye.

The fluorescent dye Thioflavin T

In the literature the use of optically-active probes employed in *in vitro* experiments to monitor aggregation kinetics or characterize their products is quite relevant. For example the fluorescent dye 1-anilinonaphthalene-8-sulfonate (ANS) is largely employed to monitor amorphous aggregates production, while the absorption properties of the dye Congo Red or the fluorescence features of dye Thioflavin T (ThT) have been used to reveal the presence of amyloid fibrils *in vitro* and *in vivo*. Moreover, ThT is nowadays widely employed to monitor *in situ* fibril formation, under the fundamental hypothesis that this probe does not influence the aggregation processes. Although in some particular cases this hypothesis was actually proved [21, 135], the fact that ThT presence does not alter the amyloid formation pathway appears to be rather assumed than demonstrated.

There is also a renovated attention for this dye because it was found to slow down aging processes in the model organisms C. Elegans [24]. These unexpected health benefits seem to be related to ThT capability of suppressing protein-aggregation-associated paralysis in toxic protein models in multiple tissues [24]. It was intriguingly suggested that the presence of ThT may affect the amount or the size of proteins prone to aggregate [161].

In this work ThT was used to show that, in the employed experimental conditions, this dye stronlgy influences the aggregation pathways of both Aβ(1-40) and αSN (in absence of trifluoroethanol alcohol). Also, ThT spectroscopic properties were employed to monitor *in situ* fibril formation during Aβ(1-40) aggregation process triggered by the dye, and during αSN aggregation kinetics in the presence of trifluoroethanol (not influenced by the dye).

Here the main structural and spectroscopic characteristics and binding modes to fibrils of ThT are briefly presented. For a proper description of ThT structural and optical features and for deeply reviewing this subject, it is suggested to refer to a more specialized work carried out in the biophysics research group in Palermo [162].

The benzothiazole dye Thioflavin T is an organic molecule, soluble in aqueous solvents, positively charged in solutions at a pH in the range 2-7. Its structure can be split in three rather rigid fragments: the benzothiazole group (I), the benzene ring (II) and the dimethylamino group (III) [163] (Fig. 2.1). In water the dye is characterized by an absorption band centered around 412 nm. As it is well-assessed, the fluorescence signal of ThT in aqueous solution is almost vanishing for the presence of highly efficient internal non-radiative channels, whereas the fluorescence intensity shows a dramatic increase in the presence of amyloid fibrils both in vivo and in vitro [21, 164–166]. To explain the enhanced quantum yield in the presence of fibrils in 2003 Voropai et al. and in 2008

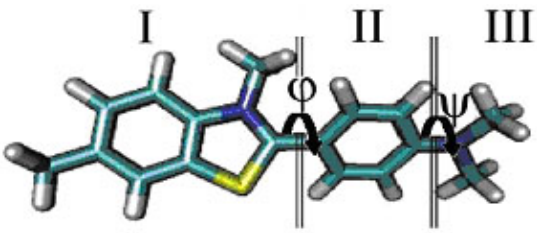

Figure 2.1: Schematic representation of Thioflavin T structure. Three ThT fragments are shown: benzthiazole ring (I), benzene ring (II), and dimethylamino group (III). Adapted from the original paper [163].

Stsiapura and coworkers formulated the model of molecular rotor [167]. Starting from this model Stsiapura et al. performed quantum-chemical calculations of ThT in the ground and excited singlet states [167]. On the basis of the obtained results, the authors concluded that the angle φ of a ThT molecule in its ground state assumes a value of about 37°. The arrival of electromagnetic radiation on a ThT molecule induces the transition to a locally excited (LE) state, characterized by the same value for the angle φ ($\sim$ 37°). From this state the reverse transition can take place trough a direct radiative channel, if the molecule is locked in the initial conformation. On the other hand, if it is not locked, the transition through a non-radiative channel is more probable to occur. This consists in a torsional relaxation of LE toward a state characterized by a value of 90° for the angle φ, followed by a not radiative deactivation to the ground state. On the basis of this model, binding to fibrils locks ThT molecules preventing rotation.

The mechanism by which ThT recognizes and binds fibrils, amyloid plaques in diseased tissues or other β-rich self-assembled peptides has been matter of debate in the last years [166, 168–171]. The main proposed models involve the presence of ThT micelles [168], formation of ThT dimers [169], or highly directional monomer binding into β-sheet structured cavities with ThT long axis parallel to the elongation axis of the fibrils [166]. However, this last model was recently confirmed by experimental and theoretical works, and it is the most accepted one [172–174].

Fluorescence microscopy

Fluorescence microscopy employs the intrinsic or extrinsic fluorescent properties of samples to acquire microscopy measurements. This technique allows one to enhance the contrast of biological sample, with respect to the case of simple optical microscopy. Moreover, by means of different fluorescent dyes, emitting in different spectral regions and specifically binding to different regions of the sample, it is possible to selectively investigate it.

The sample can be excited by means of electromagnetic radiation both in the visible or infrared region of the electromagnetic spectrum, resulting in one photon or two photon

excitations, respectively. In the first case the emitted electromagnetic radiation comes not only from the focused plan, but also from the adjacent out of focus planes, leading to blurry imagines. To overcome this drawback, in confocale microscopy, a pinhole is employed in order to remove the out of focus radiation. In the case of two photon excitation the incoming beam is able to effectively excites only the focused portion of the sample, making unnecessary the use of the pinhole. The use of two photon excitation microscopy is particularly useful when one wants to avoid radiation damage of samples and/or dyes.

Besides the acquisition of microscopy imagines, fluorescence microscopy can be used to determinate the average size of particles in solution, under the instrumental resolution, which is around 200 nm. Shortly, in FRAP measurements a small sample region containing a fluorescent dye is illuminated with an high intensity laser beam. Its wavelength is chosen within the dye absorption band, in order to bleach the largest possible number of dye molecules in this area. Then the fluorescence intensity recovery as a function of time is acquired. By means of its temporal behaviour it is possible to establish the degree of homogeneity of the sample (single or multiple exponential growth) and the average values of the diffusion coefficients. Indeed, after bleaching the fluorescence is recovered by the diffusion of unbleached molecules inside the pre-bleached area. In this work the Kapitza model [175] was used to analyse fluorescence recovery data.

2.1.2 Circular dichroism

Consider the two circular polarized components (right and left circularly-polarized beams) of a beam of linearly polarized light passing through a sample. CD signal is defined as the difference in absorption of left and right polarized light, and is usually expressed in term of molecular ellipticity according to the following formula:

$$[\theta] = \frac{4500}{\pi} ln(10) \left(\varepsilon_L - \varepsilon_R\right) \tag{2.1}$$

where ε_L and ε_R are the molecular extinction coefficients for the left and right circularly-polarized light, respectively. From the Lambert-Beer low, their difference is given by:

$$\varepsilon_L - \varepsilon_R = \frac{1}{LC} log_{10} \left(\frac{I_R}{I_L}\right) \tag{2.2}$$

where I_R and I_L are the intensities of the right and left circularly-polarized transmitted light beams, respectively.

Circular dichroism (CD) measurements in the Far-UV region (180-240 nm) give qualitative information about protein secondary structure. The absorption in this region is due to the peptide bond. On the other hand CD spectra in the region 260-320 nm are due to aromatic residues absorption and give information on protein tertiary structure [176].

2.1.3 Small angle x-ray scattering

Small angle x-ray scattering (SAXS) is a powerful method for the structural characterization of biomolecular systems, both ordered and disordered, at a resolution level of a few nm. It is a complementary technique to the high resolution methods of x-ray crystallography and NMR, and it has the great advantage of not requiring any particular type of sample treatment. Indeed, measurements can be carried out on solutions. In particular, in the case of globular proteins this technique gives information about the global size and shape of macromolecules in solution, on their states and, during protein folding, on global conformational changes en rout to the native state. It provides three-dimensional low-resolution structures by means of *ab initio* and rigid body modelling, and allow one to asses the oligomeric state of proteins and protein complexes. SAXS is also a useful technique for the analysis of flexible systems, among which intrinsically disordered proteins.

Theoretical background

This section reports a short overview on the SAXS theoretical background. For a comprehensive treatment of this topic it is suggested to check more appropriate books (for example see [177]).

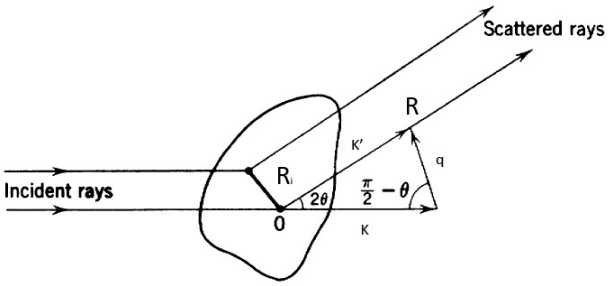

Figure 2.2: Schematic representation of the diffraction from a solution containing N particles. See the text for the description. Adapted from [177].

Consider a nonmagnetic, nonconducting, nonabsorbing medium consisting of a solvent containing N particles. Indicate with O the center of an inertial reference system, and with $\vec{R}_i$ the vector radius of the particle i with respect to O. Consider an electric field of the following form impinging upon this system:

$$\vec{E}_0(\vec{r},t) = \widehat{n}_0 E_0 \exp\left[i\left(\vec{k}\cdot\vec{r} - \omega t\right)\right] \tag{2.3}$$

where $\widehat{n}_0$ is the versor of the incident electric field, E_0 its amplitude, $\vec{k} = 2\pi/\lambda\widehat{k}$ the incident wave vector, λ and ω its wavelength and frequency, respectively (see Fig. 2.2). The electric field scattered by a particle i, respect to the pole O, measured at a distance

R much larger than interparticle distances is given by:

$$\vec{E}_s^i(\vec{R},t) \propto \widehat{n}_s f_i \frac{E_0}{R} \exp\left[i\left(\vec{k'}\cdot\vec{R} - \omega t - \Delta\varphi\right)\right] \tag{2.4}$$

where $\widehat{n}_s$ is the versor of the scattered electric field, $\vec{k'}$ is the scattering wave vector, $\Delta\varphi$ the phase difference of the scattered field with respect to O and f_i is the *scattering length amplitude* [177]. It can be shown that the phase difference is given by:

$$\Delta\varphi = \vec{q}\cdot\vec{R}_i \tag{2.5}$$

where $\vec{q}$ represents the *scattering vector* and is given by $(\vec{k'} - \vec{k})$. The total scattered field at distance $\vec{R}$ is given by the interference of the fields scattered by the N particles:

$$\vec{E}_s(\vec{R},t) \propto \widehat{n}_s \sum_{i=1}^{N} f_i \exp\left(-i\vec{q}\cdot\vec{R}_i\right) \tag{2.6}$$

As a consequence the revealed radiation intensity can be written as:

$$\langle I(\vec{q},t)\rangle = \left\langle \vec{E}_S(\vec{q},t)\,\vec{E}_S^*(\vec{q},t)\right\rangle \propto \tag{2.7}$$

$$\propto \left\langle \sum_{i=1}^{N}\sum_{j=1}^{N}\left\{ f_i(\vec{q},t)\, f_j^*(\vec{q},t)\exp\left[-i\vec{q}\cdot\left(\vec{R}_i - \vec{R}_j\right)\right]\right\}\right\rangle = \tag{2.8}$$

$$= \left\langle \sum_{i=1}^{N} |f_i(\vec{q},t)|^2\right\rangle + \left\langle \sum_{i,j(i\neq j)}\left\{ f_i(\vec{q},t)\, f_j^*(\vec{q},t)\exp\left[-i\vec{q}\cdot\left(\vec{R}_i - \vec{R}_j\right)\right]\right\}\right\rangle \tag{2.9}$$

In the case of statistically independent particles, which can be approximated by diluted solutions, the last term in equation 2.9 vanishes. So, if the system is a diluted solution of N identical particles the expression for the intensity reduces to:

$$\langle I(\vec{q},t)\rangle \propto N\left\langle |f_i(\vec{q},t)|^2\right\rangle = N\langle I_p(\vec{q},t)\rangle \tag{2.10}$$

Where $\langle I_p(\vec{q},t)\rangle$ is the scattering intensity due to the interference created by atoms within a single particle. In order to determine this quantity one can repeat an argument similar to that presented above, substituting the N particles with N_A atoms, the *scattering length amplitude* with the *atomic scattering length amplitude*. Indicating with $\vec{r}_n$ the vector radius of the atom n with respect to the pole O, the scattered electric field from this atom is given by equation 2.4, with the *atomic scattering length amplitude*, ϕ_n, in place of f_i, and $\vec{r}_n$ in place of $\vec{R}_i$ in the expression for the difference of phase equation 2.5. As a consequence, the scattered electric field due to the contributions from all the atoms inside a particle is given by:

$$\vec{E}_s^p(\vec{R},t) \propto \widehat{n}_s \sum_{n=1}^{N_A} \phi_n \exp\left(-i\vec{q}\cdot\vec{r}_n\right) \tag{2.11}$$

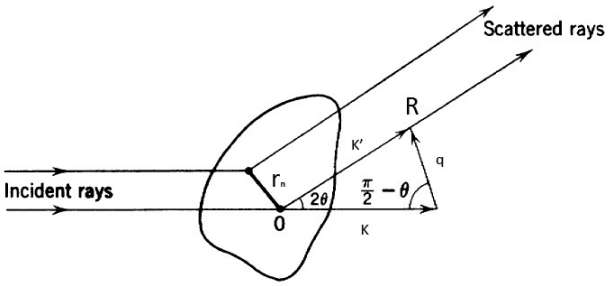

Figure 2.3: Schematic representation of the diffraction from a particle consisting of N_A atoms. See the text for the description. Adapted from [177].

From what said the expression 2.10 can be rewritten as:

$$\langle I(\vec{q},t)\rangle \propto N\left\langle \sum_{n=1}^{N_A}\sum_{m=1}^{N_A}\phi_n\phi_m^* \exp\left[-i\vec{q}\cdot(\vec{r}_n-\vec{r}_m)\right]\right\rangle = N\left\langle |F|^2\right\rangle \tag{2.12}$$

where the quantity:

$$F = \sum_{n=1}^{N_A}\phi_n \exp\left(-i\vec{q}\cdot\vec{r}_n\right) \tag{2.13}$$

is called *particle structure factor*. This depends on the conformation and shape of proteins in solution, in particular, on their globular or intrinsically disordered conformation. As explained below, this characteristic allow to easily individuate homogeneous solutions of globular proteins distinguishing them from solutions containing IDPs.

Globular proteins In the case of solutions containing globular proteins the structure factor can be evaluated approximating the macromolecules to rigid bodies. This means that a single protein is considered as a system with fixed interparticle distances. It can be shown that under this approximation the modulus squared of the structure factor is given by equation 2.14, known as Debye Equation [177]:

$$\left\langle |F|^2\right\rangle = \sum_{n=1}^{N_A}\sum_{m=1}^{N_A}\phi_n\phi_m^*\frac{sin(qr_{nm})}{qr_{nm}} \tag{2.14}$$

where $qr_{nm} = |\vec{q}||\vec{r_n} - \vec{r_m}|$. In the derivation of 2.14 the probability that $\vec{q}$ and $\vec{r}_{nm}$ form an angle between φ and $\varphi + d\varphi$ has been assumed to be $\sin(\varphi)\mathrm{d}\varphi/2$.

For $qr_{nm} << 1$ the expression 2.14 can be developed in series giving:

$$\left\langle |F|^2\right\rangle = \sum_{n=1}^{N_A}\sum_{m=1}^{N_A}\phi_n\phi_m^*\left[1 - \frac{q^2}{6}|\vec{r}_{nm}|^2 + ...\right] = \tag{2.15}$$

$$= \sum_{n=1}^{N_A}\sum_{m=1}^{N_A}\phi_n\phi_m^* - \frac{q^2}{3}\sum_{m=1}^{N_A}\phi_m^*\sum_{n=1}^{N_A}\phi_n|\vec{r}_n|^2 + \frac{q^2}{3}\sum_{m=1}^{N_A}\sum_{n=1}^{N_A}\phi_n\phi_m^*\vec{r}_n\cdot\vec{r}_m + ... \tag{2.16}$$

Let consider the center of charges, that is the point at the position:

$$\vec{R}_O = \frac{\sum_{n=1}^{N_A}\phi_n\vec{R}_n}{\sum_{n=1}^{N_A}\phi_n} \tag{2.17}$$

Choosing this point as the pole O, that is putting $\vec{R}_O = 0$, then the third term in 2.16 goes to zero and the expression can be rewritten as:

$$\langle|F|^2\rangle \approx |\sum_{n=1}^{N_A}\phi_n|^2 \exp\left(-\frac{q^2}{3}R_0^2\right) \tag{2.18}$$

where the quantity:

$$R_0^2 = \frac{\sum_{n=1}^{N_A}\phi_n|\vec{r}_n|^2}{\sum_{n=1}^{N_A}\phi_n} \tag{2.19}$$

is the electronic radius of gyration of particles.

From 2.18 and 2.12 the intensity scattered at q values such that $qr_{nm} << 1$, for diluted and homogeneous solutions containing globular proteins, can be approximated to:

$$I = I_0 \exp\left(-\frac{q^2}{3}R_0^2\right) \tag{2.20}$$

known as *Guinier approximation* [177].

For such a system the plot of ln(I) vs q^2 (Guinier Plot) shows a linear behaviour for $q < 1/R_0$ with a slope equal to $\left(-R_0^2/3\right)$, and an y axis intercept equal to $\ln(I_0)$, which can be shown to be proportional to the molecular mass of the particles. This allows one to calculate a first estimation of the electric radius of gyration, R_0, and, after suitable calibration, of the molecular mass. Moreover, the plot of $q^2I(q)$ vs q (Kratky Plot) shows a bell-shaped behaviour, giving qualitative information on the compactness of proteins in solution [178].

It should be remember that the Guinier approximation is valid under the hypothesis of a diluted and homogeneous system containing globular proteins. As a consequence, if the Guinier plot does not show a linear region at low q values this means that at least one of the above assumptions is not valid.

Disordered proteins This section briefly takes into account the case of a diluted and homogeneous solution containing intrinsically disordered proteins. Obviously, in this case, among the different approximations made above, the one concerning the assumption of proteins as rigid bodies has to be released. Indeed, in intrinsically disordered proteins

interparticle distances can not be all considered fixed. In this case the polymer can be described as a chain of N freely-jointed rigid rods of length b [179].

In order to evaluate the structure factor the distinction between "good-solvents" and "ϑ-solvents" has to be made. In the first case the polypeptide chain is fully solvated, excluding the polymer solvation layer from the configuration space of the chain. For this reason it is said to have *excluded volume*, resulting in an effective repulsive interaction between residues. In the second case the excluded volume vanishes and the chain can be equally well in contact with itself or with the solvent. The probability density for distances between points on the chain is gaussian and the chain is said to be gaussian [179].

It can been demonstrated that in both cases the Guinier plot does not show any linear region for low q values. In particular, in the presence of a ϑ-solvent the scattering intensity can be calculated averaging again the Debye equation 2.14, in order to take into account all the forms the flexible chain can acquire. The result of this averaging is given by the following expression [179]:

$$I = I_0 \frac{2}{x^2} \left[x - 1 + \exp\left(-x\right) \right] \tag{2.21}$$

where $x = q^2 R_0^2$. In the presence of a good-solvent this expression is only valid for low q values while for $q > 7/b$ the scattering intensity is given by:

$$I \sim I_0 \left[\frac{\pi}{qNb} + \frac{4}{3b^2 N q^2} \right] \tag{2.22}$$

Eventually, in both cases (good- and ϑ-solvents) the Kratky plot does not show any bell-shaped behaviour but a a monotonic increase behaviour followed by a plateau, instead [75, 179].

2.2 Instrumentation

This section reports the main features of the instrumentation employed in this work.

2.2.1 Instrumentation for the acquisition of Rayleigh scattering and fluorescence measurements

Rayleigh scattering and fluorescence measurements were acquired simultaneously using the fluorescence system whose block diagram is reported in Fig. 2.4 (ACTON Instruments). The excitation light produced by a Xenon Lamp (75 W) comes inside the excitation spectrograph SpectraPro 2150i (SP-2150i), PI Acton, 150 mm focal length. This spectrograph allows one to select the excitation wavelength by means of a dual grating turrets, a grating with a groove linear density of 150 grooves/mm, blazed at 500 nm and the other one with a density of 150 grooves/mm, blazed at 300 nm. *Grooves density* and *blaze angle* determine the spatial resolution on the wavelength selection (being much precise as bigger is the number of the lines on the grating) and efficiency as

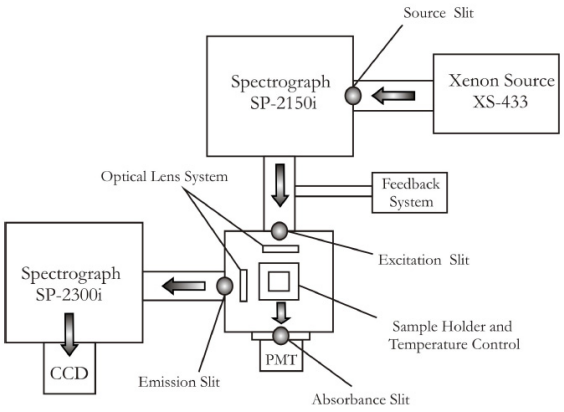

Figure 2.4: Bock diagram of the fluorescence system (ACTON instruments) used in this thesis. Adapted from [162]

a function of wavelengths, respectively. The light at the desired wavelength is focalized on the sample through a micrometer adjustable slit and an optical lens system. This instrument is able to simultaneously perform absorbance and emission measurements. Indeed, a feedback system, placed before sample compartment, reveal the intensity of incident light, while a PMT acquires the transmitted light through another micrometer adjustable slit. The light emitted from the sample, coming through a third micrometer adjustable slit, is revealed, in right-angle configuration, and focalized by a lens system in the emission spectrograph SpectraPro 2300i (SP-2300i), PI Acton, 300 mm focal length, which disperses it on the CCD camera PIXIS 400 Princeton Instruments, ACTON. The SP-2300i spectrograph is equipped with three gratings, a 1200 grooves/mm 300 nm blazed grating, a 300 grooves/mm 500 nm blazed grating and a 150 grooves/mm 300 nm blazed grating. The CCD camera is thermoelectrically air-cooled down to -75 °C to provide a low value of dark current. Grating and wavelength in excitation and emission can be set by means of the software SpectraPro and WinSpec32, respectively; while the software SpectraSense allows one to control the feedback system.

In this work, the excitation and emission grating were chosen to be the one with a density of 150 g/mm, blazed at 500 nm and the one with a density of 300 g/mm, blazed at 500 nm, respectively.

In this experimental work the system was only used to acquire emission spectra. The electron magnetic radiation coming from the sample was acquired as a function of wavelength. The emitted signal was collected at 90° with respect to the excitation beam in order to minimize sample absorption effects. This configuration allows one to simultaneously detect the Rayleigh scattering intensity, at the same wavelength of the excitation beam, and ThT fluorescence, at lower wavelengths.

Since measurements lasted several hours, care was taken to ensure that variation in

the efficiency of the lamp source will not affect the correctness of the experimental data. The source signal, acquired each minute from the feedback system, was used to normalize the emission intensity. However, the diminution of the lamp intensity was less than 3% in 50 hours of use. Moreover, for samples containing the dye ThT, correction for the primary and secondary inner filter effects and only for primary filter effects were made for scattering and fluorescence data, respectively. This was accomplished by means of the following expression[180]:

$$S_{corr} = \frac{S_{meas}}{10^{\frac{dAbs(435\ nm)}{l}}} \tag{2.23}$$

where S_{corr} is the corrected scattering signal, S_{meas} is the measured signal, Abs(435 nm) is sample absorbance at 435 nm, l is the light path to acquire the absorbance spectrum (l=1 cm), and d is the effective light path inside the sample during emission spectrum acquisition.

In this work measurements were performed in standard right-angle geometry on a 0.5 x 1.0 cm PMMA UV-cuvette (BRAND). As a consequence, d is equal to 3/4 l for scattering correction and 1/2 l for fluorescence correction. Secondary inner effects for fluorescence were not taken into account because sample absorption at 490 nm is negligible.

2.2.2 Instrumentation for the acquisition of two photons excitation microscopy measurements and fluorescence recovery after photobleaching experiments

Two photons excitation microscopy (2-PM) and fluorescence recovery after photobleaching (FRAP) measurements were carried out using a Leica TCS SP5 confocal laser scanning microscope (Leica Microsystems, Germany). With this system, images are acquired scanning a 2-D surface from the left to the right, and from the top to the bottom.

In order to describe in broad outline the system, in Fig. 2.5 a general picture of such instrumentation is reported. A description of the main devices shown is given in the following. The microscope is equipped with three laser line inputs, one for confocal measurements which allows one to choose between five lasers at different wavelengths in the visible region (1), and the other two optional, one for an UV laser (3) (not present in the instrumentation used in this work) and the other one for IR pulsed laser (2). This last is connected to a Spectra-Physics Mai-Tai Ti:Sa ultra-fast laser, and allows one to perform 2-ph excitation microscopy measurements. Pulses of the IR laser source are at a frequency of 80 MHz, with a temporal with <100 fs, average power >650 mW and peak power >80 kW. Laser wavelength and intensity, and acquisition settings can be choose by means of the software Leica application suite. In particular, the IR laser source wavelength can be tuned in the range 780-920 nm. Moreover, in Fig. 2.5, a detector (14), to acquire measurements very similar to those of the optical transmission microscopy,

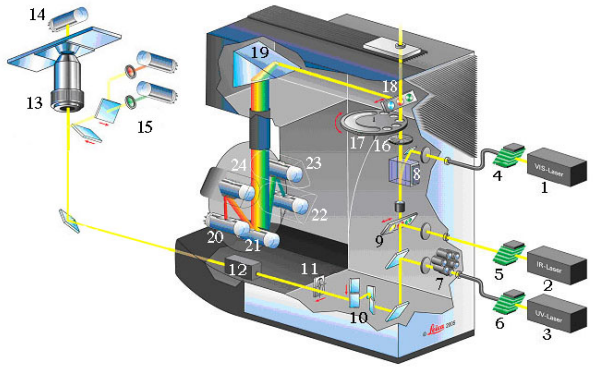

Figure 2.5: Representation of Leica TCS PS5 confocal laser scanning microscope used in the experimental work of this thesis.

and a Xenon lamp (15), which, through the eyepieces, allows one to quickly select the region of interest inside the sample, are also shown.

During 2-ph excitation microscopy image acquisition, IR pulses pass trough the electro-optic modulator (EOM) (5), a software-controlled device which fixes the beam intensity at the constant value chosen by the user, and the multi function port (MFP) (9), a type of wavelength filter which reflects IR radiation and transmits visible light. Then it goes through an optical lens system (10, 11, 12) until reaching the objective (13) and so the sample. The radiation emitted from the sample is collected by the objective and goes back through the MFP device (9). Subsequently, it impinges on the Acousto Optical Beam Splitter (AOBS) (8). This device, software-controlled, allows one to select the desired spectral range of the emitted radiation, modifying the wavelength window in the range 400-800 nm. The radiation outcoming from the AOBS device passes through the pinhole (16) and an optical system (19) and is detected by the photomultipliers (PMTs) (20-24). The pinhole is a software-controlled slit, essential to perform confocal measurements. Indeed, it is able to cut down the light emitted from sample coming from out of focus planes. During 2-ph excitation measurements, since this technique is intrinsically confocal, this slit is left open (600 μm). The optical system (19) is able to divide the radiation coming from the sample in several spectral ranges, from one to a maximum of five, in order to separately acquire them by means of the five PMTs. This characteristic is really useful since it allows one to stain the sample with dies emitting in different spectral region, separately and simultaneously acquiring the radiation from each of them.

The system is equipped with four objectives: 20x air objective NA 0.7, 40x oil objective NA 1.25, 63x oil objective NA= 1.4 and 100x air objective NA 0.9. For the measurements acquired in this work the 63x oil objective NA= 1.4 was employed.

This system is also able to perform fluorescence recovery after photobleaching (FRAP) measurements, by means of the available FRAP wizard of the LEICA control software.

These measurements allow one to obtain an averaged estimation of the hydrodynamic radius of populations in solution. This is a really useful technique to employ when the dimensions of species in solution are under the instrumental resolution (∼200 nm).

To perform FRAP experiments the confocal mode is employed. In this case one of the five visible laser is chosen. The light path inside the microscope is essentially the same than for the IR laser beam, width only slightly modifications. The only worth mentioning difference is the with of the pinhole, which in the confocal mode has to be reduced so that one can focus on the sample.

2.2.3 Instrumentation for the acquisition of circular dichroism measurements

In this work CD measurements were carried out on a Jasco J-715 spectropolarimeter, whose block diagram is reported in Fig. 2.6, equipped with a Jasco PCT 348 WI temperature controller. The light produced by a xenon lamp comes inside a double monochromator, which produces a monochromated and liner-polarized beam, reducing stray light. This linearly-polarized light is modulated by the modulator into right and left circularly-polarized beams, and sent on the sample. If these two circular polarized components (right and left circularly-polarized beams) are absorbed in different amounts the sample is said to have circular dichroism.

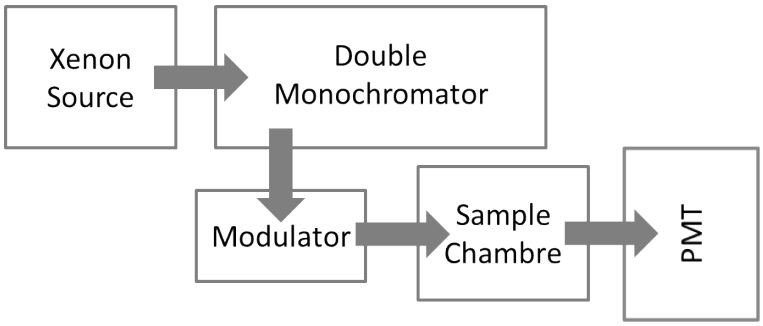

Figure 2.6: Block diagram of Jasco J-715 spectropolarimeter.

2.2.4 Instrumentation for the acquisition of SAXS measurements

Fig. 2.7 presents a typical setup for SAXS measurements. A collimated monochromatic x-ray beam is made to strike the sample, a solution of macromolecules placed in a capillary or cuvette. X-ray beam and the intensity of the scattered beam is measured as a function of the scattering angle (2θ). In solution, scattering is usually isotropic due to the random orientation of particles, but SAXS patterns are generally recorded by two-dimensional detectors, which provide better statistical accuracy of the signal after radial averaging [75]. The scattering patterns are presented as radially averaged one-dimensional curves.

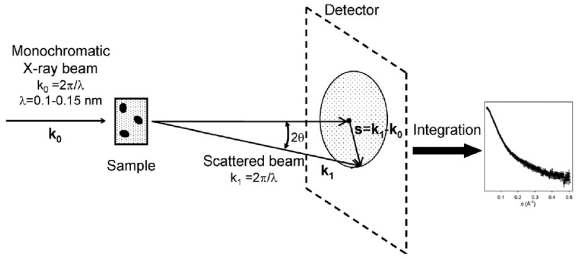

Figure 2.7: Experimental setup for the acquisition of small angle x-ray scattering measurements. Adapted from the original paper [75]

This technique is considerably sensitive to beam drift. As a consequence a typical scattering experiment is carried out measuring the scattered curves from buffer, then from sample and from buffer again. If the two acquired buffer curves superimpose within the experimental error, the averaged buffer curve is subtracted from the one of sample. If this is not the case, that is if the two buffer curves significantly differ, due to beam drift, measurements have to be repeated.

2.3 Materials and sample preparation

2.3.1 The fluorinated alcohol Trifluoroethanol

Cosolvents, and in particular alcohols, have long being employed to trigger changes in the conformation of proteins in order to study folding and unfolding kinetics in a controlled manner. In this work water-TFE mixtures at different alcohol concentrations were employed to test αSN fibril stability. TFE is known to modulate protein conformation, changing protein solvent interactions via concentration dependent effects. In particular, electrostatic interactions and relative stability of hydrogen bonds, can be tuned by varying TFE concentration [25, 27].

TFE-proteins interaction

2,2,2-Trifluoroethanol (TFE) is a fluorinated alcohol, whose molecular formula is given by $C_2H_3F_3O$. It consists in an organic molecule which differ from ethanol for the replacement of the CH_3 group by a CF_3 group.

Effects of water-TFE mixtures on the structure of peptides and proteins have been studied for more than five decades. These mixtures affect the conformation of polypeptide chains in dependence of the particular amino acid sequences, the cosolvent concentration and other solution conditions as well as of the structures involved. In particular, both stabilization and denaturation of proteins were found. As a general rule, in globular proteins high TFE concentrations lead to the unfolding of the native state and the stabilization of α-helical secondary structures; while low concentration values facilitate the formation of β-sheet aggregates [26, 27]. TFE was found to change intra- and

intermolecular H-bond interactions and, importantly, to induce changes in amyloid fibrils stability acting as a strong denaturing agent [25, 181].

By means of a large amount of experimental and computational works, performed in order to investigate the interaction TFE-proteins at molecular level, it has been shown that a single mechanism which accounts for all the different effects induced by TFE does not exist [25]. Rather, it seems that TFE acts on different sides: i) it is able to penetrate the hydrophobic cores of proteins, interacting with hydrophobic groups within proteins [25]; ii) TFE reinforces hydrogen bonds between carbonyl and amidic groups and removes water molecules in the proximity of the solute so affecting solvation/hydration properties of proteins; iii) it changes the properties of bulk water lowering the dielectric constant. In this regard, in 2003 Munishkina and coworkers showed that, if effects of single alcohol on αSN conformation can be ascribed to the reduction of the electric constant value of the solution, in the case of TFE a combination of preferential binding to the mainchain of αSN and dielectric constant effects have to be taken into account. This picture is made even more complex by the fact that balancing between the three different mechanisms depends on the particular system. As a consequence TFE acts as both a localized structural stabilizer and a global denaturant that provide different, and potentially competitive, effects depending on the element under investigation [182].

To explain how TFE strengthens intra-chain hydrogen bonds, it has been proposed that it is likely to bind preferentially to the mainchain carbonyl oxygen group (which is often able to accept two hydrogen bonds), being a better hydrogen bond donor but a poorer acceptor compared to water [25]. Since TFE molecules are nine times bigger than water molecules, this interaction leads to the expulsion of water molecules from the mainchain, resulting in the reduction of amide group solvent exposure, and, as a consequence, in the formation of intra-chain hydrogen bounds [25]. This also changes the solvation properties of proteins. On the other hand, in a recent study it has been postulated that amyloid formation and non-native helix induction upon addition of cosolvents can be governed by differential values of dielectric constant [183]. High concentration of cosolvents would enhance cosolvent-peptide backbone association resulting into dropping off the dielectric constant by removal of water molecules from vicinity of peptide backbone and mediate intra-peptide hydrogen bonding to induce helicity [183].

For its features, TFE is generally used to probe structural characteristics of the enzymes. More in detail, it was used in enzymatic denaturation studies, providing insights into the folding pathways, enzymatic catalysis and thermal stability [184, 185]. Moreover, it is used to mimic some features of *in vivo* environment. Indeed, mimicking the cell environment in *in vitro* studies is usually accomplished acting on three different aspects: i) crowding, which provides the typical excluded volume effect experienced by proteins in living cell, ii) viscosity and iii) solvation/hydration of proteins. It is nowadays well accepted that TFE can be used to mimic the last two aspects [17]. Furthermore, it has been reported that water-TFE mixtures at different cosolvent concentrations can be used to reproduce the effects of membrane on protein-protein electrostatic interactions, at different distances from membranes [27].

To conclude, TFE is reported to mimic cell environment accounting for solvation/hydration of proteins in cell, viscosity and dielectric constant effects.

2.3.2 β Amyloid peptide (1-40)

Aβ(1-40) peptide pretreatment

Aβ(1-40) peptide was purchased from Biopeptide (purity>95%) and pretreated before use. The employed pretreatment consists in a slightly modified Fezoui protocol[186]. The peptide was dissolved in a 2 mM NaOH aqueous solution (pH 10), sonicated for 30 min in an ice-water bath, divided in aliquots of 200 μl and freeze-dried before being stored at -80 °C. All phases were accomplished in a cold room. This preliminary procedure promotes peptide solvation in buffer solution at pH values higher than its isoelectric point (5.5), reducing the probability that Aβ samples contain aggregation nuclei right after peptide dissolution. This is essentially due to the fact that dissolving the peptide for example in a buffer at physiological pH the peptide does not pass through its isoelectric point, where the solubility in aqueous solution is minimized. Moreover, this treatment leads to the creation of twin aliquots of about 0.2 mg each, reducing peptide waste.

Aβ(1-40) sample preparation and experimental settings

Commercial ThT was purchased from Sigma Aldrich (purity 65-75%). Recrystallized ThT was kindly provided by Minna Groenning, Department of Pharmacy, University of Copenhagen [187].

Immediately before use, the pretreated peptide power (see above) was dissolved in 50 mM sodium phosphate buffer, pH 7.4, with or without ThT, and filtered through a 0.20 μm filter (Sartorius 17761). Dissolution procedure was accomplished in a cold room in order to avoid seeds formation. Aβ(1-40) and dye concentrations were estimated by means of absorbance measurements using a molar extinction coefficient of 1390 M^{-1} cm^{-1} at 276 nm and 36000 M^{-1} cm^{-1} at 412 nm, respectively.

Fluorescence and Rayleigh scattering measurements were carried out simultaneously during the incubation of the sample at the desired temperature. Measurement were acquired every 1 minute, in standard right-angle geometry on a 0.5 x 1.0 cm PMMA UV-cuvette (BRAND), under excitation at 435 nm, using the fluorescence system described in Section 2.2.1. The temporal window for acquiring the light was set 250 ms. Rayleigh scattering signal at 90° was measured as the maximum of the elastic peaks of excitation light (435 nm). Data were corrected for possible lamp intensity fluctuations as reported in Section 2.2.1. All the reported aggregation kinetics were measured in quiescent conditions and experiments were repeated several times showing an high degree of reproducibility.

For TEM measurements grids were prepared as described by Foderá and co-workers[188]. Briefly, 5 μl of the sample were loaded onto copper 400 mesh grids (Agar Scientific, Stansted, UK) coated with Formvar and carbon film. After 60 s, 10 μl of distilled water was added and excess water was removed. Subsequently, 10 μl of 2% (w/v) uranyl acetate (Agar Scientific) was placed on the grid and left for 30 s. Finally, 2x10 μl distilled water

were added and again excess water removed. The grid was then left to dry. The same procedure was used for the two samples under investigation. Images were collected using a CM100 transmission electron microscope operating at an acceleration voltage in the range of 40-100 kV.

Before to carry out FRAP measurements Aβ(1-40) samples after incubation at 41 °C were cooled down in an ice-water bath. Drops (10 μl) were placed in chambered coverglass and imaged using the system described in Section 2.2.2. The confocal experiments were performed using the available FRAP wizard of the LEICA control software.

Far-UV CD measurements were carried out on a sample cell with a path of 0.5 mm. Spectra were acquired at 25 °C using a scan speed of 50 nm/min, data pitch of 0.1 nm, response of 2 sec, number of accumulations 4. Measurements on thermally treated samples were carried out just after cooling down in an ice-water bath.

Classical MD simulations were performed in collaboration with the Biophysics Group of University of Rome-Tor Vergata. People from this research group computationally analysed the system containing five ThT molecules and one Aβ(1-40) molecule, using GROMACS package [189].

2.3.3 α-Synuclein

Expression and purification of wild type α-synuclein

Expression and purification of recombinant human wild type αSN were performed at the laboratories of BioSAXS group, University of Copenhagen, Denmark. The expression construct was kindly provided by Bioneer, Horsholm, Denmark. The Escherichia coli plasmid vector p-ET11-a was transfected into an Escherichia coli BL21 (DE 3) cell line for expression of αSN. Purification of αSN was performed following the protocol developed by Huang et al. [190]. We slightly modified the procedure and performed an additional boiling of the lysate and size-exclusion chromatography before and after ion-exchange chromatography respectively. This is in agreement with previously reported protocols [22]. In short, the periplasmic αSN was released by resuspending cell pellets in an osmotic shock buffer (30 mM TRIS, 40% sucrose, 2 mM EDTA, pH 7.2). Impurities in the lysate were precipitated by boiling at 95 °C for a maximum of 15 minutes. After filtration, solution was subsequently loaded onto a HiTrap Q FF column after buffer exchange to 20 mM Tris-HCl pH 8.0. The fractions containing αSN were analyzed by SDS-PAGE and loaded onto a HiLoadSuperdex 75 column. Fractions solely showing a 14.5 kDa band on SDS-PAGE were pooled and dialyzed against MQ-water over-night. Lyophilization was performed prior to storage at -20 °C.

αSN sample preparation and experimental settings for fresh prepared αSN samples investigation and aggregation kinetics

Thioflavin T (ThT) (purity 65-75%) and Trifluoroethanol alcohol (TFE) (purity$\geq$99%) were purchased from Sigma Aldrich and used without further purification. All the measurements were performed in aqueous solution: immediately prior to each experiment,

αSN was dissolved in 50 mM sodium phosphate buffer, pH 7.4, and filtered through 0.20 μm filters (WVR cod. 514-0060). Buffer, TFE and water-ThT solution were added in suitable volumes in order to obtain 1.2 mg/ml αSN samples in the required TFE concentration, and containing 20 μM ThT. αSN and dye concentrations were estimated by means of UV absorbance measurements using a molar extinction coefficient of 5120 M^{-1} cm^{-1} at 280 nm [191] and 36000 M^{-1} cm^{-1} at 412 nm [192], respectively.

SAXS experiments on fresh prepared αSN samples were performed at beamline I911-4 at MAX-lab, Lund, Sweden, using a 61-period, 3.5 T, multipole-wiggler operating at a wavelength of 0.91 $\AA$. Beam area was of 0.3 x 0.3 mm^2. The scattering was registered on a Pilatus detector in the momentum transfer range of $0.008 < q < 0.45$ $\AA^{-1}$. Sample exposure was 2 min. Buffers were measured before and after sample exposure, and averaged before background subtraction. Repeated exposure did not reveal any radiation damage. The bioXTAS RAW software was used for radial averaging and background subtraction [193].

For CD measurements in the Far-UV region sample cell path was 0.1 mm. Spectra were acquired at 25 °C using a scan speed of 50 nm/min, data pitch of 0.1 nm, response of 1 sec, number of accumulations 10.

Fluorescence measurements were carried out every 1 minute, in standard right-angle geometry on a 0.5 x 1.0 cm PMMA UV-cuvette (BRAND), under excitation at 435 nm using the fluorescence system described in Section 2.2.1. The temporal window for acquiring the light was 250 ms. Rayleigh scattering signal at 90° was simultaneously measured as the maximum of the elastic peaks of excitation light. Because of long time measurements of several hours, data were corrected for lamp intensity variations as reported in Section 2.2.1. All the reported aggregation kinetics were measured in quiescent conditions.

For 2-PM measurements samples were stained with ThT right before microscopy measurements. Aliquots of 10 μl were placed in chambered coverglasses and imaged at 1024x1024 pixel resolution using the system described in Section 2.2.2. Two-photon laser excitation wavelength was set at 880 nm. The measurements were performed using a scanning frequency of 400 Hz, detecting the emitted light in the spectral range 470-600 nm.

αSN sample preparation and experimental settings for fibril stability investigation

αSN samples in 15% TFE v/v, prepared as described above, were incubated for 27 hours at 50 °C. After that, samples were cooled down in ice-water bath for 15 min. Then an aliquot (control sample) was withdrawn and checked by means of 2-PM. The remaining aggregated sample was spun down at 13000 rpm for 10 min. The supernatant was removed and investigated by means of CD and 2-PM. These two techniques did not show neither a detectable CD protein signal nor aggregates within the microscope resolution. Four identical aliquots were withdrawn from the pellet and diluted 1:10 in buffer containing suitable TFE concentrations. Four samples (A, B, C, D) at different

final TFE concentrations were obtained: Sample A at TFE 15% v/v, Sample B at 30% TFE v/v, Sample C at 60% TFE v/v and Sample D at TFE 1.5% v/v.

CD measurements in the Far-UV region were carried out on sample cells with paths of 0.1 mm for control sample, 1 mm for supernatant aliquots and 0.5 mm for A, B, C, D samples. Spectra were acquired using a scan speed of 50 nm/min, data pitch of 0.1 nm, response of 1 sec. Number of accumulations was set to 10 for control, A, B, C, D samples and 3 for supernatant.

2-PM measurements were curried out as described in the precedent section.

Experimental Section

Chapter 3

Aβ(1-40) aggregation pathways controlled by Thioflavin T

In the last two decades several experimental and computational works highlighted how IDPs conformation are strongly affected by their environment [17, 18]. A change in pH or addition of co-solvents, metals or co-solutes can reshape the energy landscape generating deeper minima, so inducing a partially folding, possibly influencing the aggregation processes [26, 88, 94, 103, 104]. In this regard, to take advantage of this aspect for therapeutic purposes, the possibility of using small molecules to modulate the aggregation pathway and isolate the occurring species has recently been considered [194–198], in particular, in order to prevent the formation of cytotoxic species. Indeed, although the ideal case would be completely inhibiting the aggregation process, it would be significant, however, to be able to generate new, more likely, aggregation pathways bypassing the events generating toxic species. Such molecules can delay the fibril formation, stabilize specific intermediate species or even disrupt the final aggregate [199, 200]. Evidence for the occurrence of such events has driven an increasing interest towards the understanding of small molecule-peptide interaction [201, 202]. In particular the role of specific residues in the peptide-molecule interactions and the possible change in conformation upon interaction should be clarified.

In the case of Aβ peptide, it has been established that the hydrophobic core, consisting of residues 17-21 (Leu17-Val18-Phe19-Phe20-Ala21), plays a key role in the interaction with small molecules influencing the fibrillation process. Masuda and co-workers reported that the small molecule Curcumin can affect both Aβ(1-40) and Aβ(1-42) [196] amyloid fibril formation, with 12th and 17-21st residues of the peptide Aβ(1-42) mainly involved in the interaction [202]. Moreover, Tjernberg and co-workers showed that the peptide fragment including residues 16-20 (Lys16-Leu17-Val18-Phe19-Phe20) is the shortest one displaying a high binding capacity to the full length Aβ(1-40) peptide and the ability of inhibiting in vitro fibrils formation [203]. Recently, Viet and co-workers demonstrated that this fragment binds to residues near the N-terminal, Gly9 and His13 [204]. For

such kind of studies both experiments and simulations have been employed. Specifically, Molecular Dynamic (MD) has been recently employed in the emerging field of metallo-proteins and protein-metal interactions [205]. In the case of the Aβ peptide, MD results have been employed not only to guide experiments, but have also been instrumental in designing potential Aβ aggregation inhibitors [206].

In this context, this chapter presents the effect of Thioflavin T (ThT), a commonly used probe for the detection of amyloid-like species, on the Aβ(1-40) conformation, stability and aggregation and singles out the Aβ(1-40) residues involved in the interaction with ThT.

3.1 Results and discussion

Fig. 3.1 shows the typical time evolution of Rayleigh scattering intensity measured at 435 nm for 150 μM of Aβ(1-40) in 50 mM sodium phosphate buffer at pH 7.4, incubated at 41°C for 46 hours (black line). Green line refers to the measurements on Aβ(1-40) at the same concentration in the same buffer containing ThT (20 μM) (hereafter Aβ-ThT). Since Rayleigh scattering gives qualitative information about average size of all aggregates in solution [207], acquiring its intensity as a function of time allow one to monitor the growth of all type of aggregates in solution, that is the overall aggregation process. As it is observed, for the Aβ(1-40) sample the scattering intensity remains constant during the incubation time. This behaviour indicates that the average size of the particles in solution remains unchanged at least up to 46 hours. Interestingly, in the presence of ThT (green line), the scattering signal shows a two-step kinetics: In the first phase it slowly increases almost linearly, then it undergoes an abrupt growth after about 23 hours (t_0). This behaviour resembles the biphasic kinetics consisting of a lag and a growth phases which usually indicates nucleated polymerisation mechanisms in Aβ fibrillation [125]. In panel b) we also report, as control, the corresponding scattering measurement on an Aβ sample containing Fluorescein at a concentration of 25 μM, instead of ThT. As well as in the Aβ(1-40) alone sample, changes in the scattering signal are not observed indicating that the increase of scattering in the presence of ThT is not barely due to the presence of small organic molecules in solution. Since the acquisition of Thioflavin T fluorescence signal gives information on the presence/growth of fibrils [20], the time evolution of ThT fluorescence intensity in the Aβ-ThT sample was acquired, in order to monitor in situ fibril formation during the aggregation kinetics. In Fig. 3.1-c) the ThT fluorescence behavior, simultaneously measured with the scattering signal showed in panel a), is reported. The combination of the two methods can be used to outline different features of the amyloid growth, and highlight the possible presence of interconnected aggregation mechanisms. As is observed from Fig. 3.1, in parallel with the first slight increase of scattering intensity ($t < t_0$) ThT fluorescence shows a first concave growth, followed by a linear temporal increase after t_0. It is worth to note that the first temporal behavior resembles the kinetics usually observed in seeded nucleated processes, when elongation

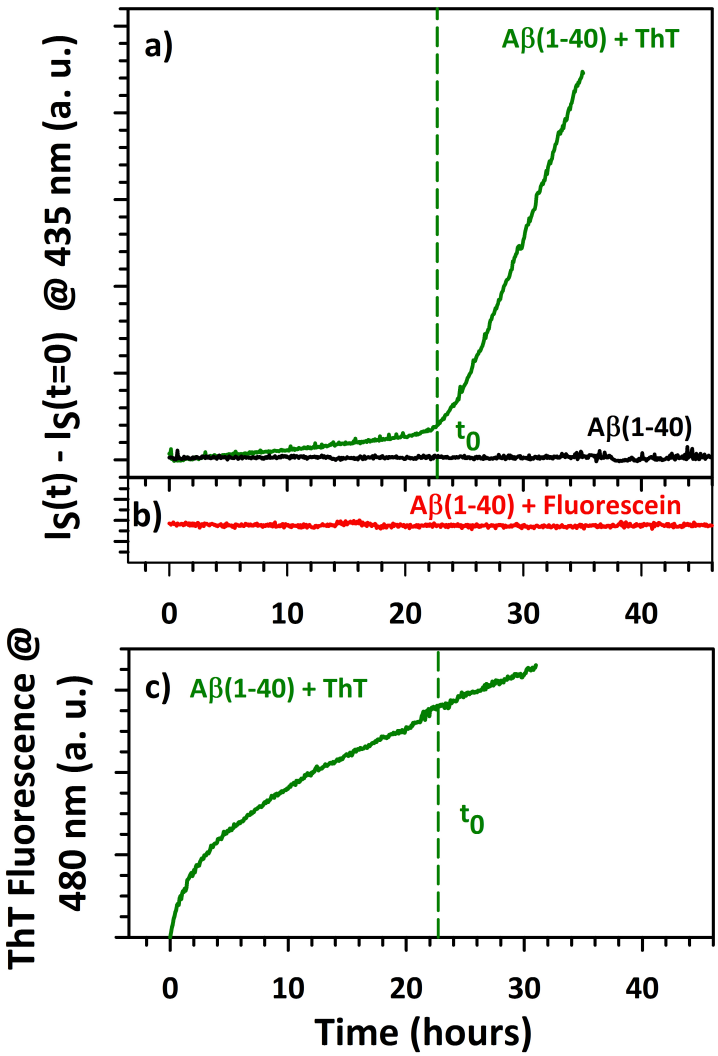

Figure 3.1: (a,b) Rayleigh scattering intensities at 435 nm as a function of time for samples incubated at 41 °C: Black line refers to the sample of Aβ(1-40) at a concentration of 150 μM; green line corresponds to a similar sample with the addition of 20 μM of ThT; red line corresponds to a similar sample with the addition of Fluorescein. (c) Fluorescence intensity at 490 nm as a function of time in the Aβ(1-40) sample containing 20 μM of ThT. The vertical dashed green lines represent the time of the abrupt increasing of the scattering signal (t_0) [187].

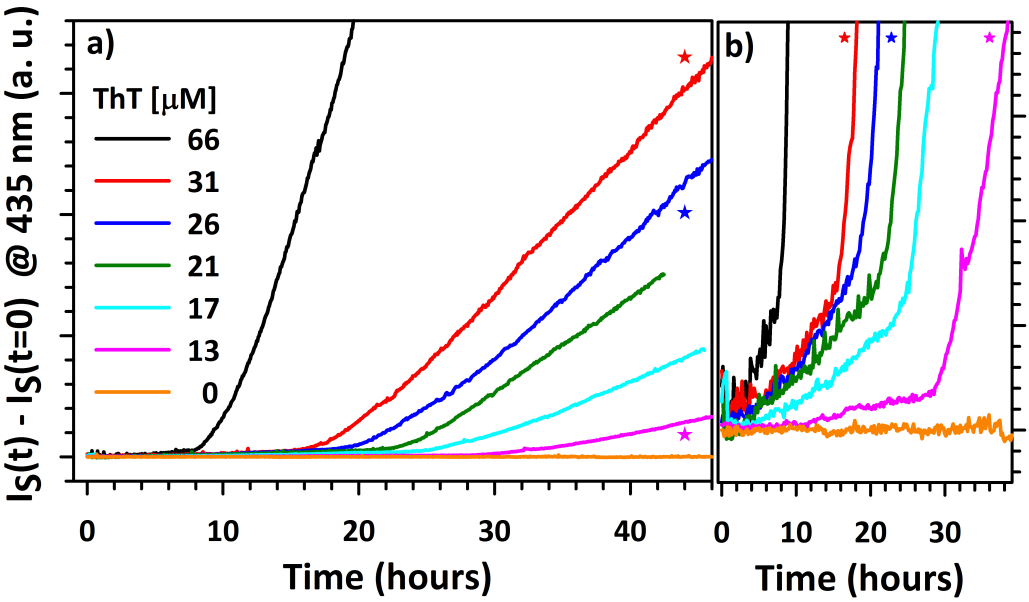

Figure 3.2: (a) Rayleigh scattering intensities at 435 nm as a function of incubation time for seven representative samples with different ThT concentrations. (b) Enlarged scale of panel a. For both panels, the curves labeled with stars refer to samples containing recrystallized ThT [187].

from polymer ends is more effective than primary nucleation [134] (see also Section 1.2). Since light scattering intensity takes into account the average size of all aggregates in solution, and ThT gives information only on amyloid aggregates, the experimental observation of a clear non correlation between these two observable has a quite great importance. Indeed, it indicates that more complex underlyning processes are taking place in solution.

In Fig.3.2 the time evolution of ThT fluorescence intensity in Aβ(1-40) samples at different ThT concentrations ([ThT]) in the range 0-66 μM, is reported. To guarantee that the observed effect of ThT was not due to the presence of impurities in the commercial ThT (purity of 65-75%), measurements (labeled with stars) were performed also with ThT purified by a recrystallization procedure where the proton-containing organic impurities and excess salts were removed. All measured scattering kinetics present the same biphasic trend (except for data with [ThT]=0): An almost linearly increase in the first hours and a subsequent abrupt growth after a time t_0 which depends on ThT concentration. Interestingly, as it is pointed out in Fig. 3.3-a), t_0 decreases as [ThT] increases. Moreover, the slope of the first increasing part of scattering data ($t<t_0$) increases linearly with [ThT] (see Fig. 3.3-b).

Fig.3.4 shows the behaviour of ThT fluorescence as a function of incubation time, normalized at 3 hours. In all samples the ThT fluorescence intensities grow almost monotonically as a function of time. In the first part the data perfectly overlap and after

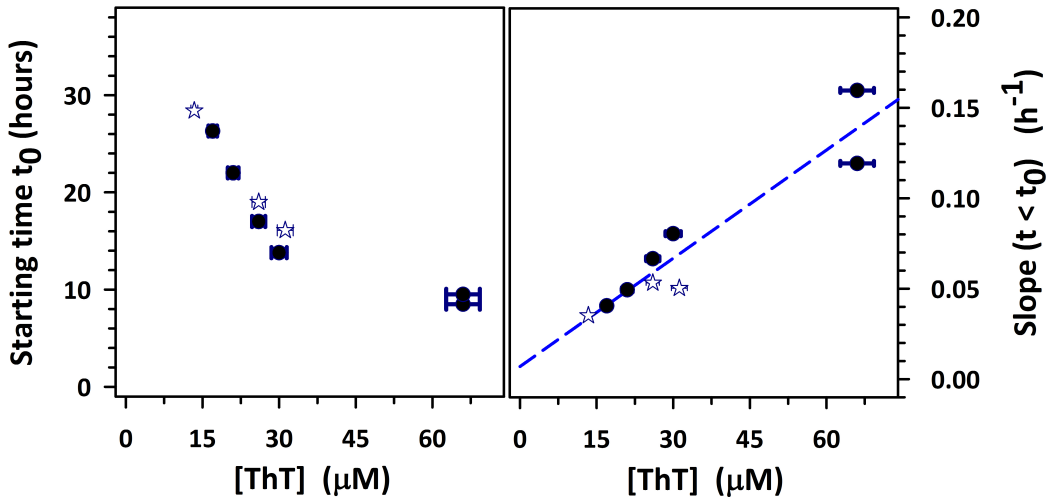

Figure 3.3: (a) Starting time t_0 as a function of ThT concentration. (b) Slope of the lag-phase ($t<t_0$) of scattering kinetics as a function of ThT concentration. The dashed line represents the best linear fit to the points. For both panels, stars refer to samples containing recrystallized ThT [187].

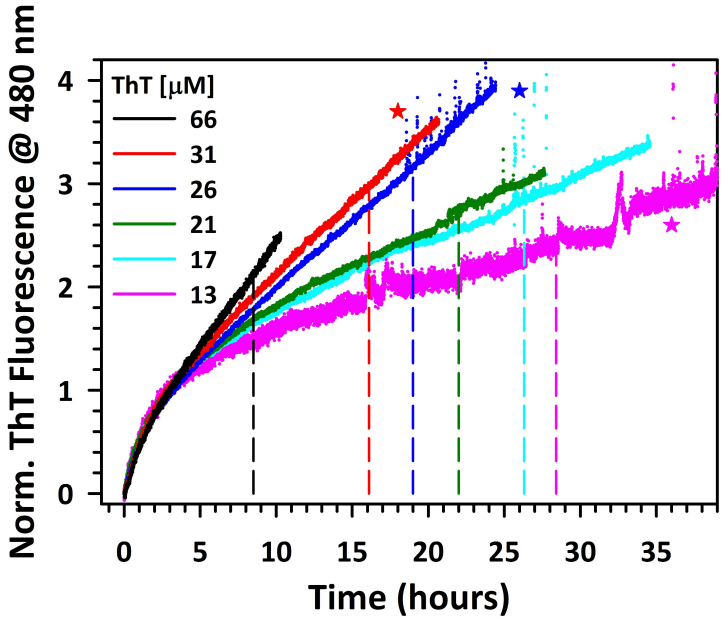

Figure 3.4: ThT fluorescence intensities at 490 nm normalized at 3 h as a function of incubation time for six representative samples with different ThT concentrations. The vertical dashed lines correspond to the times t_0 when corresponding signals of Fig. 3.2 show a dramatic scattering increase. Stars refer to samples containing recrystallized ThT [187].

about five hours the signal increase depends on [ThT].

These results clearly indicate that, in the experimental condition used, the Aβ(1-40) peptide does not aggregate except when ThT is present in the solution. Upon ThT addition Rayleigh scattering signal shows a typical biphasic kinetics (lag and growth phases). The rate of aggregate formation and the lag time, t_0, critically depend on ThT concentration and the progressive increase of ThT fluorescence indicates that structures which bind this dye are progressively formed. The fact that ThT addition to the Aβ samples favours its aggregation is confirmed by the experimental observation that the starting time t_0 approaches infinity as [ThT] approaches to zero (see Fig. 3.3-a). That is, the more the ThT concentration is increased the more the Aβ aggregation speeds up.

It is worthy to note that kinetics profiles and lag times, t_0, are repeatable. This does not clearly evidence the possible absence of a stochastic nucleation mechanism, especially for the observed concave first growth of ThT fluorescence kinetics resembling the typical behavior of seeded experiments [134]. Moreover, Rayleigh scattering as a function of time and ThT fluorescence signal time behaviour do not correlate. The first observable acquired as a function of time gives information about the overall aggregation process, while the second one only monitors fibril formation. This allows one to speculate the presence of different interconnected aggregation pathways, likely characterized by different intermediate species and different energy barriers[40]. On the basis of concave ThT fluorescence kinetics reported, and the surprising result of ThT triggered peptide aggregation process, it is possible to speculate that, already from the early time instants of kinetics, the formation of ThT-triggered Aβ seeds occurs. In order to investigate the presence of such species and their morphology, as well as to reveal possible differences between Aβ samples with and without the addition of the dye TEM measurements were carried out.

In Fig.3.5, representative transmission electron microscopy (TEM) measurements are reported for a 150 μM Aβ samples in the presence of 30 μM ThT (panel A, B) and in the absence (C, D) of ThT before incubation. The two samples were freshly prepared using identical protocols and then dried on the sample holder. Large quantities of aggregates are found in the sample where ThT is present (A and B), in particular a network of tiny aggregates possibly formed by elongated substructures is observed. On the contrary, samples where ThT is not present show very few aggregates of smaller size and with lower level of organization (C and D). Obviously, these measurements do not reflect actual conditions at the first stage of the kinetics, since samples underwent (identical) drying procedure before imaging, possibly favouring aggregation. However, it is worth stressing that, since the preparation protocol for the two samples is identical, any difference between them can only be ascribed to ThT. This means that, Fig.3.5A-D reveal for Aβ(1-40) an increased tendency to aggregate when ThT is present, even at room temperature. These measurements indicate that changes induced by the presence of ThT in solution are effective right after the sample preparation and before thermal treatment. To gain further insights into the different phases of the process, the morphology of the species possibly formed before and after thermal incubation at 41°C and during the lag phase were investigated by means of imaging techniques. Moreover, the peptide

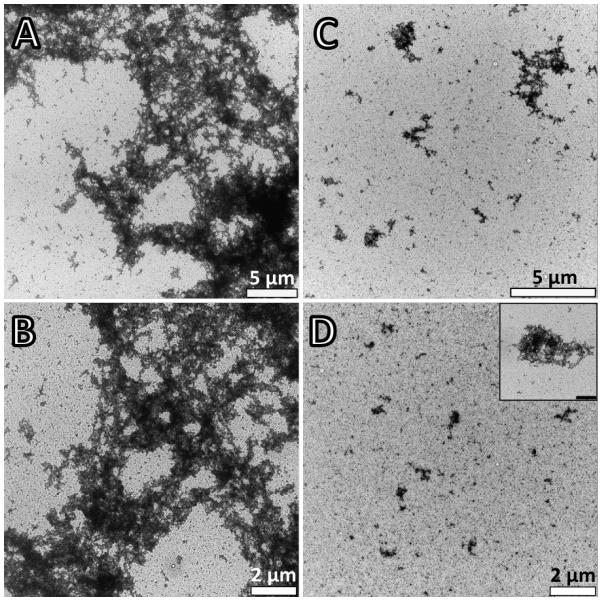

Figure 3.5: Panels A, B, C and D: Representative transmission electron microscopy measurements on Aβ(1-40) samples prepared dissolving the peptide in 50 mM sodium phosphate buffer, pH 7.4, with (A and B) and without (C and D) the addition of 30 μM of ThT. The inset scale bar in panel D is 2 μm.

secondary structure (with and without ThT, before and after thermal treatment) was analyzed by means of circular dichroism measurements. Aβ(1-40) samples after 6 hours of incubation at 41° in the presence of ThT were analyzed, as an example.

Fig. 3.6-A reports a representative single colour confocal microscopy measurement. ThT fluorescence signal (green pixels) is uniformly distributed in the sample (Higher fluorescence intensity at the border indicates higher local concentration of aggregates probably due to surface effects) suggesting the presence of small aggregate structures which bind ThT and whose size is below the instrumental resolution (200 nm). It is possible to quantify the size of these aggregates using Fluorescence Recovery After Photobleaching (FRAP) technique. Several FRAP experiments were performed in different areas of the samples showing a homogeneous presence in solution of small aggregates bound to ThT. In Fig. 3.6-B a typical profile of fluorescence recovery curve from a circular area of 10 μm-radius is reported. According to such fluorescence recovery, standard analysis using the Kapitza model [175] allows one to calculate a diffusion coefficient D = 29 $\mu m^2/s$. Similar measurements on different solution areas using bleaching regions (with radius from 5 to 30 μm) reveal the presence in solution of small aggregates (bound to ThT) with hydrodynamic radius ranging between 5 nm and 25 nm. In contrast with other standard techniques (e.g. light scattering or bulk ThT fluorescence), these measurements allow one to isolate the contribution of the population of molecules which bind to ThT and contribute to its fluorescence enhancement, determining also their size. These aggregates

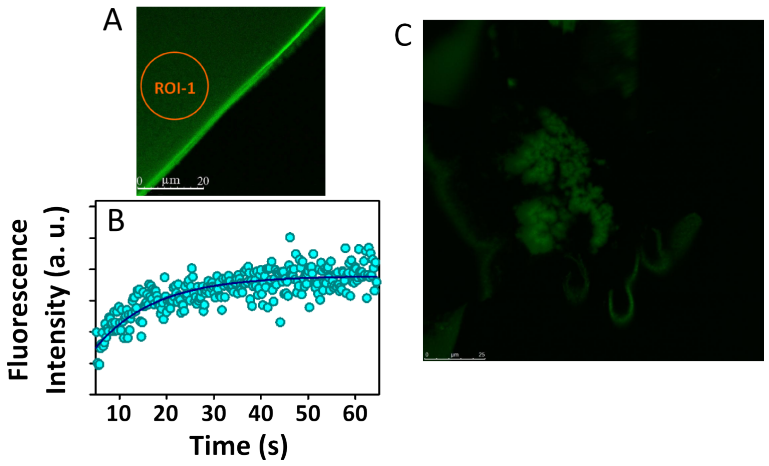

Figure 3.6: Panel A: 512X512 confocal image of the edge of a drop of an Aβ(1-40) sample prepared dissolving the peptide in 50 mM sodium phosphate buffer, pH 7.4, with the addition of 30 μM of ThT. This sample was incubated at 41 ^{c}ircC and images acquired during the first stage of the kinetics. Panel B: Typical Fluorescence recovery profile obtained from FRAP experiments on a circular region of 20 μm radius (ROI-1) on sample in panel A. Panel C: 1024X1024 confocal image representative of the Aβ(140) in Panel A after 45 hours of incubation.

of fibrillar nature also contribute to the first scattering growth observed in Fig. 3.1-C, Fig. 3.2 and Fig. 3.8-B and, importantly, they are uniformly distributed in the whole sample (within instrumental resolution). These structures can either 1) constitute seeds for further aggregation, 2) represent propagons [42, 194] that may further interact with non-fluorescent species or 3) be involved in an independent assembly pathway acting in competition with massive aggregation observed in the second part of the kinetics. In panel C a representative image of the Aβ-ThT sample incubated for about 45 h is reported. At this stage, the presence of large fibrils is clearly evident.

Fig. 3.7 shows representative FAR-UV CD spectra for two identical A*beta*(1-40) samples prepared dissolving the peptide in 50 mM sodium phosphate buffer, pH 7.4, with and without the addition of 30 μM of ThT. Spectra were acquired just after thermal incubation at 41 ^{c}ircC. Moreover, for comparison, the CD spectrum for the sample containing ThT after 45 hours of incubation is also reported. No significant differences are found in FAR-UV CD spectra between the sample containing ThT dye and the one without. Even after incubation, i.e. when large aggregates are present, the secondary structure is unvaried. This indicates that most of the peptide secondary structure remains in the (mostly disordered) initial state, both after ThT addition and thermal treatment.

As detected by fluorescence microscopy and revealed by ThT fluorescence as a function of time, aggregation kinetics in the presence of ThT leads to the formation of large aggregates able to bind the dye. However, it is possible to infer that only a small fraction of the sample is converted into fibrils, leaving a significant part of the molecule with a nearly unchanged secondary structure. In this case, as also commented by Arosio et

al. [194], the resolution of CD technique may not allow one for the detection of small fractions of aggregates/peptides with a modified secondary structure.

Fig. 3.8-A reports the time evolution of Rayleigh scattering growth as a function of time for three identical 120 μM Aβ (1-40) samples containing 33 μM ThT and incubated at 37 °C (green squares), 41 °C (blue squares) and 45 °C (red squares). Moreover, in Fig. 3.8-B shows ThT fluorescence intensity kinetics simultaneously acquired during the scattering measurements. Data are normalized to the ThT intensity value after 3 hours of incubation. This is mainly because the evaluation of the absolute values of fluorescence intensity at the different temperatures is not possible due to the dependence of the quantum yield on temperature [180]. However, the comparison of the temporal profile of fluorescence signals during isothermal experiments still provides significant information about the activation times and growth rates of the occurring processes.

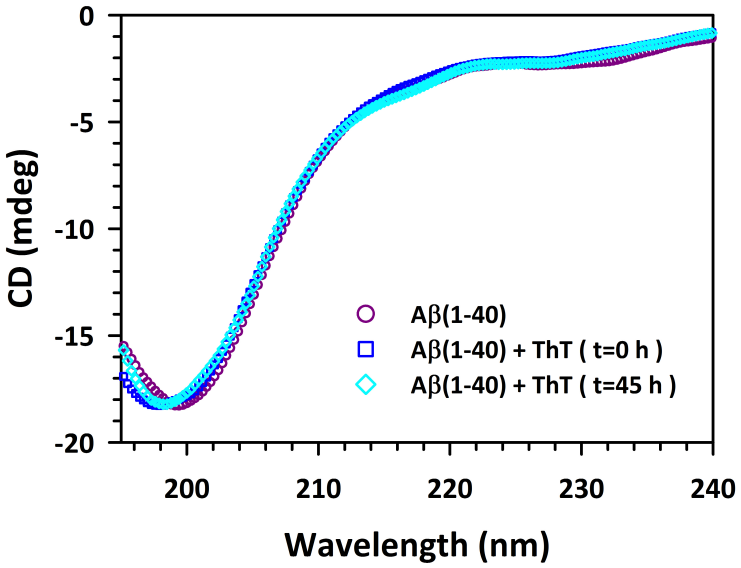

Figure 3.7: Far-UV CD spectra acquired at RT, before thermal incubation, for two A*beta*(1-40) samples prepared dissolving the peptide in 50 mM sodium phosphate buffer, pH 7.4, with and without the addition of 30 μM of ThT. The spectrum of the sample containing ThT after 45 hours of thermal incubation at 41 ^{c}ircC is also reported for comparison.

As shown in Fig. 3.1, the scattering signal shows a two-step kinetics with a high degree of reproducibility: a lag-phase (indicated by dashed lines) in which the signal slowly increases almost linearly, and a subsequent abrupt growth. The duration of the lag-phase and the slope of the signal growth in the second phase are critically dependent on temperature, being the whole process faster at higher temperatures. ThT fluorescence kinetics in Fig. 3.8-B again shows a first concave growth for $t<t_0$ (before dashed lines) and a second linear growth. Moreover, the absence of correlation between scattering and Thioflavin T signals as a function of the time is confirmed also at 37 °C and 45 °C.

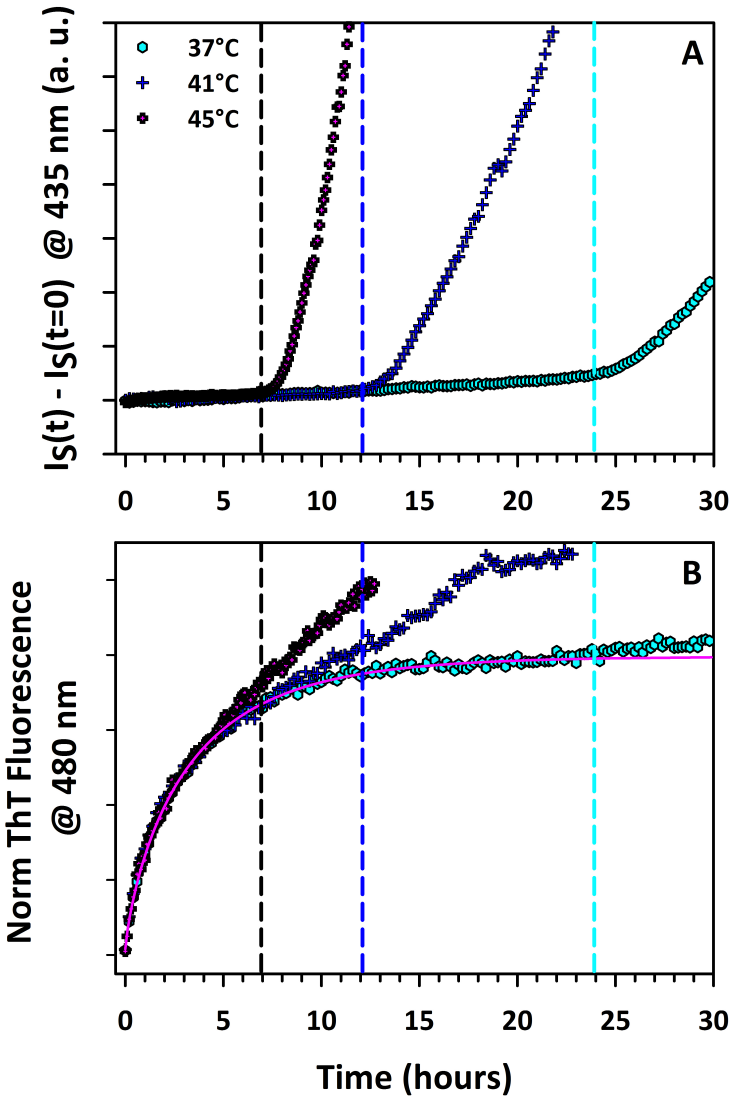

Figure 3.8: A) Normalized Rayleigh scattering intensity at 435 nm as a function of time for Aβ(1-40) samples at three different temperatures. The peptide was dissolved in 50 mM sodium phosphate buffer, pH 7.4, containing 33 μM of ThT, to a final concentration of 115 μM; B) ThT fluorescence intensity as a function of time simultaneously acquired to Rayleigh scattering. The fluorescence curves were normalized to the ThT fluorescence intensity value after 3 hours of incubation in order to compare the temporal profiles. Pink solid line indicates the stretched exponential fit (see text). Vertical dashed lines correspond to the end of the lag phase (t_0) for the three temperatures.

The occurrence of the second phase and its slope strongly depend on temperature. The kinetic ThT profile in the first phase overlaps for 6-7 hours not showing any significant temperature dependence. It is possible to infer that, in the observed conditions and at least in the early stages, ThT growth is characterized by the same kinetic profile for experiments at different temperature, and that only for the sample incubated at 37 °C a plateau is reached before the onset of the second phase, as detected by light scattering (Fig. 3.8-A).

Concave ThT fluorescence growth was previously observed in Aβ supramolecular assembly process characterized by a nucleation process occurring in the presence of seeds [134, 194]. The first concave growth in the kinetics at 37 °C can be fitted using a stretched exponential function y=$\{1 - exp\lfloor(-\beta * t)^{\gamma}\rfloor\}$ with $\beta \approx 0.37$ sec^{-1}, $\gamma \approx 0.72$ (pink line in Fig. 3.8-B). Stretched exponential function ($\gamma < 1$) can be used to provide a description of phenomena characterised by the presence of a highly heterogeneous sequence of events or species regulated by a distribution of activation energies. The stretched exponential function ($\gamma < 1$) has been also attributed to systems in which the growth of larger aggregates takes place primarily by reaction with smaller aggregates [208]. This is the case, for example, of aggregation reactions occurring in pre-seeded samples, in the particular case in which the process of monomers addition to the polymers ends prevail over nucleation of new aggregates or fragmentation [134]. In this case the free monomer concentration decrease with an exponential approach to equilibrium behaviour.

Rayleigh scattering as a function of time and ThT fluorescence signal time behaviour do not correlate. While the temporal behaviour of Rayleigh scattering gives information about the overall aggregation process, the second one only monitors fibril formation. As a consequence, the data shown clearly indicate the presence of at least two aggregation pathways with different temperature dependence. In particular, the first phase is not affected by a small increase or decrease in temperature. This could be associated with a conformational change, driven by specific interactions with ThT, but affecting only a small fraction of the sample, as suggested by CD experimental results. This conformational change could be a kind of "ThT-induced partial folding" which acts as rate limiting step for fibril formation, responsible for the concave ThT fluorescence signal growth.

The analysis previously presented qualitatively indicates the presence of a series of interconnected mechanisms, including a specific role for ThT, that needs to be clarified. The initial increase of the ThT signal is independent of the dye concentration and the temperature. Such enhancement in the fluorescence can potentially be attributed to changes in the secondary structure of the peptide in the presence of the dye. Indeed, as already said, it has been widely reported that this dye selectively binds to fibrillar structures, resulting in the enhancement of its quantum yield.

The dependence of the temporal features of the aggregation kinetics on the peptide concentration is not obvious. Fig. 3.9 shows the time evolution of Rayleigh scattering intensity (A) and ThT fluorescence intensity (B), acquired for five Aβ(1-40) samples with peptide concentration ranging between 25 μM and 150 μM, containing a constant concentration of ThT (28 μM), during isothermal incubation at 41 °C. Fig. 3.10 in panel (A) and (B) respectively report Rayleigh scattering and Thioflavin T intensity as a

function of time for three Aβ(1-40) samples incubated at 37 °C at a peptide concentrations of 50 μM, 115 μM and 160 μM.

The duration of the first phase (t_0) has a very weak dependence on the peptide monomer concentration, and no ThT fluorescence growth is observed for samples at peptide concentration lower than 65 μM during the whole incubation time. Only at higher peptide concentrations a monotonic concave ThT growth is observed, being larger at higher peptide concentration. This indicates that there is an interaction of the native peptide molecules with ThT, resulting in an increased quantum yield of fluorescence since the very early stages. This last evidence indicates that the protein-solvent-dye balance of different interactions is also regulated by peptide concentration. It is worthwhile to note that, in samples where ThT fluorescence intensity growth is not observed, Rayleigh scattering signal shows anyway a biphasic behavior, with the slope of the first linear growth not being significant. In samples at higher peptide concentration, the ThT growth is paralleled by scattering increase, with higher slope at higher concentration. This is more evident for 150 μM sample when the first 25 hours are considered. This suggests that the scattering species during this phase are of amyloid-like origin. The duration of the first phase remains unvaried when protein concentration is increased from 25 μM to 65 μM (i.e. when ThT fluorescence signal growth is not significant) and it is slightly enhanced when also a ThT fluorescence increase takes place. Specifically, in samples at peptide concentration of 100 μM and 150 μM the duration of the first phase increases by about 3 hours with respect to the 25 μM one. This is more evident for data obtained at 37 °C (Fig. 3.10) where the the first phase becomes shorter at lower concentration of peptide. All the different stages in the observed reaction are regulated by the rate constants and the number of multiple reacting species occurring at each point in time and on their relative concentrations and interactions, which can be regulated in different ways by external factors. This atypical peptide concentration dependence together with the high repeatability of the observed kinetics (generally observed in the case of templated processes) indicates a main role of ThT in the aggregation process. In fact, data in Fig. 3.9 and Fig. 3.10, in combination with the experiments reported in Fig. 3.2, suggest that peptide-ThT interaction dominates the aggregation process in such a way that the rate constants of the processes (formation of aggregates binding the ThT and massive aggregation) depend on the ratio between dye and peptide concentrations. This indicates that the self-assembly process is modulated by ThT-mediated interactions. If the process would have been regulated only by pure peptide-peptide interaction, the aggregation process would have occurred via stochastic nucleation mechanisms (i.e. low degree of reproducibility [46]) with a strong dependence of the lag phase on the peptide concentration [36, 44]. This is not observed in our experiments performed in quiescent conditions. On the contrary, we found that ThT presence in solution clearly alters the balance between monomer-oligomers-fibrils populations (Fig. 3.5), so that classical scaling laws for nucleated process are not followed. It is anyway worth noting that the growth of aggregates able to bind the dye is dependent on the concentration of peptide, and that, at higher peptide concentration, these structures undergo a further reorganization leading to the concave profile typical of assembly kinetics regulated by complex nucleation

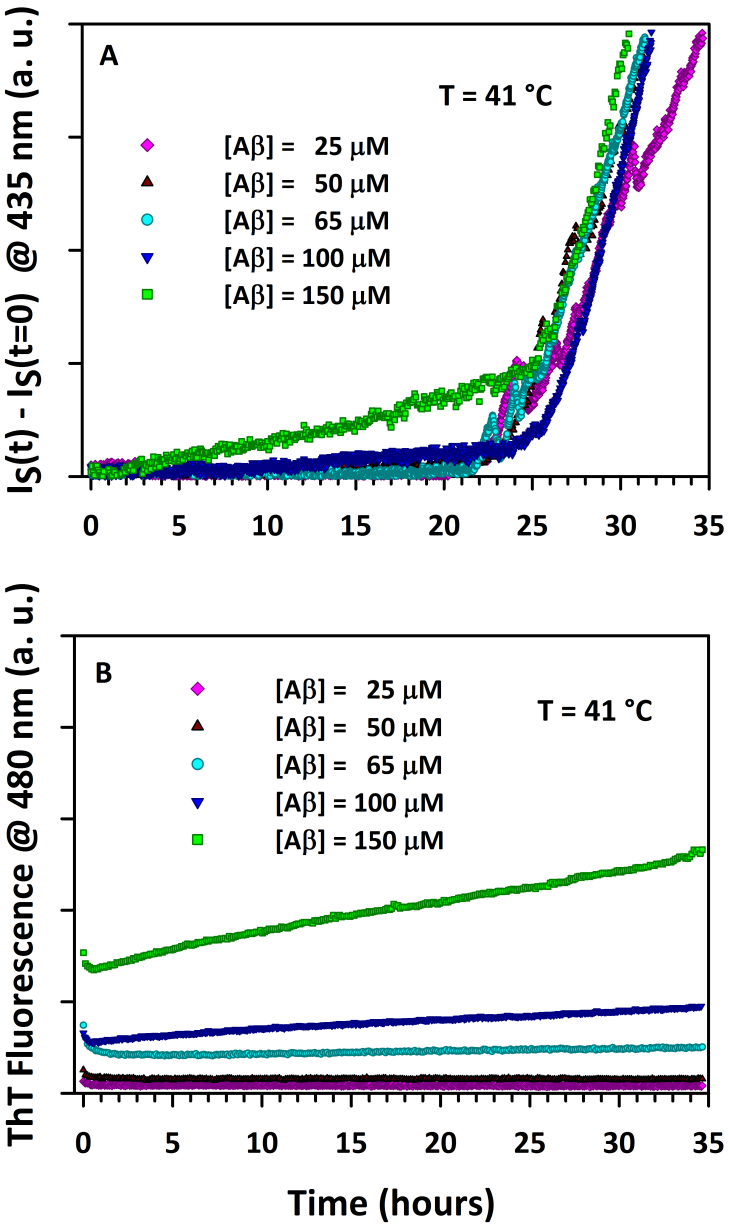

Figure 3.9: Panel A: Rayleigh scattering intensity at 435 nm as a function of time for Aβ(1-40) samples at different peptide concentrations, incubated at 41 °C. The peptide was dissolved in 50 mM sodium phosphate buffer, pH 7.4, containing 28 μM of ThT. Panel B: ThT fluorescence intensity as a function of time simultaneously acquired to Rayleigh scattering in panel A.

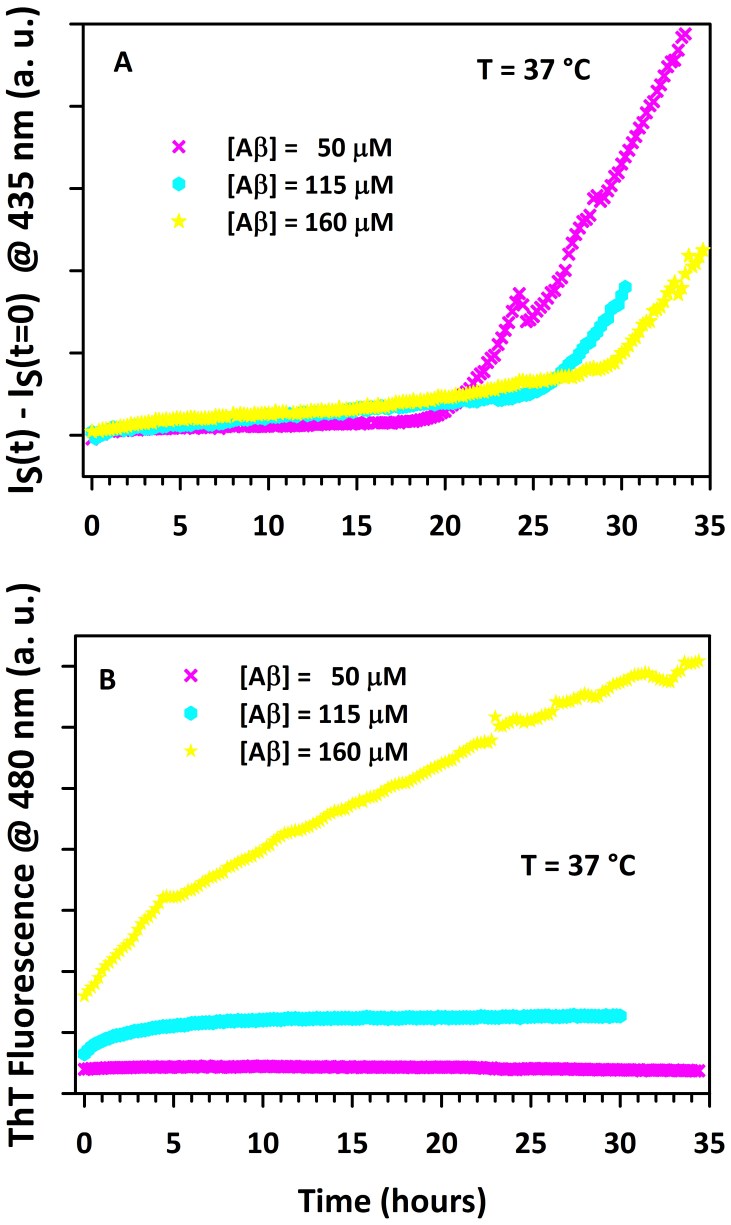

Figure 3.10: Panel A: Rayleigh scattering intensity at 435 nm as a function of time for Aβ(1-40) samples, incubated at 37 °C. The peptide was dissolved in 50 mM sodium phosphate buffer, pH 7.4, containing 33 μM of ThT. Panel B: ThT fluorescence intensity as a function of time simultaneously acquired to Rayleigh scattering in panel A.

mechanisms.

The selected approach gives detailed information on the time evolution of Aβ(1-40) fibrillation highlighting multiple aggregation pathways and different aggregate species. Indeed, data reported so far show that Aβ(1-40) aggregation process, in the experimental conditions investigated, occurs only in the presence of ThT and suggest that the observed supramolecular association involves at least two different aggregation mechanisms acting in competition. In the first step, small oligomers, which bind ThT, are formed (provided that a sufficient amount of ThT is present) via non nucleated polymerization mechanism, their number increasing as the peptide concentration rises. This process appear to be a rate limiting step for fibril growth, responsible for the observed concave ThT fluorescence kinetics. Furthermore, Rayleigh scattering data reveal that the abrupt aggregates growth, observed in the second part of the process (t> t_0), occurs only if the ThT is present in solution and may occur even in the absence of an increased ThT fluorescence growth. That is, the formation of small aggregates that bind to ThT is not directly linked to the occurrence of the massive aggregation at t> t_0, but the presence of the dye is a *condicio sine qua non* for the activation of the massive aggregation. This indicates that both processes are triggered by ThT but with different mechanisms and different peptide concentration-dependences. Moreover, the early formation of ThT-positive species may act in competition with massive aggregation observed at longer time. This effect is emphasized at lower temperature (Fig. 3.9, insets). At increasing peptide concentration, an enhanced population of ThT-positive aggregates is initially formed (Fig. 3.9) probably having as a direct effect a depletion of the peptide pool. This would in turn determine the apparent "reverse" dependency on the t_0 as a function of the nominal Aβ(1-40) concentration (Fig. 3.9) observed at 37 °C and barely visible at higher temperatures. Importantly, since such an effect is more evident at lower temperature, we can also conclude that the two aggregation pathways have different temperature dependencies, as suggested also by data reported in Fig. 3.8. Regarding the activation of the massive aggregation, we can infer that ThT presence templates the formation and the enrichment of a population of a reactive species during the lag-phase [209]. These species may constitute critical nuclei for further nucleation mechanisms. Alternatively, the "lag time" may be the time necessary for the activated species to cross a particular solubility limit. This is supported by the absence of clear peptide concentration dependence for this process [209], while a strong ThT concentration dependence is observed. This templated process could resemble the aggregation mechanisms followed by an ensemble of proteins in the presence of preformed seeds[134, 194].

Given the complex landscape just described, it would be an important piece of information to obtain insights into the way the dye interacts with a single peptide triggering the aggregation process. The effect of promoting Aβ(1-40) aggregation has to be feature of ThT molecules, since the addition of Fluorescein in the solution (an aromatic molecule with similar molecular weight as ThT) does not trigger any effects in the first 46 hours (see Fig. 3.1). Interactions between ThT and the peptide seem

somehow specific and the effect could be related to the symmetry of the molecule and specific side groups. Hydrophobic and electrostatic interactions between Aβ and ThT may favour supra-molecular association. In particular, aggregates formation may be due to the interaction between ThT aromatic rings and non-polar aromatic side chains of Aβ molecules in solution[164]. It should be noted that the same effect was not found in amyloid fibril formation from globular proteins [161], [210]. This may be explained taking into account that Aβ(1-40) is known to have a disordered structure in aqueous solution[174] so that various conformations are available at the equilibrium for a single molecule, giving to reactive groups in the chain the possibility of being exposed and to interact with correspondent groups of the ThT dye. The presence of ThT molecules in solution may induce conformational changes trapping a specific conformation prone to supra-molecular assembly, so that this effect could be considered as a possible example of template-dependent fibrillation [187]. This was shown for other small molecules able to stabilize different intermediates during the supra-molecular assembly modulating the fibrillation pathway and determining the final morphology of the aggregates [211–216]. In order to verify the validity of these hypotheses, allowing the investigation at atomistic level of the mechanisms involved in the interaction between Aβ(1-40) and ThT molecules, Classical MD simulations of a model system where one Aβ(1-40) peptide is dissolved in water together with 5 ThT molecules were performed. The rationale for this choice is to monitor in the behavior of a system where a sufficiently high number of ThT molecules are in position of interacting with the Aβ(1-40) peptide. It should be noted that, at variance with the situation simulated in MD, all the experiments previously presented were performed in conditions where the peptide concentration exceeds that of ThT. However, it has been emphasized several times that the time behaviour of Rayleigh scattering and that of ThT fluorescence do not correlate. Since, the first observable gives qualitative information on the average size of particle in solution, by means of its evolution one can monitor the overall aggregation process. On the other hand ThT fluorescence temporal behaviour monitors the formation of only amyloid fibrils. As a consequence multiple population of Aβ(1-40) molecules, both interacting and non-interacting with ThT, are seen to exist in solution. As a consequence, it is possible to conclude that the effective ThT-to-peptide concentration ratio is significantly higher than the nominal one.

Analysis of the effect of the presence of 5 ThT molecules on the peptide structure and conformation was performed starting from the Aβ(1-40) NMR structure ID:1IYT [217]. Data were compared to the case of Aβ(1-40) peptide in water and in the absence of ThT.

Fig. 3.11A shows the Root Mean Square Displacement (RMSD) as a function of time including only the peptide backbone atoms of the Aβ(1-40) (green points) and Aβ(1-40)-ThT (magenta points) systems along the 90 ns of the NpT simulation.

The RMSD is a measure of the configurational modifications [218] of the Aβ(1-40) structure as a function of the time with respect to a reference one. RMSD(t) is calculated according to the formula:

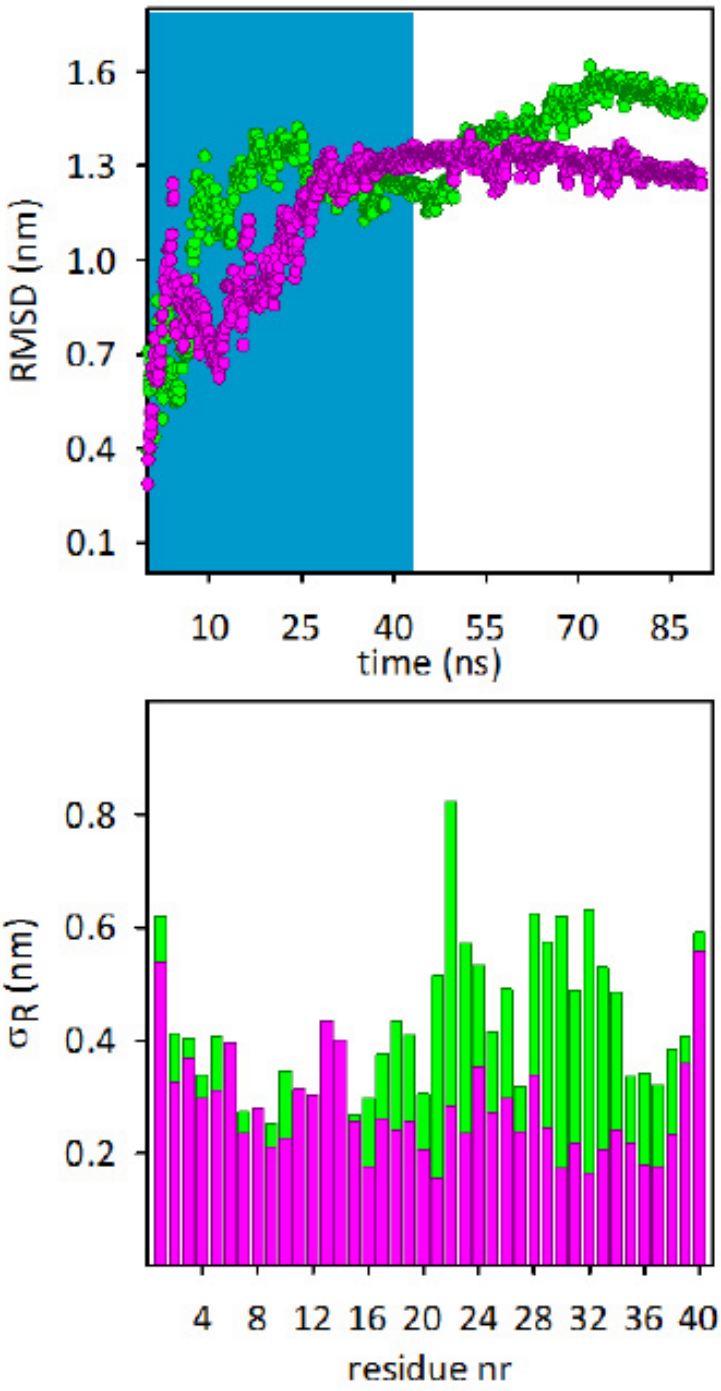

Figure 3.11: A) Aβ(1-40) peptide RMSD(t) as a function of time in the absence (green) and in the presence (magenta) of ThT molecules along the 90 ns NpT simulation. The cyan area indicates the initial equilibration time. B) Mobility of Aβ(1-40) residues. Colour code is as before. Only the last 60 ns of the simulation were used.

$$RMSD(t) = \left[\frac{1}{N} \sum_{i=1}^{N} |r_i(t) - r_i(t_0)|^2 \right]^{\frac{1}{2}} \tag{3.1}$$

where the coordinates $\{r_i(t), i=1,...,N\}$ in the equation are obtained after minimizing the expression in square parenthesis over the rigid roto-translations of the current atomic configuration. The coordinates at the initial time t_0 are those of the PDB structure from which MD simulations have been started. The time behavior of RMSD was computed by means of the g_rms [218] GROMACS' tool. As can be seen in the region between 30 ns and 90 ns, the value of RMSD as a function of time is quite stable in the presence of ThT (magenta) while in the absence of dye molecules (green) it reaches a plateau only in the last 20 ns (Fig. 3.11A). Moreover, in the first 30 ns (dark cyan area), the two systems display quite a different approach to equilibrium. In the absence of ThT the RMSD of the Aβ(1-40) system (green) moves rapidly to a plateau, while the Aβ(1-40)-ThT system (magenta) gradually approaches it. A comparison of the mobility of the two systems can be performed in terms of the quantity:

$$\sigma_R = \left[\frac{1}{T} \sum_{t} \frac{1}{N_R} \sum_{j} |r_j(t) - \langle r_j \rangle|^2 \right]^{\frac{1}{2}} \tag{3.2}$$

where T is the length of the MD trajectory, $\{ r_j(t), j=1,..., N_R \}$, are the positions of the N_R atoms belonging to the residue R and $\langle r_j \rangle$ represents the average position of each residue atom along the trajectory. For the computation of this quantity only the last 60 ns of the simulation were used. The behaviour of σ_R as a function of the amino acid residue position for the two systems of interest is displayed in Fig. 3.11B. The mobility σ_R is computed using the g_rmsf GROMACS routine. The kind of values taken by σ_R at the amino acid residue position clearly suggest that the interaction with ThT imposes constraints, reducing the size of the basin of the peptide accessible conformations. The 1-16 region does not show any significant mobility differences, while they are well visible in the 17-38 region. This latter includes the central hydrophobic cluster 17-Leu-Val-Phe-Phe-Ala-21, which is known to form the core of the minimum fibril forming sequence [219] that is considered crucial in the aggregation process. Indeed, planar aromatic interactions involving the two Phe residues were proposed to stabilize the fibrillar structure and to determine the main structure of the amyloid fibrils [220]. These modifications can be ascribed to the direct interaction of ThT molecules with specific Aβ(1-40) residues. To verify such hypothesis, Fig. 3.12 reports the measured time evolution of the distance between the Aβ peptide and each one of the 5 ThT molecules.

In particular, for each ThT molecule, the occurrence of an event where a ThT molecule approaches a specific Aβ(1-40) residue is reported as a function of the simulation time. Specifically, a given symbol is drawn in the plot if the center of mass of the n-th ThT

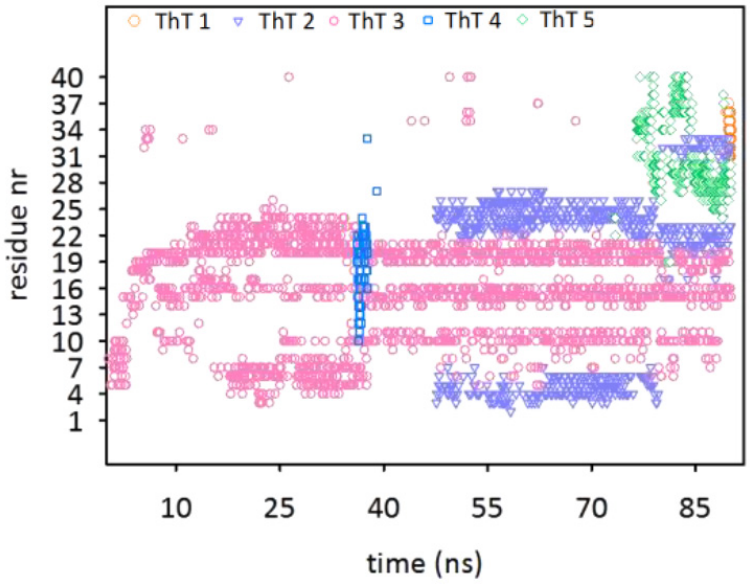

Figure 3.12: ThT molecules whose center of mass is within 8 $\AA$ from the Aβ(1-40) backbone atoms as a function of simulation time. Data are reported only for the ThT molecules directly approaching the Aβ(1-40) backbone atoms. (The Aβ(1-40) amino acid sequence is DAEFRHDSGYEVHHQKLVFFAEDVGSNKGAIIGLMVGGVV).

molecule is found within 8 $\AA$ from anyone of the Aβ(1-40) backbone atoms. As shown in Fig. 3.12 all the five ThT molecules approach the peptide. However, the time of permanence in the peptide vicinity is quite different. In particular, both ThT nr. 1 and nr. 4 approach the peptide for a very short time, the former at the end of the simulation trajectory and the latter in the interval 36-39 ns. ThT molecule nr. 2, instead, comes close the Aβ(1-40) peptide after about 48 ns and remains in its vicinity until the end of the simulation. Specifically, it interacts with the residues located at the two extremes of the fragment 3-26.

It is interesting to note that ThT nr. 2 interacts with an unstructured region by acting as a "lock" that imposes stable hairpin like structure. ThT molecule nr. 3 approaches the peptide backbone (fragment 5-25) immediately after the simulation starting and remains in this position for the whole simulation. As is clear from Figure 5, both ThT nr. 2 and nr. 3 are found to predominantly interact with aromatic residues. ThT nr. 2 interacts with the peptide in the region 3-6 namely with the sequence Glu-Phe-Arg-His, and 24-27 i.e. Val-Gly-Ser-Asn while ThT nr. 3 interacts very stably along the whole simulation time with the peptide in regions 10-11 (Tyr-Glu) and 19-21 (Phe-Phe-Ala), forcing these last residues in a more rigid conformation as shown in Fig. 3.11B. Finally ThT molecule nr. 5 is found in the vicinity of the peptide (28-40 region) in the last 14 ns close to the β-sheet structure. It cannot be excluded that this ThT molecule may possibly have a role in the peptide-peptide interaction. Indeed, the vicinity of the molecule to the β-sheet structure could favour intermolecular interactions [164] able to block the ThT molecule in

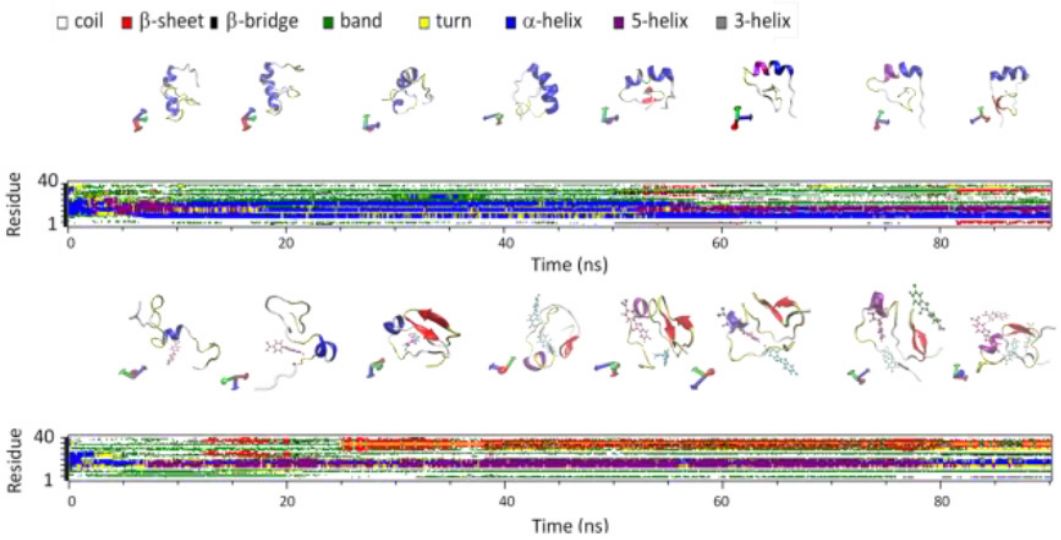

Figure 3.13: Aβ1-40 DSSP secondary structure as function of simulation time of Aβ(1-40) peptide in the absence (panel A) and in the presence (panel B) of ThT. The tridimensional structure of the most representative configuration of each 10 ns simulation are drawn as cartoons.

between two peptide molecules. Secondary structure evolution during the simulation was monitored using a protocol for the definition of secondary structure of proteins (DSSP) previously proposed [221] and implemented in GROMACS in the do_dssp tool. Fig. 3.13 shows DSSP results ad a function of the simulation time for the Aβ(1-40) peptide both in the absence (panel A) and in the presence (panel B) of ThT.

Above each DSSP panel, the photograms showing the most representative tridimensional structures of each 10 ns interval are drawn. As can be seen in the Aβ(1-40)-ThT system, the α-helix structure (blue) is immediately completely lost. At the same time, β-sheet (red) and turn (yellow) structures in the 28-38 segment, together with a 13-20 segment of 5-helix, appear and remain almost stable for the whole simulation time. We report in Table 1 the relative content of secondary structure as computed along the final 60 ns.

	Coil	β-Sheet	β-Bridge	Bend	Turn	α-Helix	5-Helix
Aβ	39%	2%	2%	19%	7%	23%	8%
Aβ-ThT	42%	10%	3%	20%	7%	4%	13%

It is worth mentioning here that the influence of ligands on the Aβ(1-40) aggregation propensity relies on their ability of altering the peptide secondary structure organization. As an example, ligands able to increase Aβ helix stability are found to reduce fibrils

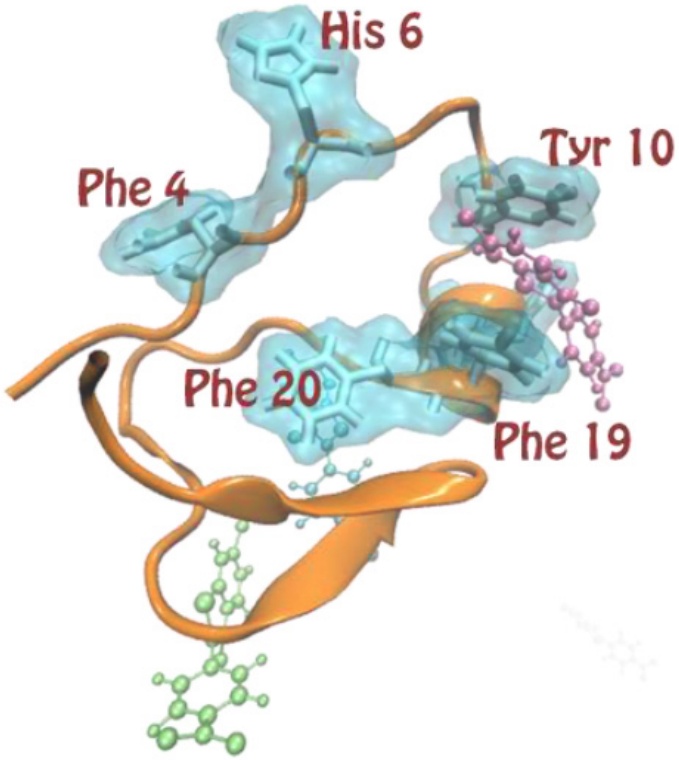

Figure 3.14: 3D structure of Aβ(1-40)-ThT system as obtained after 90 ns of equilibration during the Molecular Dynamic Simulations.

formation, whereas compounds with no effects on secondary structure do not seem to affect fibril formation [214]. The ThT-peptide interaction is found to "lock" the peptide in a closed chain conformation where the hydrophobic region 28-38 is forced to form a short β-sheet that may constitute a reactive site for peptides intermolecular interactions. In fact, looking at Fig. 3.12 and Fig. 3.13, it can be noticed that, when ThT nr. 3 starts interacting stably with Tyr10 and Phe 19, Aβ(1-40) assumes the β-sheet structure in the 28-38 region and do not lose this structure irrespective of how many other ThT molecules approach the peptide. The observed differences in Aβ(1-40) fold, together with the close interaction of ThT nr. 2 and Tht nr. 3 stabilizing an extended β-sheets structure in the first steps of the simulation represents a proof on the role of the dye in controlling the secondary structure of the peptide, likely enhancing the overall aggregation propensity of the peptide ensemble. It is worth noting that, at the end of the simulation, ThT nr. 5 and, for a reduced time, ThT nr. 1 approach the peptide exactly in the β-sheet region, neither interfering with ThT nr. 3 nor with the stability of the 28-38 secondary structure. A representative structure of the last 10 ns of simulation is reported in Fig. 3.14, where three ThT molecules are present.

As it is evident, the ThT nr. 3 templates protein conformation in a way that mimic

the usual configuration in which Thioflavin T molecules binds amyloidal structures [164]. The two aromatic rings in ThT nr. 3 are packed in between the aromatic rings of Tyr10 and Phe19. This configuration leads to the critical exposure of other aromatic residues which may take part in supra-molecular association. Although it is evident that simulation conditions are far by the experimental ones, MD data can elucidate the experimentally observed effects of ThT on Aβ(1-40) stability. The "locked" ThT-induced conformation contains a short β-sheet in the hydrophobic region and its subsequent reduced mobility may indeed change the energetic equilibria of the peptide ensemble. This could probably lead to favorable stacking interactions also due to the varied spatial organization of aromatic residues in the presence of the dye as well as to the directionality and the orientation of new intermolecular bonding. This would be in agreement with the tendency to aggregation experimentally observed by TEM imaging even at room temperature (Fig. 3.5) and the ability of ThT in inducing aggregation processes (Fig. 3.1 and Fig. 3.9) otherwise not occurring in its absence (Fig. 3.1). Specifically, it can be postulated that this "locked" conformation may favour intermolecular interaction both with "templated" molecules and unstructured monomers giving rise to the two different aggregation pathways experimentally observed. In particular, a direct interaction of such ThT-induced conformation could in principle give rise to the formation of the aggregates binding the dye, while interaction of such state with unstructured monomers could be at the basis of the observed massive aggregation. Moreover, MD simulation results are in good agreement with CD measurements. According to the MD data, the $[ThT/A\beta(1-40)]$ ratio should be extremely high to observe an overall conversion of secondary structure in the peptide ensemble (i.e. balance shifted towards Aβ(1-40)-ThT species). For the occurrence of potential artifacts, such high ratio can not be reproduced in the presented experiments. As a consequence, in the experimental conditions employed only a fraction of the Aβ(1-40) sample would be able to interact with ThT, so that the extent of the expected secondary structure changes cannot be appreciated by CD, being them within the experimental error.

3.2 Conclusions

As main and quite surprising result, experimental data reported in this chapter demonstrate that the *in vitro* Aβ(1-40) aggregation process, in the experimental condition investigated, is triggered by the fluorescent dye Thioflavin T. Indeed, it has been shown that this process occurs in the presence of the dye, while do not occurs in identical samples not containing it. Molecular dynamics simulations presented in this chapter show that, as a consequence of the ThT presence, a rigid Aβ(1-40) conformation can occur. This finding and experimental data suggest that the presence of such novel conformation shifts the balance toward a more aggregation-prone ensemble of molecules. Aggregation kinetics were monitored by means of Rayleigh scattering and ThT fluorescence measurements, simultaneously acquired as a function of time. The observation that the temporal evolutions of these two observables do not correlate leads to the conclusion that

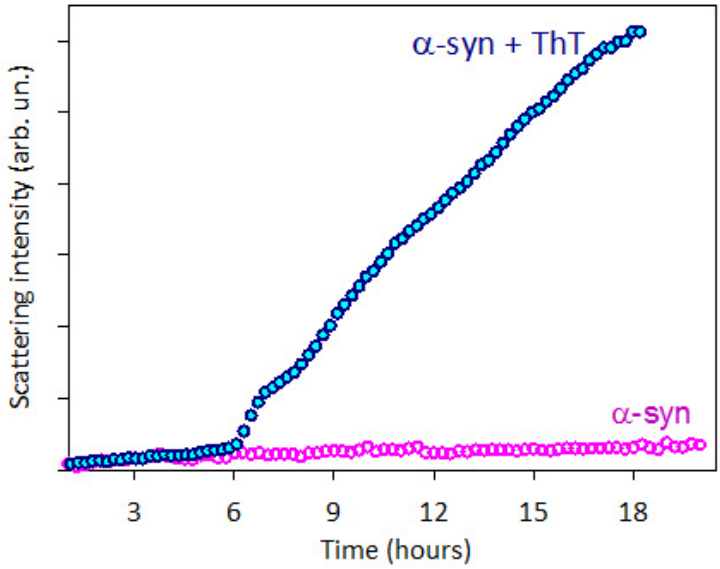

Figure 3.15: Rayleigh scattering signals as a function of time for two αSN sample at the concentration of 1.2 mg/ml, incubated at 50 °C. The protein was dissolved in 50 mM sodium phosphate buffer, pH 7.4, with (cyan) and without (pink) the addition of 20 μM of ThT. Rayleigh scattering remains constant for all the incubation time (about 20 hours) in the case of the sample non containing the dye, while a biphasic behavior is observed for the sample containing ThT. The reported kinetics are repeatable. The aggregation process of αSN is triggered by ThT.

the observed *in vitro* aggregation process is characterized by interconnected molecular mechanisms. Indeed, while ThT fluorescence as a function of time is related with the formation of only fibril aggregates, Rayleigh scattering gives qualitative information about the average size of particles in solution, and so about the overall aggregation process, whatever the type of aggregates.

More in detail, experimental data show the existence of at least two interconnected and competing pathways of aggregation, occurring in the presence of ThT, and leading to the formation of both aggregates binding the ThT and aggregates that do not bind the dye. Both processes are triggered by ThT but with different mechanisms and different peptide concentration-dependences. Moreover, the early formation of ThT-positive species may act in competition with massive aggregation observed at longer time. Further studies are needed to detect the intermediate steps and aggregated species involved in the observed supramolecular assembly.

This important result indicates that ThT can act as template to change the Aβ(1-40) random conformation in a β-aggregated form ready to form amyloid fibrils. This result could be really significant in the perspective that ThT may favor the conversion of possible toxic oligomers into less reactive amyloid fibrils, having strong implications in

the evolution of amyloid related aging processes in living organisms [24]. Moreover, the finding reported here constitutes a relevant warning for the scientific community, since in *in vitro* experiments the spectroscopic properties of this dye are widely used *in situ* to monitor fibril formation during protein aggregation processes, under the hypothesis that it not influence the aggregation processes [20–22]. As a consequence, this work further brings about the need of developing label-free techniques for a reliable quantitative investigation of the aggregation process for Aβ(1-40).

To conclude, it is worth to note that Aβ(1-40) peptide in close experimental conditions, differing from that reported in this study only for the incubation volume, it has been reported to aggregate trough heterogeneous nucleated mechanisms [125]. In the light of this observation, the results reported in this chapter give a clear example of how much strong can be the influence of the environment on IDPs conformation and aggregation propensity [17, 18]. This consideration is made even more significant by the fact that, in the same experimental conditions, an analogous effect was also observed for the other IDP object of this work, α-synulcein (see Fig. 3.15 and Chapter 4). This suggest a thermodynamic drive toward the stabilization of exposed groups in natively unfolded proteins by interaction with ThT specific groups. On the other hand ThT has been reported does not affect the fibrillation process of most globular protein, such as lys, Con A, BSA, HSA, BLG. This is essentially due to the fact that globular protein in their native state are characterized by a well folded conformation corresponding to a deep minimum in the intramolecular energetic landscape (see Fig. 1.1). This results in the hiding of hydrophobic and aromatic residues from the solvent and, as a general feature, made globular proteins less sensible to the environment than IDPs.

Chapter 4

α-synuclein aggregation process modulated by Trifluoroethanol

In the last decades several experimental works have highlighted that IDPs conformation and aggregation propensity can be strongly influenced by the environment [17, 18], much more than globular proteins. As reported in Chapter 1, this is essentially due to the fact that they are characterized by a shallow energetic landscape, being able to explore different conformational substates. This leads to exposition of aromatic and hydrophobic residues to the solvent.

The results reported above, establishing that Aβ(1-40) peptide aggregation process, in the reported experimental conditions, is triggered by interaction with the small molecule ThT, is a relevant example which well insert in this context. Indeed, it has been suggested that, as a general rule, if for ordered proteins the first critical step in fibrillogenesis is the partial unfolding, the earliest stage of fibrillation of IDPs is their partial folding [23]. This statement has been verified to be true in particular for αSN, whose fibrillation propensity is negligible in absence of partial folding [222, 223]. As a consequence, *in vitro* αSN fibrillation experiments are usually accomplished inducing its partial folding [26, 104], for example by means of mechanical agitation [22], or changing the pH of the solution [104]. It is well known that trifluoroethanol (TFE) is able to induce modifications in the 3D conformation of the chain by changing the equilibria in hydrophobic, ionic and hydrogen bonding interactions. This effect highly depend on TFE concentration. In particular, TFE-water mixtures are able to modulate αSN conformation on the basis of different TFE percentages. It has been shown that, at a protein concentration of 0.5 μM, in TFE-water mixtures, αSN samples at least three different secondary structure conformations in dependence of TFE concentration: an unfolded conformation, which is approximated by the 0% v/v TFE point; a partially folded structure populated at moderate TFE concentrations; and an α-helical conformation, which is approximated by the the 60% v/v TFE point [26]. The partially folded structure consists in a monomeric, partly α-helical, conformation, existing in equilibrium with the disordered conformation at low TFE concentrations, and with the α-helical rich state at high TFE percentages.

Aggregation kinetics performed in the presence of 15% v/v of TFE, monitored by means of CD measurements, show that the population of the partially folded structure strongly correlates with fibril production. In conclusion, the partial helical intermediate is on-pathway to the TFE induced formation of both the highly helical monomeric conformation and the fibrillar species [26]. At higher protein concentrations these intermediates are not observable due to the speeding up of the reaction. In this case the formation of β-oligomeric species is observed already from the early instants of time [26, 27]. Low or medium concentrations of TFE, leading to the population of partially structured states, enhance αSN fibrillation propensity, while the induction of helical rich states inhibits the aggregation process. It was shown that αSN folding in the presence of TFE can be attributed to a decrease in the solvent dielectric constant [27]. Such a decrease resembles the one of water at the water-membrane interface [224]. In this experimental work TFE-water mixtures at different TFE concentrations were used to monitor their effect on native αSN, to test αSN fibril stability and investigate different aggregates morphologies. Direct evidence on how αSN fibril stability strongly depends on TFE concentration, and how fibrils disaggregation can be obtained by simply reducing TFE concentration, is reported.

4.1 Results and discussion

4.1.1 αSN aggregation process modulated by TFE

Fig. 4.1 shows the typical circular dichroism spectra for seven identical samples of αSN at concentration of 1.2 mg/ml. The protein was dissolved in 50 mM sodium phosphate buffer, pH 7.4, containing different TFE concentrations. In absence of TFE, a shape typical of disordered structures, with a minimum at about 198 nm is obtained. In the presence of TFE at concentration higher than 7.5% αSN CD spectrum is characterized by a minimum at about 216 nm, typical of β-sheet structures, confirming αSN folding induced by TFE. Analogous results were previously ascribed to TFE-induced αSN oligomerization [26, 27]. Further increment of the TFE concentration leads αSN to mainly adopt the expected α-helical structure. These data clearly demonstrate how αSN secondary structure can be modulated by adding TFE to the solution.

In Fig. 4.2A the time evolution of Rayleigh scattering intensity as a function of time is reported for three identical samples of αSN at the concentration of 1.2 mg/ml. Measurements were carried out incubating the protein at 50 °C in 50 mM sodium phosphate buffer, pH 7.4 (black), in buffer with the addition of 20 μM of ThT (dark cyan) and in buffer plus 20 μM of ThT and 15% v/v of TFE (pink). Fig. 4.2B reports the time evolution of ThT fluorescence intensity as a function of time acquired together the scattering for the two samples containing the dye. Rayleigh scattering measurements qualitatively give information about the average size of particles in solution. As consequence, by means of the temporal behaviour of the Rayleigh scattering signal one can monitor the overall aggregation process. On the other hand ThT fluorescence signal acquired as a function of time only reveals the formation of fibrils [21]. From Panel A it is evident that, in absence

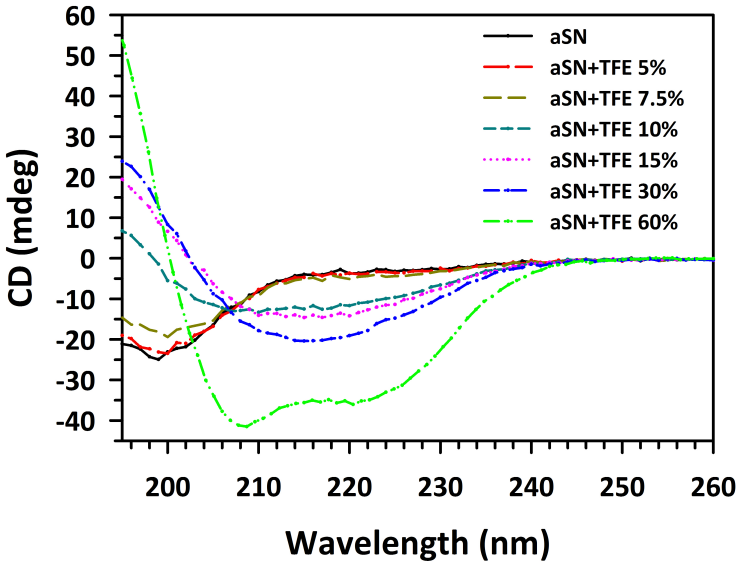

Figure 4.1: Far-UV CD spectra for samples of αSN dissolved in 50 mM sodium phosphate buffer, pH 7.4, with the addition of TFE at different concentrations, as indicated. All measurements were performed at RT.

of cosolvent and dye, the scattering intensity remains constant during the incubation time. This behaviour indicates that the average size of the particles in solution remains unchanged at least up to 20 hours. This is in line with several in vitro studies reported in the literature, pointing out that αSN fibril formation in aqueous solution, at physiological pH, and in quiescent conditions is highly unfavoured [222, 223]. ThT addition to the solution generates a biphasic scattering curve: the scattering signal remains unchanged during the first 7 hours of incubation. Then it undergoes a slow, almost linear, increase. This behaviour resembles that of nucleation processes, characterized by a lag-phase and a growth-phase. As in the case of Aβ peptide, this suggests a sort of template effect generated by the dye. However, the acquired ThT fluorescence intensity as a function of time remains constant during the whole incubation time. This means that ThT addition does not trigger the formation of fibrils, at least in the experimental conditions employed. Nevertheless, this is a quite important finding. Indeed, together with the main result of Chapter 3, it is a clear example of how much strong can be the influence of the environment on IDPs conformation and aggregation propensity [17, 18].

When TFE is present in solution Rayleigh scattering signal increases from the early time instants of kinetics. An almost monotonic increase is observed characterized by a first concave growth followed by a linear increase. Together with it, ThT fluorescence signal as a function of time presents the same behaviour. No lag phase is observed and a strong correlation between the time behaviours of ThT fluorescence and scattering growth exists. Also, it is important to highlight the fact that these kinetics are highly

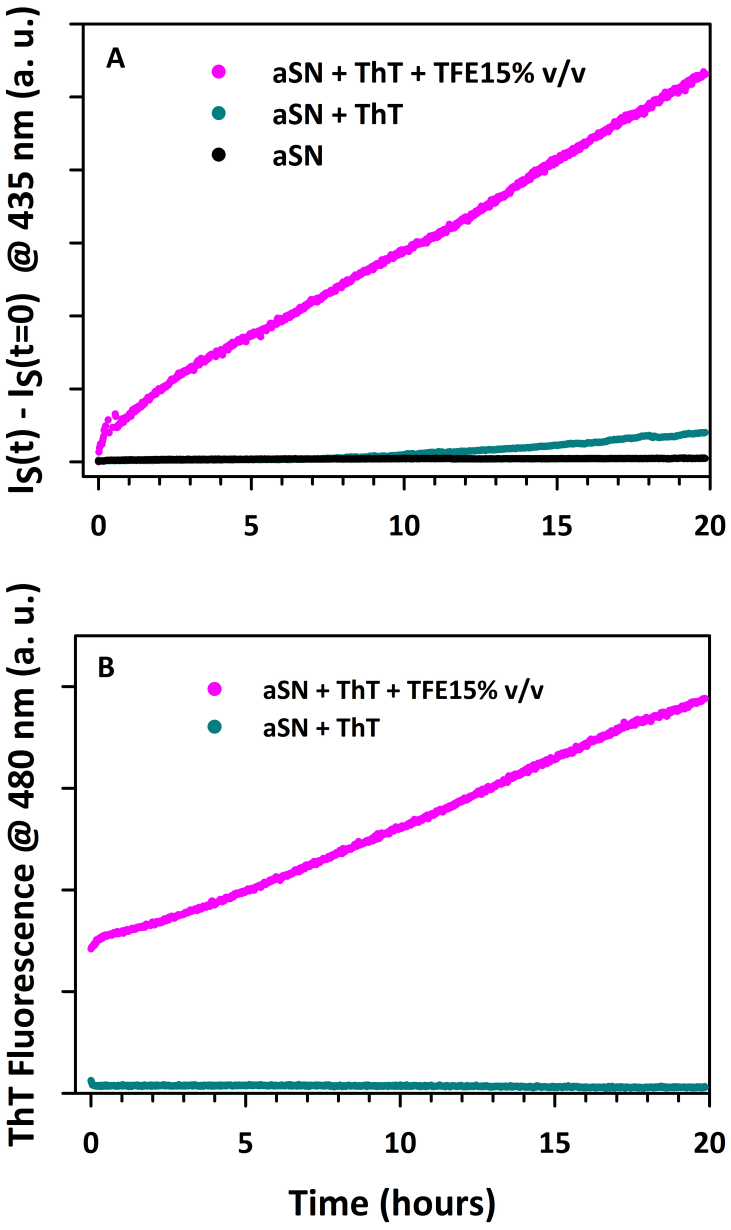

Figure 4.2: Panel A Rayleigh scattering as a function of time for three identical αSN samples at a concentration of 1.2 mg/ml. The protein was dissolved in 50 mM sodium phosphate buffer, pH 7.4, with and without the addition of 20 μM of ThT and 15% v/v of TFE, as indicated; Panel B ThT fluorescence simultaneously acquired to scattering for samples containing the dye. Samples were incubated at 50 °C.

reproducible. These observations suggest that supra-molecular assemblies capable of ThT binding are formed already at the earlier stages of aggregation kinetics and that oligomeric species are present in solution, forming larger aggregates as a function of time. Indeed, confirming this hypothesis, the absence of a lag-phase, the initial concave behaviour and the observed reproducibility remind seeded nucleation processes (see Section 1.2).

These data clearly show that TFE dramatically affects the aggregation process, more than ThT. Indeed, the biphasic behaviour completely disappears: there is not any lag-phase and after about 7 hours incubation, in correspondence of the beginning of the growth-phase observed for the sample without TFE, the scattering signal continues its linear growth. Moreover, the correlation between the two acquired signals observed in the presence of TFE leads to the conclusion that in this case all the produced species are ThT-positive. As a consequence, a complex process with one aggregation pathway activated by TFE and another activated by ThT can be excluded, at least within the experimental error. In view of these data, it is possible to conclude that the aggregation process of αSN in the presence of TFE is not influenced by ThT addition. In this case ThT plays the only role of a probe, monitoring fibril formation. This is another really relevant example of how IDPs aggregation processes can be strongly influenced by the environment. Indeed, it is possible to infer that ThT addition to the protein solution, not containing TFE, modulates αSN energy landscape in such a way that an amorphous aggregation pathway is triggered. However, TFE modifies the landscape more strongly, probably creating minima so deep and barriers so high that the addition of ThT is not more able to affect αSN aggregation process.

Fig. 4.3 shows small angle x-ray scattering (SAXS) data for two sample of αSN at a concentration of 1.2 mg/ml. The protein was dissolved in 50 mM sodium phosphate buffer, pH 7.4, with the addition of 20 μM of ThT and 15% v/v of TFE (pink) and without dye and alcohol addition (black). These data confirm the induction of oligomerization as a result of TFE addition, at a concentration of 15% v/v. Panel A shows the scattering intensity as function of the scattering angle ($q = 4\pi sin(\theta)/\lambda$, where λ is the x-ray wavelength and 2θ is the scattering angle); Panel B shows the relative Kratky plot for the two samples. From Panel A it is evident that the sample containing TFE presents an I(0) value higher than that of sample without TFE. This indicates the presence of larger species in the sample with TFE in comparison with the other one. Moreover, panel B clearly shows the typical shape of disordered conformation in absence of TFE, while a bell shape, typical of globular proteins, for the sample containing alcohol [75] (see also Section 2.1.3). This means that αSN is characterized by a high degree of flexibility when dissolved in buffer at physiological pH and in absence of co-solvents, while the presence of TFE forces αSN into a structured conformation.

In summary, data in Fig. 4.1, Fig. 4.2 and Fig. 4.3 show that the aggregation process originates from oligomeric species having a β-sheet secondary structure and able to bind the dye. This explanation agrees with the fact that the aggregation process in the presence of TFE (pink data set in Fig. 4.2) is reproducible.

Fig. 4.4 reports two photon excitation microscopy measurements representative of

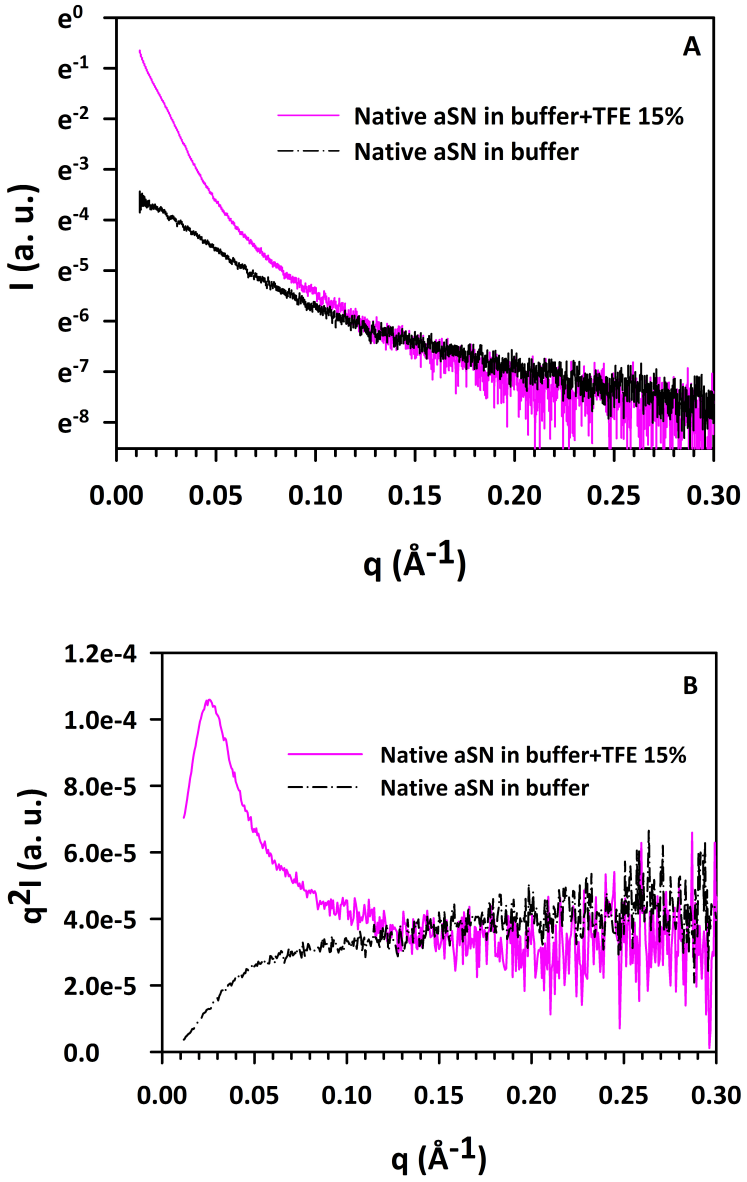

Figure 4.3: Panel A SAXS data for two samples of αSN, dissolved in 50 mM sodium phosphate buffer, pH 7.4, with and without the addition of 20 μM of ThT and 15% v/v of TFE; Panel B Kratky plot of A. Measurements were acquired at RT.

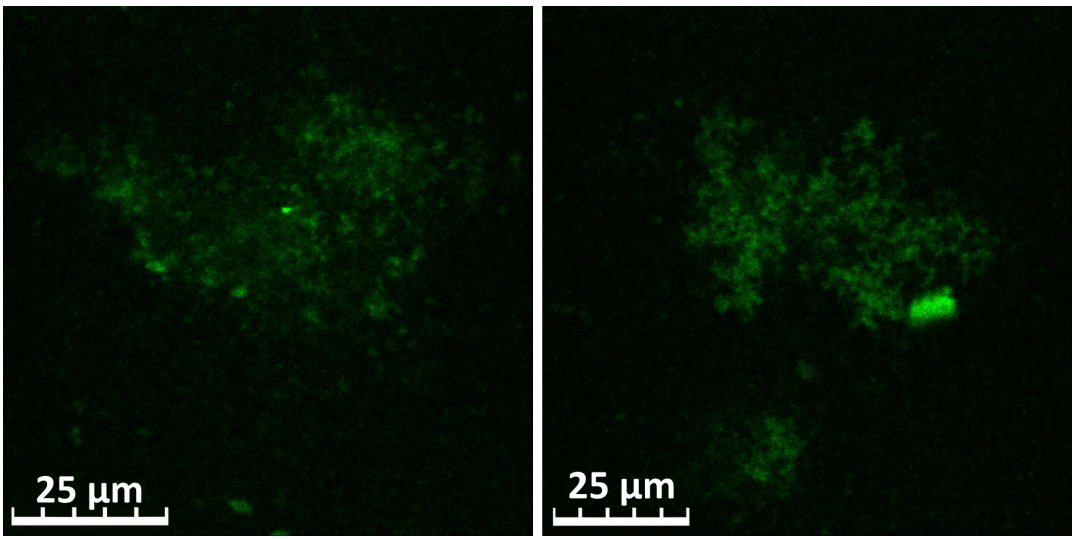

Figure 4.4: Two photon excitation microscopy measurements representative of αSN samples at a concentration of 1.2 mg/ml. The protein was dissolved in 50 mM sodium phosphate buffer, pH 7.4, containing 20 μM of ThT and 15% v/v of TFE. Samples were incubated at 50 °C for about 27 hours. Microscopy measurements were performed right after thermal incubation and cooling down in a ice-water bath.

αSN aggregates, obtained incubating the samples at 50 °C for about 27 hours. The corresponding Rayleigh scattering and ThT fluorescence measurements, acquired as a function of time in order to monitor the aggregation kinetics, are shown in Fig. 4.2 (see pink data sets). αSN was dissolved in 50 mM sodium phosphate buffer, pH 7.4, containing 20 μM of ThT and 15% v/v of TFE. The protein concentration was 1.2 mg/ml. Since in these measurements the revealed signal is the fluorescence of the dye ThT, one can conclude that the observed green structures are large fibril clusters surrounded by "grainy" fibrillar aggregates. Indeed, ThT is usually employed to reveal the *in vivo* or *in vitro* presence of fibrils.

4.1.2 αSN fibrils stability modulated by TFE

In this section results about the stability of the already formed αSN fibrils, as a function of TFE concentration, are reported. This aspect is really important to take into account since nowadays fibrils are considered as reservoirs of actual cytotoxic species, which can be released if fibrils stability is modified [13].

αSN fibrils were produced dissolving the protein in 50 mM sodium phosphate buffer, pH 7.4, containing 20 μM of ThT and 15% v/v of TFE. Samples were incubated at 50 °C for about 27 hours. Aggregation kinetics were monitored by means of Rayleigh scattering and ThT fluorescence measurements. The typical scattering and ThT fluorescence signals as a function of time are reported in Fig. 4.2, panel A and B (pink data sets) (see above

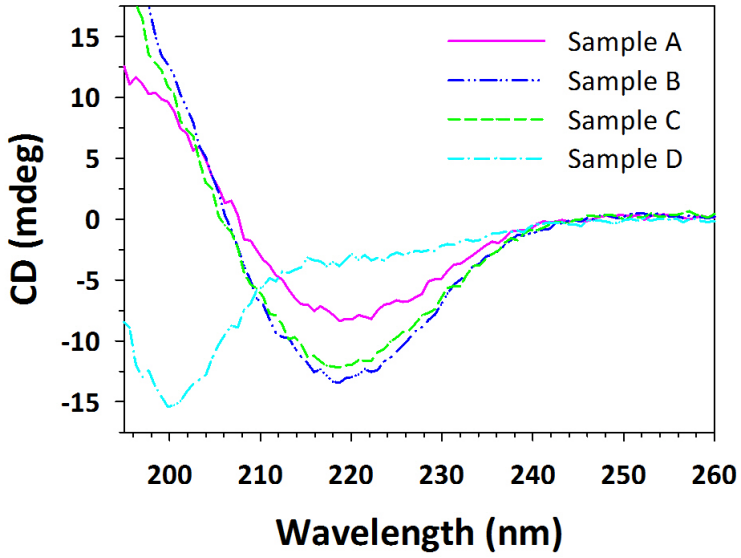

Figure 4.5: CD spectra for four samples containing αSN aggregates formed in the presence of 15% v/v TFE, diluted in 50 mM sodium phosphate buffer, pH 7.4, with the TFE adjustment to final concentrations of 15% v/v (A), 30% v/v (B), 60% v/v (C) and 1.5% v/v (D). All the measurements were acquired at RT.

for the description). After the incubation samples were cooled down, and split in two parts, one aliquot was left as it was and the other one was treated as shortly described in the following. The treated aliquot was obtained by spinning down one part of the sample. Then the pellet was diluted 1:10 in sodium phosphate buffer containing TFE, in order to obtain samples at different TFE concentrations: A) 15% v/v i.e. unchanged compared to aggregation conditions, TFE concentration at B) 30% v/v and C) 60% v/v and D) 1.5% v/v. In Fig. 4.5 the CD spectra of the four samples A, B, C, D are reported. Samples B and C are characterized by an intensified minimum, at the same position as for sample A. This suggests a further increase in the relative content of β-strand secondary elements at increasing TFE concentrations. It is worth nothing that this effect cannot be ascribed to partially structured conformation induced by TFE on not-aggregated αSN, (possibly present in the sample). In fact the spectrum referring to sample C (60% TFE) is in stark contrast to the spectrum recorded in similar experimental conditions for non thermally treated αSN samples (Fig. 4.1), which shows the typical shape assigned to α-helix conformation. This is further emphasized by a control CD experiment on supernatant from spun down samples, which do not show any detectable signal. It can be hence ruled out that the suspension of the fibrils into increased concentrations of TFE causes dissolution. Data in Fig. 4.5 indicates that changes obtained by increasing TFE concentration are related to the increase of order in the β-sheet structures within the fibrils. On the contrary, upon dilution to 1.5% v/v TFE concentration, CD spectra show

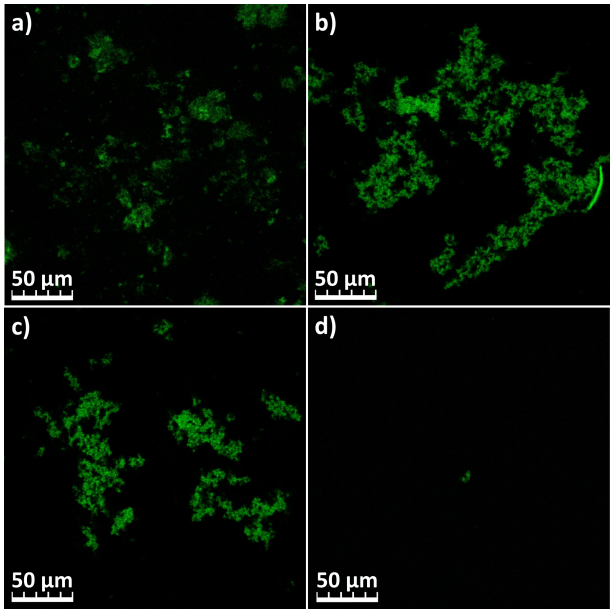

Figure 4.6: Representative two-photon excitation fluorescence microscopy measurements for samples containing αSN aggregates diluted in 50 mM sodium phosphate buffer, pH 7.4 and stained with ThT (green in images), at different TFE concentrations of 15% v/v (A) (panel a)), 30% v/v (B) (panel b)), 60% v/v (C) (panel c)) and 1.5% v/v (D) (panel d)).

a strong modification of the secondary structure of the aggregates, with negligible β-sheet content in favour of a partially random coil conformation, thus suggesting dissolution of the fibrils.

With the aim of further investigating and confirming the effect of TFE concentration on the stability of aggregates, two photon excitation microscopy measurements on the four samples are reported in Fig. 4.6. Data in panel a) clearly show that large fibril clusters surrounded by "grainy" aggregates are present in sample at 15% v/v TFE. These aggregate present the same morphology of that reported in Fig. 4.4, performed on the sample right after thermal incubation. This last consideration indicates that spinning down the sample and diluting it in the same buffer do not modify sample characteristics, at least under the instrument resolution ($\sim$200 nm). Images obtained at 30% or 60% v/v TFE concentration (panel b) and panel d)), in exactly the same conditions, show similar morphology but a higher level of supra-molecular organization of fibrils, corroborating the stabilization of the fibrillar state as suggested by the CD data. Moreover, aggregates appear brighter, possibly indicating that ThT quantum yield is higher at these TFE concentrations, i.e. a different arrangement in the local environment around the dye. The sample at 1.5% v/v TFE concentration shows a reduced and almost vanishing content of ThT-positive aggregates, in line with CD measurements in Fig. 4.5.

Globally, results indicate that TFE content regulates αSN conformation, affecting β-sheet content and inducing changes in the aggregate secondary structure, overall

macroscopic morphology or, alternatively, partial/total dissolution. It is worth noting that the occurrence of changes in aggregate secondary structure which does not destroy the supra-molecular assemblies is unlikely, since the decrease of the β-sheet signature in the CD experiment is coupled with an almost complete disappearance of signals in the microscopy images.

4.1.3 αSN aggregation process as a function of TFE concentration

In this section some interesting, although preliminary, results are shown, highlighting that incubation of αSN samples containing different TFE concentrations leads to different aggregate morphologies. Samples were prepared dissolving the protein in 50 mM sodium phosphate buffer containing 20 μM of ThT. Moreover, TFE was added to the two solutions at the concentrations 15% v/v or 1% v/v, respectively. Samples were incubated at 50 °C for about 27 hours. Fig. 4.7 and Fig.4.8 show two-photon excitation microscopy measurements representative of two αSN aggregates. The measurements were performed rather after incubation and cooling down of samples in a ice-water bath. Aggregates

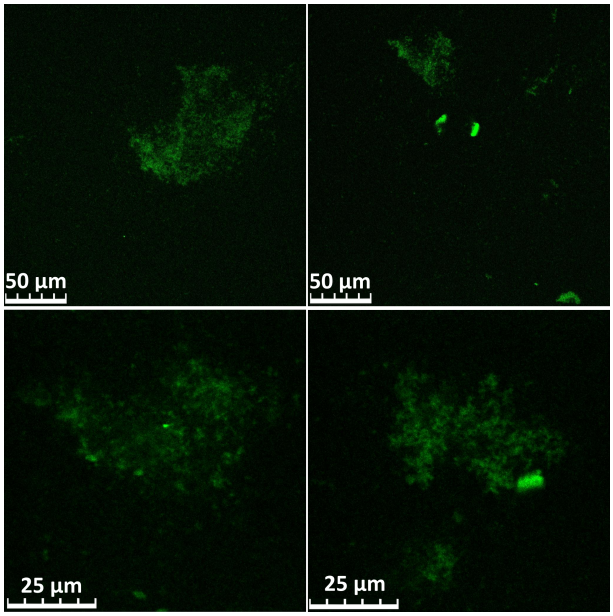

Figure 4.7: Two photon excitation microscopy measurements representative of αSN samples at a concentration of 1.2 mg/ml. The protein was dissolved in 50 mM sodium phosphate buffer, pH 7.4, containing 20 μM of ThT and 15% v/v of TFE. Samples were incubated at 50 °C for about 27 hours. Microscopy measurements were performed right after thermal incubation and cooling down in a ice-water bath.

obtained in the presence of 15% v/v of TFE appear as large "curly" fibril clusters surrounded by "grainy" aggregates. Incubation at lower TFE concentration leads to the formation of thinner straight fibrils and fibril clusters. Surprisingly, there are also

few aggregates in which fibrils are arranged radially with respect to a brilliant area, usually named precursor. These particular 3D fibril arrangements are usually referred with the term of spherulites. It is matter of debate if precursors originate from a random aggregation, with consequent fibril growth outward from the precursor [225] or if growth of the central part is due to fibril collapse [141]. However, it is generally accepted that spherulites grow from precursors by sequential addition of protein molecules rather than from preformed fibrils [11]. Moreover, Fig. 4.8 (top, left) shows a lot of brilliant spherical aggregates which seams to be spherulite precursors. This hypothesis is confirmed by two-photon excitation microscopy measurements reported in Fig. 4.9, representative of an identical sample incubated for about 45 hours. It is evident that after longer incubation time this kind of aggregates disappear and bigger and thicker spherulites appear, beside to a large network of thin free fibrils.

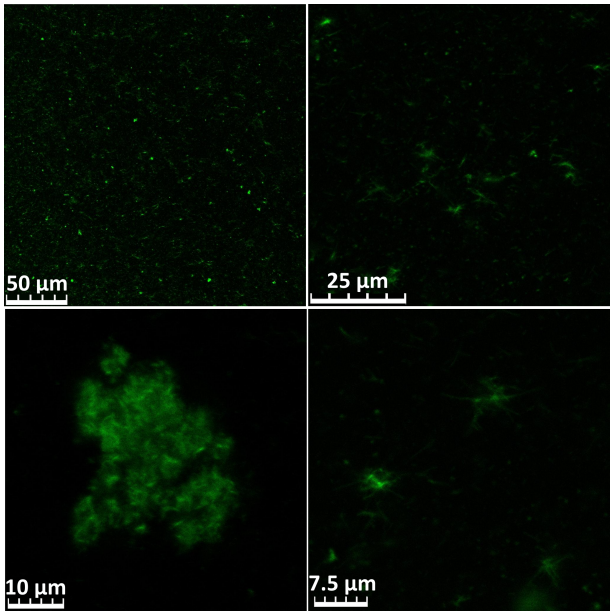

Figure 4.8: Two photon excitation microscopy measurements representative of αSN samples at a concentration of 1.2 mg/ml. The protein was dissolved in 50 mM sodium phosphate buffer, pH 7.4, containing 20 μM of ThT and 1% v/v of TFE. Samples were incubated at 50 °C for about 27 hours. Microscopy measurements were performed right after thermal incubation and cooling down in a ice-water bath.

These, although preliminary, are really interesting results since *in vitro* formation of αSN spherulites have never been reported in literature, although a recent study demonstrated for the first time their existence in cellular environment [143]. Moreover, these data show how changing TFE concentration leads to the formation of different supramolecular aggregates. This last being a quite important finding because it highlights the importance of protein environment in the aggregation processes. At the present state it is only possible to speculate that the mechanisms through which TFE is able

to modulate aggregate morphology are driven by electrostatic interactions. Indeed, it is known from the literature that 3D organization of protein aggregates is driven by electrostatic forces [80], and that TFE at different concentrations, changing protein-protein electrostatic interactions, may be able to modulate them. In order to understand the mechanisms involved and highlight the possible presence of interconnected aggregation pathways, it could be really important to investigate αSN aggregation kinetics in samples containing different TFE concentrations. For all these reasons this study is definitely worth to be deepened.

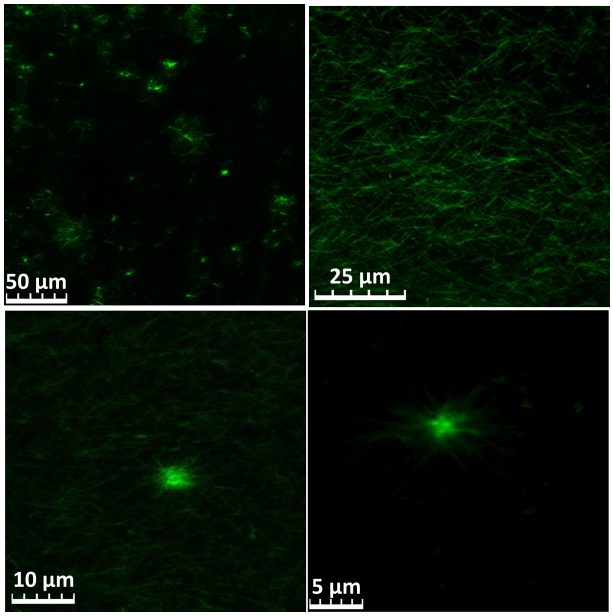

Figure 4.9: Two photon excitation microscopy measurements representative of αSN samples at a concentration of 1.2 mg/ml. The protein was dissolved in 50 mM sodium phosphate buffer, pH 7.4, containing 20 μM of ThT and 1% v/v of TFE. Samples were incubated at 50 °C for about 45 hours. Microscopy measurements were performed right after thermal incubation and cooling down in a ice-water bath.

4.2 Conclusions

This chapter draws the attention on αSN aggregation kinetics in relation to the environment. In line with the literature, data confirm that the initial αSN conformation and aggregation state is strongly affected by the addition of TFE. This alcohol affects protein secondary structure and stability on the basis of its concentration [26, 27]. It acts changing protein solvation properties, but also lowering the dielectric constant of the solution [25]. As a result, for example, protein-protein electrostatic interactions are changed.

Importantly, data univocally show that αSN aggregate structure and conformation

can be tuned by changing the environmental conditions. In particular preformed fibrillar structures brought at TFE concentration higher than the ones employed in the aggregation kinetics, appear to be stabilized and show the tendency in forming larger macroscopic clusters. Changes in the environment induce an increased ThT quantum yield and changes towards an enhanced organization at the secondary structure level with a more pronounced β-sheet content. These conditions thus favour both intra-fibril structure, via ordering of hydrogen bonding in the β-sheets, and inter-fibril structure, via increased clustering. Interestingly, when the TFE concentration is reduced, the β-sheet structures almost completely dissolve and micron-scale fibrils disappear.

Moreover, it is worth to note that αSN aggregation kinetics performed in the presence of a low TFE concentration lead to the formation of αSN spherulites. This is a quite surprisingly finding because it has never been reported for αSN in vitro studies. Anyway, since a recent study demonstrated for the first time their existence in cellular environment [143], it is worth to deeper investigate this aspect. Further studies are needed to reveal mechanisms through which TFE is able to modulate the 3D supramolecular organization of αSN fibrils.

Conclusions

Results reported in this thesis are aimed at highlighting the effects of environmental conditions in the modulation of the fundamental interactions, which trigger or modify aggregation processes and aggregate stability. In particular, aggregation processes of Aβ(1-40) peptide and the stability of αSN fibrils were analysed. These two intrinsically disordered proteins were selected since their aggregation is known to be related with the high impact neurodegenerative diseases AD and PD.

In Chapter 3, the effects of ThT dye on the aggregation kinetics of Aβ(1-40) peptide were studied. ThT is a small molecule usually employed to reveal *in vivo* and *in vitro* amyloid fibril deposits. Importantly, it is nowadays widely used *in situ* to monitor fibril formation *in vitro*, under the assumption that it does not affect the process itself. Surprisingly, the results here reported reveal that the presence of ThT in solution triggers Aβ(1-40) supramolecular assembly in a time scale where aggregation is not observed in absence of ThT. Results indicate that steric and chemical properties of the ThT molecule may modulate the peptide conformation. Moreover, the observed increase of fluorescence of the dye suggests that the interactions with the peptide are similar to the ones that usually drive the binding of this dye to the already formed amyloid structures. Experimental observations show that the overall rate of aggregation process increases as ThT concentration rises and that Rayleigh scattering and ThT fluorescence growth do not proceed in parallel. This, together with a not obvious dependence of the aggregation rate on Aβ(1-40) concentration, led to the conclusion that at least two interconnected pathways of aggregation occur in the presence of ThT, leading to the formation of both ThT-positive and ThT-negative aggregates. It was shown that ThT-peptide interactions are able to modify the equilibrium structure of Aβ(1-40) polypeptide chain with respect to the one in water. In particular, Aβ tridimensional organization is modified together with secondary structure organization. Moreover, in collaboration with the Biophysics Group of University of Rome-Tor Vergata and by means of classical molecular dynamics simulations, three sites of interaction for ThT molecules were identified: i) regions 3-6 namely with the sequence Glu-Phe-Arg-His, and 24-27 i.e. Val-Gly-Ser-Asn; ii) regions 10-11 (Tyr-Glu) and 19-21 (Phe-Phe-Ala) iii) region 28-40. The interaction with ThT molecules leads to a rigid partially folded Aβ(1-40) conformation where a short beta strand is exposed. The results suggest that ThT templated conformation leads to favourable interactions also due to the changed spatial organization of aromatic residues

due to the presence of the dye as well as to the directionality and the orientation of new intermolecular binding. Importantly, it was postulated that the conformation imposed may favour intermolecular interactions both with "templated" molecules and unstructured monomers, giving rise to the two different aggregation pathways experimentally observed.

From a general point of view and in light of other results in the literature, which indicate that small molecules can be used to control aberrant aggregation for the modulation of inter-protein interactions, this result add pieces of information that may have important medical implications. Indeed, ThT may favour the conversion of possible toxic Aβ oligomers into less reactive amyloid fibrils.

On the other hand, this result is a fundamental warning for experiments where ThT is used as a fluorescent probe. The same effect was not observed, in similar experimental conditions, for globular proteins but it was observed for αSN in this experimental work. So, it is possible to infer that ThT induces a thermodynamic drive toward the stabilization of exposed groups in natively unfolded proteins which are expected to populate conformations that are different from each other on all possible length scales. It may mediate a selection process toward a specific structure whose presence favours the self-assembly process in these proteins.

In Chapter 4, αSN fibril stability in water-TFE mixtures was analyzed. The study was performed in collaboration with the BioSAXS group of the University of Copenhagen. This study is aimed at analyzing the equilibrium of fundamental interactions at the basis of supramolecular assemblies stability. The idea that the presence of small molecules may change the aggregation pathways of intrinsically disordered properties by changing protein-protein and protein-solvent interactions was extended and tested on already formed aggregates. In particular, αSN stability was analysed in water solution at different TFE concentrations. TFE is known to modulate protein conformations, changing protein-solvent interactions via concentration dependent effects. In particular, electrostatic interactions and relative stability of hydrogen bonds, can be tuned by varying TFE concentration [25, 27].

Direct evidence was presented on how αSN fibril stability critically depends on TFE concentration, and how fibril disaggregation can be obtained by simply reducing TFE concentration i.e. altering the balance of electrostatic interactions and H-bonds.

It has been suggested that water-TFE mixtures at different alcohol concentrations would qualitatively mimic the effects of the membrane, at different distances, on the protein-protein electrostatic interactions [27].

Results indicate that, in the reported experimental conditions, making TFE concentration double (or more) induces clustering of αSN fibrils and strengthening of β-sheet structures. Importantly, a drastic reduction of TFE concentration leads to fibril dissolution. This adds a further evidence to the view of the fibrils as reservoirs of toxic oligomers [13]. Indeed, in the highly dynamic cellular environment fibrils coul experience different conditions favouring a disassembly process with a consequent release of oligomeric species, or monomers, from large aggregate clusters. This can result in the production of potential toxic species able to affect cell integrity and/or in the formation

of new seeds with higher diffusion coefficients, able to trigger aggregation in different areas of the brain. For examples, taking in account that TFE-water mixtures have been proposed to mimic the effect of membrane proximity on αSN, the reported results may indicate that αSN β-stranded aggregate stability could be strongly modulated, being either increased or reduced to complete dissolution, by the membrane presence in the aggregate surroundings. This may have a particular relevance in the PD aetiology, possibly being relevant in the inter-neuronal diffusion of αSN aggregates [226].

In conclusion, the reported results highlight the importance of the environment in protein-protein interactions in aggregation processes and fibril stability of intrinsically disordered proteins. As known, IDPs are characterized by shallow free energy landscapes with multiple local minima and without global energy minimum typical for the ordered proteins. This thesis gives two qualitative examples of how, in such free energy landscapes, minima can be created or made deeper or barriers made higher by the modification of some chemical or physical environmental factors.

Bibliography

[1] D. J. Selkoe, "Folding Proteins in Fatal Ways", *Nature*, **426** (2003), 900. (document), 1.1.1, 1.2

[2] V. N. Uversky, "The triple power of D: protein intrinsic disorder in degenerative diseases", *Front Biosci (Landmark Ed)*, **19** (2014), 181. (document), 1.4, 1.4

[3] C. L. Masters, G. Simms, N. A. Weinman, G. Multhaup, B. L. McDonald and K. Beyreuther, "Amyloid plaque core protein in Alzheimer disease and Down syndrome", *Proceedings of the National Academy of Sciences*, **82(12)** (1985), 4245. (document)

[4] K. S. KoSIK, C. L. Joachim and D. J. Selkoe, "Microtubule-associated protein tau (tau) is a major antigenic component of paired helical filaments in Alzheimer disease", *Proceedings of the National Academy of Sciences*, **83(11)** (1986), 4044. (document)

[5] M. G. Spillantini, R. A. Crowther, R. Jakes, M. Hasegawa and M. Goedert, "α-Synuclein in filamentous inclusions of Lewy bodies from Parkinsons disease and dementia with Lewy bodies", *Proceedings of the National Academy of Sciences*, **95(11)** (1998), 6469. (document), 1.4

[6] M. Goedert, M. G. Spillantini, K. Del Tredici and H. Braak, "100 years of Lewy pathology", *Nature Reviews Neurology*, **9(1)** (2012), 13. (document), 1.4

[7] M. Stefani, "Protein misfolding and aggregation: new examples in medicine and biology of the dark side of the protein world", *Biochimica et Biophysica Acta (BBA)-Molecular Basis of Disease*, **1739(1)** (2004), 5. (document), 1.2

[8] T. R. Jahn and S. E. Radford, "The Yin and Yang of protein folding", *Febs Journal*, **272(23)** (2005), 5962. (document), 1, 1.1.1, 1.2

[9] M. Fändrich, J. Meinhardt and N. Grigorieff, "Structural polymorphism of Alzheimer Abeta and other amyloid fibrils", *Prion*, **3(2)** (2009), 89. (document), 1.2, 1.2.2, 1.2.2, 1.7, 1.8, 1.3

[10] A. T. Petkova, R. D. Leapman, Z. Guo, W.-M. Yau, M. P. Mattson and R. Tycko, "Self-Propagating, Molecular-Level Polymorphism in Alzheimer's β-Amyloid Fibrils", *Science*, **307(5707)** (2005), 262. 1.2.2

[11] Foder, Vito and Donald, AM, *The Formation of Amyloid-like Superstructures: On the Growth of Amyloid Spherulites*. (document), 1.2.2, 1.9, 1.2.2, 4.1.3

[12] M. Fändrich, "Oligomeric Intermediates in Amyloid Formation: Structure Determination and Mechanisms of Toxicity", *J. Mol. Biol.*, **10.1016/j.jmb.2012.01.006(0)** (2012), In press. (document)

[13] M. Stefani, "Structural features and cytotoxicity of amyloid oligomers: implications in Alzheimer's disease and other diseases with amyloid deposits", *Progress in neurobiology*, **99(3)** (2012), 226. (document), 4.1.2, 4.2

[14] W. S. Gosal, I. J. Morten, E. W. Hewitt, D. A. Smith, N. H. Thomson and S. E. Radford, "Competing Pathways Determine Fibril Morphology in the Self-assembly of β¡ sub¿ 2¡/sub¿-Microglobulin into Amyloid", *Journal of molecular biology*, **351(4)** (2005), 850. 1.2

[15] V. Vetri, R. Carrotta, P. Picone, M. Di Carlo and V. Militello, "Concanavalin A aggregation and toxicity on cell cultures", *Biochimica et Biophysica Acta (BBA)-Proteins and Proteomics*, **1804(1)** (2010), 173. (document)

[16] R. M. Koffie, M. Meyer-Luehmann, T. Hashimoto, K. W. Adams, M. L. Mielke, M. Garcia-Alloza, K. D. Micheva, S. J. Smith, M. L. Kim, V. M. Lee *et al*, "Oligomeric amyloid β associates with postsynaptic densities and correlates with excitatory synapse loss near senile plaques", *Proceedings of the National Academy of Sciences*, **106(10)** (2009), 4012. (document)

[17] J. Habchi, P. Tompa, S. Longhi and V. N. Uversky, "Introducing Protein Intrinsic Disorder", *Chemical reviews*. (document), 1.1.1, 1.1.2, 1.1.2, 1.4, 1.1.3, 1.2, 2.3.1, 3, 3.2, 4, 4.1.1

[18] V. N. Uversky, "Natively unfolded proteins: a point where biology waits for physics", *Protein Science*, **11(4)** (2002), 739. (document), 1.1.1, 1.1.2, 1.1.3, 3, 3.2, 4, 4.1.1

[19] G. Tiana and L. Sutto, "Equilibrium Properties of Realistic Random Heteropolymers and their Relevance for Globular and Naturally Unfolded Proteins", *Phys. Rev. E*, **84** (2011), 061910. (document)

[20] H. LeVine III, "Thioflavine T interaction with synthetic Alzheimers disease β-amyloid peptides: Detection of amyloid aggregation in solution", *Protein Science*, **2** (1993), 404. (document), 3.1, 3.2

[21] LeVine III, Harry, *Quantification of β-sheet Amyloid Fibril Structures with Thioflavin T*. 2.1.1, 2.1.1, 4.1.1

[22] L. Giehm, N. Lorenzen and D. E. Otzen, "Assays for α-synuclein aggregation", *Methods*, **53(3)** (2011), 295. (document), 1.2, 2.3.3, 3.2, 4

[23] V. N. Uversky, C. J. Oldfield and A. K. Dunker, "Intrinsically disordered proteins in human diseases: introducing the D2 concept", *Annu. Rev. Biophys.*, **37** (2008), 215. (document), 1.2, 4

[24] S. Alavez, M. C. Vantipalli, D. J. S. Zucker, I. M. Klang and G. J. Lithgow, "Amyloid-binding Compounds Maintain Protein Homeostasis During Ageing and Extend Lifespan", *Nature*, **472** (2011), 226. (document), 2.1.1, 3.2

[25] M. Buck, "Trifluoroethanol and colleagues: cosolvents come of age. Recent studies with peptides and proteins", *Quarterly reviews of biophysics*, **31(03)** (1998), 297. (document), 2.3.1, 2.3.1, 4.2, 4.2

[26] V. L. Anderson, T. F. Ramlall, C. C. Rospigliosi, W. W. Webb and D. Eliezer, "Identification of a helical intermediate in trifluoroethanol-induced alpha-synuclein aggregation", *PNAS*, **107(44)** (2010), 28042815. (document), 1.1.3, 1.2, 2.3.1, 3, 4, 4.1.1, 4.2

[27] L. A. Munishkina, C. Phelan, V. N. Uversky and A. L. Fink, "Conformational Behavior and Aggregation of a-Synuclein in Organic Solvents: Modeling the Effects of Membranes", *Biochemistry*, **42**. (document), 1.1.3, 2.3.1, 2.3.1, 4, 4.1.1, 4.2, 4.2

[28] V. N. Uversky and A. L. Fink, "Conformational constraints for amyloid fibrillation: the importance of being unfolded", *Biochimica et Biophysica Acta (BBA)-Proteins and Proteomics*, **1698(2)** (2004), 131. 1, 1.2

[29] V. N. Uversky, J. R. Gillespie and A. L. Fink, "Why are natively unfolded proteins unstructured under physiologic conditions?", *Proteins: Structure, Function, and Bioinformatics*, **41(3)** (2000), 415. 1, 1.1.2, 1.1.2, 1.3, 1.1.2, 1.1.3, 1.2

[30] P. Romero, Z. Obradovic, X. Li, E. C. Garner, C. J. Brown and A. K. Dunker, "Sequence complexity of disordered protein", *Proteins: Structure, Function, and Bioinformatics*, **42(1)** (2001), 38. 1.1.2, 1.2, 1.2

[31] S. E. Permyakov, I. S. Millett, S. Doniach, E. A. Permyakov and V. N. Uversky, "Natively unfolded C-terminal domain of caldesmon remains substantially unstructured after the effective binding to calmodulin", *Proteins: Structure, Function, and Bioinformatics*, **53(4)** (2003), 855. 1.1.1, 1.1.3

[32] M. Brucale, B. Schuler and B. Samorì, "Single-Molecule Studies of Intrinsically Disordered Proteins", *Chemical reviews*, **114(6)** (2014), 3281. 1, 1.1, 1.1.2

[33] P. Tompa, "Intrinsically disordered proteins: a 10-year recap", *Trends in biochemical sciences*, **37(12)** (2012), 509. 1, 1.1.1

[34] J. T. Bendor, T. P. Logan and R. H. Edwards, "The Function of a-Synuclein", *Neuron*, **79**.

[35] H. A. Pearson and C. Peers, "Physiological roles for amyloid β peptides", *The Journal of Physiology*, **575(1)** (2006), 5. 1, 1.3

[36] F. A. Ferrone, J. Hofrichter and W. A. Eaton, "Kinetics of sickle hemoglobin polymerization: II. A double nucleation mechanism", *Journal of molecular biology*, **183(4)** (1985), 611. 1, 1.2.1, 3.1

[37] F. Ferrone, "[17] Analysis of protein aggregation kinetics", in R. Wetzel (Ed.), *Amyloid, Prions, and Other Protein Aggregates*, vol. 309 of *Methods in Enzymology*, Academic Press (1999), 256 – 274. 1.2, 1.2.1, 1.2.1, 1.5

[38] F. Librizzi and C. Rischel, "The kinetic behavior of insulin fibrillation is determined by heterogeneous nucleation pathways", *Protein Science*, **14**. 1, 1.2, 1.2.1, 1.2.1, 1.5

[39] V. Vetri, M. Leone, L. A. Morozova-Roche, B. Vestergaard and V. Fodera, "Unlocked Concanavalin A Forms Amyloid-like Fibrils from Coagulation of Long-lived Crinkled Intermediates", *PloS one*, **8(7)** (2013), e68912.

[40] V. Vetri, C. Canale, A. Relini, F. Librizzi, V. Militello, A. Gliozzi and M. Leone, "Amyloid Fibrils Formation and Amorphous Aggregation in Concanavalin A", *Biophys. Chem.*, **125(1)** (2007), 184. 1, 1.2, 3.1

[41] A. M. Morris, M. A. Watzky and R. G. Finke, "Protein aggregation kinetics, mechanism, and curve-fitting: A review of the literature", *Biochimica et Biophysica Acta*, **1794**. 1, 1.2

[42] S. I. Cohen, M. Vendruscolo, C. M. Dobson and T. P. Knowles, "From macroscopic measurements to microscopic mechanisms of protein aggregation", *Journal of molecular biology*, **421(2)** (2012), 160. 1, 1.2.1, 3.1

[43] C. Frieden, "Protein aggregation processes: in search of the mechanism", *Protein Science*, **16(11)** (2007), 2334. 1, 1.2

[44] F. A. Ferrone, J. Hofrichter, H. Sunshine and W. Eaton, "Kinetic studies on photolysis-induced gelation of sickle cell hemoglobin suggest a new mechanism", *Biophysical journal*, **32(1)** (1980), 361. 1, 1.2, 3.1

[45] W.-F. Xue, S. W. Homans and S. E. Radford, "Systematic analysis of nucleation-dependent polymerization reveals new insights into the mechanism of amyloid self-assembly", *Proceedings of the National Academy of Sciences*, **105(26)** (2008), 8926. 1.2.1

[46] V. Foderà, S. Cataldo, F. Librizzi, B. Pignataro, P. Spiccia and M. Leone, "Self-organization pathways and spatial heterogeneity in insulin amyloid fibril formation", *The journal of physical chemistry B*, **113(31)** (2009), 10830. 1.2.1, 3.1

[47] S. I. Cohen, M. Vendruscolo, M. E. Welland, C. M. Dobson, E. M. Terentjev and T. P. Knowles, "Nucleated polymerization with secondary pathways. I. Time evolution of the principal moments", *The Journal of chemical physics*, **135(6)** (2011), 065105. 1, 1.2, 1.2.1, 1.2.1

[48] E. Fischer, "Einfluss der Configuration auf die Wirkung der Enzyme", *Berichte der deutschen chemischen Gesellschaft*, **27(3)** (1894), 2985. 1.1.1

[49] C. B. Anfinsen, E. Haber, M. Sela and F. White Jr, "The kinetics of formation of native ribonuclease during oxidation of the reduced polypeptide chain", *Proceedings of the National Academy of Sciences of the United States of America*, **47(9)** (1961), 1309. 1.1.1

[50] K. Lang, A. Wrba, H. Krebs, F. X. Schmid and J. J. Beintema, "Folding kinetics of mammalian ribonucleases", *FEBS letters*, **204(1)** (1986), 135.

[51] J. Phillips, A. LeGrand and W. Lehnert, "Protein folding observed by time-resolved synchrotron x-ray scattering. A feasibility study", *Biophysical journal*, **53(3)** (1988), 461.

[52] O. Ptitsyn, R. H. Pain, G. Semisotnov, E. Zerovnik and O. Razgulyaev, "Evidence for a molten globule state as a general intermediate in protein folding", *FEBS letters*, **262(1)** (1990), 20.

[53] A. Hansen, M. Jensen, K. Sneppen and G. Zocchi, "Hot and cold denaturation of proteins: Critical aspects", *The European Physical Journal B-Condensed Matter and Complex Systems*, **10(1)** (1999), 193. 1.1.1

[54] C. Levinthal, "How to fold graciously", *Mossbauer spectroscopy in biological systems* (1969), 22. 1.1.1

[55] C. B. Anfinsen *et al*, "Principles that govern the folding of protein chains", *Science*, **181(4096)** (1973), 223. 1.1.1

[56] J. D. Bryngelson and P. G. Wolynes, "Spin glasses and the statistical mechanics of protein folding", *Proceedings of the National Academy of Sciences*, **84(21)** (1987), 7524. 1.1.1

[57] J. D. Bryngelson, J. N. Onuchic, N. D. Socci and P. G. Wolynes, "Funnels, pathways, and the energy landscape of protein folding: a synthesis", *Proteins: Structure, Function, and Bioinformatics*, **21(3)** (1995), 167. 1.1.1

[58] A. D. Miranker and C. M. Dobson, "Collapse and cooperativity in protein folding", *Current opinion in structural biology*, **6(1)** (1996), 31. 1.1.1

[59] H. S. Chan and K. A. Dill, "Protein folding in the landscape perspective: Chevron plots and non-Arrhenius kinetics", *Proteins: Structure, Function, and Bioinformatics*, **30(1)** (1998), 2. 1.1.1

[60] C. M. Dobson, A. Šali and M. Karplus, "Protein folding: a perspective from theory and experiment", *Angewandte Chemie International Edition*, **37(7)** (1998), 868.

[61] A. R. Dinner, A. Šali, L. J. Smith, C. M. Dobson and M. Karplus, "Understanding protein folding via free-energy surfaces from theory and experiment", *Trends in biochemical sciences*, **25(7)** (2000), 331. 1.1

[62] P. G. Wolynes, "Energy landscapes and solved protein–folding problems", *Philosophical Transactions of the Royal Society A: Mathematical, Physical and Engineering Sciences*, **363(1827)** (2005), 453. 1.1.1

[63] J. Wang, L. Xu and E. Wang, "Optimal specificity and function for flexible biomolecular recognition", *Biophysical journal*, **92(12)** (2007), L109. 1.1.1

[64] V. N. Uversky, "The most important thing is the tail: multitudinous functionalities of intrinsically disordered protein termini", *FEBS letters*, **587(13)** (2013), 1891. 1.1.1

[65] A. K. Dunker, J. D. Lawson, C. J. Brown, R. M. Williams, P. Romero, J. S. Oh, C. J. Oldfield, A. M. Campen, C. M. Ratliff, K. W. Hipps *et al*, "Intrinsically disordered protein", *Journal of Molecular Graphics and Modelling*, **19(1)** (2001), 26. 1.1.1, 1.1.2

[66] J. A. Marsh, S. A. Teichmann and J. D. Forman-Kay, "Probing the diverse landscape of protein flexibility and binding", *Current opinion in structural biology*, **22(5)** (2012), 643. 1.1.1

[67] A. K. Dunker, M. M. Babu, E. Barbar, M. Blackledge, S. E. Bondos, Z. Dosztányi, H. J. Dyson, J. Forman-Kay, M. Fuxreiter, J. Gsponer *et al*, "Whats in a name? Why these proteins are intrinsically disordered", *Intrinsically Disordered Proteins*, **1(1)** (2013), 0. 1.1.1

[68] P. Romero, Z. Obradovic, C. Kissinger, J. Villafranca and A. Dunker, "Identifying disordered regions in proteins from amino acid sequence", in *Neural Networks, 1997., International Conference on*, vol. 1, IEEE (1997), 90–95. 1.1.2

[69] B. D. Ambercrombie, G. G. Kneale, C. Crane-Robinson, E. M. Bradbury, G. H. Goodwin, J. M. Walker and E. W. Johns, "Studies on the Conformational Properties of the High-Mobility-Group Chromosomal Protein HMG 17 and Its Interaction with DNA", *European Journal of Biochemistry*, **84(1)** (1978), 173. 1.1.2, 1.1.2, 1.1.3

[70] K. M. Campbell, A. R. Terrell, P. J. Laybourn and K. J. Lumb, "Intrinsic structural disorder of the C-terminal activation domain from the bZIP transcription factor Fos", *Biochemistry*, **39(10)** (2000), 2708. 1.1.2, 1.1.2

[71] L. Fisher, D. Torchia, B. Fohr, M. Young and N. Fedarko, "Flexible structures of SIBLING proteins, bone sialoprotein, and osteopontin", *Biochemical and biophysical research communications*, **280(2)** (2001), 460. 1.1.2

[72] P. H. Weinreb, W. Zhen, A. W. Poon, K. A. Conway and P. T. Lansbury, "NACP, a protein implicated in Alzheimer's disease and learning, is natively unfolded", *Biochemistry*, **35(43)** (1996), 13709. 1.1.2

[73] O. Tcherkasskaya and V. N. Uversky, "Denatured collapsed states in protein folding: example of apomyoglobin", *Proteins: Structure, Function, and Bioinformatics*, **44(3)** (2001), 244. 1.1.2

[74] V. Receveur-Bréchot, J.-M. Bourhis, V. N. Uversky, B. Canard and S. Longhi, "Assessing protein disorder and induced folding", *Proteins: Structure, Function, and Bioinformatics*, **62(1)** (2006), 24. 1.1.2, 1.1.3

[75] P. Bernadó and D. I. Svergun, "Structural analysis of intrinsically disordered proteins by small-angle X-ray scattering", *Molecular biosystems*, **8(1)** (2012), 151. 1.1.2, 2.1.3, 2.2.4, 2.7, 4.1.1

[76] M. R. Jensen and M. Blackledge, "Testing the validity of ensemble descriptions of intrinsically disordered proteins", *Proceedings of the National Academy of Sciences*, **111(16)** (2014), E1557. 1.1.2

[77] V. N. Uversky, "Unusual biophysics of intrinsically disordered proteins", *Biochimica et Biophysica Acta (BBA)-Proteins and Proteomics*, **1834(5)** (2013), 932. 1.1.2, 1.1.3

[78] M. Sandal, F. Valle, I. Tessari, S. Mammi, E. Bergantino, F. Musiani, M. Brucale, L. Bubacco and B. Samorì, "Conformational equilibria in monomeric α-synuclein at the single-molecule level", *PLoS biology*, **6(1)** (2008), e6. 1.1.2

[79] S. A. Dames, M. Martinez-Yamout, R. N. De Guzman, H. J. Dyson and P. E. Wright, "Structural basis for Hif-1α/CBP recognition in the cellular hypoxic response", *Proceedings of the National Academy of Sciences*, **99(8)** (2002), 5271. 1.1.2, 1.1.3

[80] A. C. M. Ferreon, J. C. Ferreon, P. E. Wright and A. A. Deniz, "Modulation of allostery by protein intrinsic disorder", *Nature*, **498(7454)** (2013), 390. 1.1.2, 1.1.3, 4.1.3

[81] H. S. Cho, C. W. Liu, F. F. Damberger, J. G. Pelton, H. Nelson and D. E. Wemmer, "Yeast heat shock transcription factor N-terminal activation domains

are unstructured as probed by heteronuclear NMR spectroscopy", *Protein science*, **5(2)** (1996), 262. 1.1.2, 1.1.3

[82] C. M. Fletcher, A. M. McGuire, A.-C. Gingras, H. Li, H. Matsuo, N. Sonenberg and G. Wagner, "4E binding proteins inhibit the translation factor eIF4E without folded structure", *Biochemistry*, **37(1)** (1998), 9. 1.1.2, 1.1.3

[83] A. P. Minton, "The influence of macromolecular crowding and macromolecular confinement on biochemical reactions in physiological media", *Journal of biological chemistry*, **276(14)** (2001), 10577. 1.1.3

[84] C. Szasz, A. Alexa, K. Toth, M. Rakacs, J. Langowski and P. Tompa, "Protein disorder prevails under crowded conditions", *Biochemistry*, **50(26)** (2011), 5834. 1.1.3

[85] S. L. Flaugh and K. J. Lumb, "Effects of macromolecular crowding on the intrinsically disordered proteins c-Fos and p27Kip1", *Biomacromolecules*, **2(2)** (2001), 538.

[86] D. Johansen, C. M. Jeffries, B. Hammouda, J. Trewhella and D. P. Goldenberg, "Effects of macromolecular crowding on an intrinsically disordered protein characterized by small-angle neutron scattering with contrast matching", *Biophysical journal*, **100(4)** (2011), 1120.

[87] E. A. Cino, M. Karttunen and W.-Y. Choy, "Effects of molecular crowding on the dynamics of intrinsically disordered proteins", *PloS one*, **7(11)** (2012), e49876. 1.1.3

[88] T. D. Kim, S. R. Paik, C.-H. Yang and J. Kim, "Structural changes in [alpha]-synuclein affect its chaperone-like activity in vitro", *Protein Science*, **9(12)** (2000), 2489. 1.1.3, 3

[89] G. Yamin, C. B. Glaser, V. N. Uversky and A. L. Fink, "Certain metals trigger fibrillation of methionine-oxidized α-synuclein", *Journal of Biological Chemistry*, **278(30)** (2003), 27630. 1.1.3

[90] J. Ejnik, J. Robinson, J. Zhu, H. Försterling, C. F. Shaw III and D. H. Petering, "Folding pathway of apo-metallothionein induced by Zn¡ sup¿ 2+¡/sup¿, Cd¡ sup¿ 2+¡/sup¿ and Co¡ sup¿ 2+¡/sup¿", *Journal of inorganic biochemistry*, **88(2)** (2002), 144. 1.1.3

[91] Q. Ma, Y. Li, J. Du, H. Liu, K. Kanazawa, T. Nemoto, H. Nakanishi and Y. Zhao, "Copper binding properties of a tau peptide associated with Alzheimer's disease studied by CD, NMR, and MALDI-TOF MS", *Peptides*, **27(4)** (2006), 841. 1.1.3

[92] S. Zirah, S. A. Kozin, A. K. Mazur, A. Blond, M. Cheminant, I. Ségalas-Milazzo, P. Debey and S. Rebuffat, "Structural changes of region 1-16 of the Alzheimer

disease amyloid β-peptide upon zinc binding and in vitro aging", *Journal of Biological Chemistry*, **281(4)** (2006), 2151. 1.1.3

[93] S. S. Leal, H. M. Botelho and C. M. Gomes, "Metal ions as modulators of protein conformation and misfolding in neurodegeneration", *Coordination Chemistry Reviews*, **256(19)** (2012), 2253. 1.1.3

[94] S. J. C. Lee, J. W. Lee, T. S. Choi, K. S. Jin, S. Lee, C. Ban and H. I. Kim, "Probing Conformational Change of Intrinsically Disordered α-Synuclein to Helical Structures by Distinctive Regional Interactions with Lipid Membranes", *Analytical chemistry*, **86(3)** (2014), 1909. 1.1.3, 3

[95] C. M. Pfefferkorn, Z. Jiang and J. C. Lee, "Biophysics of a-synuclein membrane interactions", *Biochimica et Biophysica Acta*, **1818**. 1.4

[96] A. B. Sigalov and G. M. Hendricks, "Membrane binding mode of intrinsically disordered cytoplasmic domains of T cell receptor signaling subunits depends on lipid composition", *Biochemical and biophysical research communications*, **389(2)** (2009), 388.

[97] M. Hundertmark, R. Dimova, J. Lengefeld, R. Seckler and D. K. Hincha, "The intrinsically disordered late embryogenesis abundant protein LEA18 from¡ i¿ Arabidopsis thaliana¡/i¿ modulates membrane stability through binding and folding", *Biochimica et Biophysica Acta (BBA)-Biomembranes*, **1808(1)** (2011), 446. 1.1.3

[98] K. C. Hite, A. A. Kalashnikova and J. C. Hansen, "Coil-to-helix transitions in intrinsically disordered methyl CpG binding protein 2 and its isolated domains", *Protein Science*, **21(4)** (2012), 531. 1.1.3

[99] Y.-C. Chang and T. G. Oas, "Osmolyte-induced folding of an intrinsically disordered protein: folding mechanism in the absence of ligand", *Biochemistry*, **49(25)** (2010), 5086. 1.1.3

[100] R. Cuchillo and J. Michel, "Mechanisms of small-molecule binding to intrinsically disordered proteins.", *Biochemical Society transactions*, **40(5)** (2012), 1004. 1.1.3

[101] J. Michel and R. Cuchillo, "The impact of small molecule binding on the energy landscape of the intrinsically disordered protein C-myc", *PloS one*, **7(7)** (2012), e41070. 1.1.3

[102] J. McLaurin, R. Golomb, A. Jurewicz, J. P. Antel and P. E. Fraser, "Inositol stereoisomers stabilize an oligomeric aggregate of Alzheimer amyloid β peptide and inhibit Aβ-induced toxicity", *Journal of Biological Chemistry*, **275(24)** (2000), 18495. 1.1.3

[103] M. Kjaergaard, A. Norholm, R. Hendus-Altenburger, S. Pedersen, F. Poulsen and B. B. Kragelund, "Temperature-dependent structural changes in intrinsically

disordered proteins: Formation of -helices or loss of polyproline II", *Protein Science*, **19(8)** (2010), 1555. 1.1.3, 3

[104] V. N. Uversky, J. Li and A. L. Fink, "Evidence for a Partially Folded Intermediate in a-Synuclein Fibril Formation", *The Journal of Biological Chemistry*, **276(14)** (2001), 10737. 1.1.3, 1.2, 1.4, 1.4, 1.11, 3, 4

[105] R. L. Baldwin, "Temperature dependence of the hydrophobic interaction in protein folding", *Proceedings of the National Academy of Sciences*, **83(21)** (1986), 8069. 1.1.3

[106] T. D. Kim, H. J. Ryu, H. I. Cho, C.-H. Yang and J. Kim, "Thermal behavior of proteins: heat-resistant proteins and their heat-induced secondary structural changes", *Biochemistry*, **39(48)** (2000), 14839. 1.1.3

[107] K. Klement, K. Wieligmann, J. Meinhardt, P. Hortschansky, W. Richter and M. Fändrich, "Effect of different salt ions on the propensity of aggregation and on the structure of Alzheimers Aβ (1-40) amyloid fibrils", *Journal of molecular biology*, **373(5)** (2007), 1321. 1.2

[108] A. Roostaee, S. Beaudoin, A. Staskevicius and X. Roucou, "Aggregation and neurotoxicity of recombinant α-synuclein aggregates initiated by dimerization", *Mol. Neurodegener*, **8(5)**. 1.2, 1.4

[109] D. M. Walsh and D. J. Selkoe, "Aβ oligomers–a decade of discovery", *Journal of neurochemistry*, **101(5)** (2007), 1172. 1.2

[110] M. Bucciantini, E. Giannoni, F. Chiti, F. Baroni, L. Formigli, J. Zurdo, N. Taddei, G. Ramponi, C. M. Dobson and M. Stefani, "Inherent toxicity of aggregates implies a common mechanism for protein misfolding diseases", *Nature*, **416(6880)** (2002), 507. 1.2

[111] R. Kayed, E. Head, J. L. Thompson, T. M. McIntire, S. C. Milton, C. W. Cotman and C. G. Glabe, "Common structure of soluble amyloid oligomers implies common mechanism of pathogenesis", *Science*, **300(5618)** (2003), 486. 1.2

[112] D. M. Walsh, I. Klyubin, J. V. Fadeeva, M. J. Rowan and D. J. Selkoe, "Amyloid-β Oligomers: their Production, Toxicity and Therapeutic Inhibition", *Biochem. Soc. T.*, **30** (2002), 552. 1.2

[113] K. A. Conway, S.-J. Lee, J.-C. Rochet, T. T. Ding, R. E. Williamson and P. T. Lansbury, "Acceleration of oligomerization, not fibrillization, is a shared property of both α-synuclein mutations linked to early-onset Parkinson's disease: implications for pathogenesis and therapy", *Proceedings of the National Academy of Sciences*, **97(2)** (2000), 571. 1.2

[114] V. Foderà, A. Zaccone, M. Lattuada and A. M. Donald, "Electrostatics controls the formation of amyloid superstructures in protein aggregation", *Physical Review Letters*, **111(10)** (2013), 108105. 1.2, 1.2.2

[115] L. Di Michele, E. Eiser and V. Foderà, "Minimal Model for Self-Catalysis in the Formation of Amyloid-Like Elongated Fibrils", *The Journal of Physical Chemistry Letters*, **4(18)** (2013), 3158. 1.2, 1.2.1, 1.3

[116] A. J. Modler, K. Gast, G. Lutsch and G. Damaschun, "Assembly of Amyloid Protofibrils¡ i¿ via¡/i¿ Critical OligomersA Novel Pathway of Amyloid Formation", *Journal of molecular biology*, **325(1)** (2003), 135. 1.2

[117] E. van der Linden and P. Venema, "Self-assembly and aggregation of proteins", *Current Opinion in Colloid & Interface Science*, **12(4)** (2007), 158. 1.2

[118] M. D. Kirkitadze, M. M. Condron and D. B. Teplow, "Identification and characterization of key kinetic intermediates in amyloid β-protein fibrillogenesis", *Journal of Molecular Biology*, **312(5)** (2001), 1103 . 1.2, 1.3

[119] P. H. Nguyen, M. S. Li, G. Stock, J. E. Straub and D. Thirumalai, "Monomer adds to preformed structured oligomers of Aβ-peptides by a two-stage dock–lock mechanism", *Proceedings of the National Academy of Sciences*, **104(1)** (2007), 111. 1.2, 1.3

[120] A. R. Hurshman, J. T. White, E. T. Powers and J. W. Kelly, "Transthyretin aggregation under partially denaturing conditions is a downhill polymerization", *Biochemistry*, **43(23)** (2004), 7365. 1.2

[121] L. Nielsen, R. Khurana, A. Coats, S. Frokjaer, J. Brange, S. Vyas, V. N. Uversky and A. L. Fink, "Effect of environmental factors on the kinetics of insulin fibril formation: elucidation of the molecular mechanism", *Biochemistry*, **40(20)** (2001), 6036. 1.2

[122] A. Lomakin, D. B. Teplow, D. A. Kirschner and G. B. Benedek, "Kinetic theory of fibrillogenesis of amyloid β-protein", *Proceedings of the National Academy of Sciences*, **94(15)** (1997), 7942. 1.2, 1.3

[123] T. R. Serio, A. G. Cashikar, A. S. Kowal, G. J. Sawicki, J. J. Moslehi, L. Serpell, M. F. Arnsdorf and S. L. Lindquist, "Nucleated conformational conversion and the replication of conformational information by a prion determinant", *Science*, **289(5483)** (2000), 1317. 1.2

[124] M. M. Pallitto and R. M. Murphy, "A Mathematical Model of the Kinetics of β-Amyloid Fibril Growth from the Denatured State", *Biophysical journal*, **81(3)** (2001), 1805. 1.2

[125] C. T. Z. G. Hortschansky P., Schroeckh V. and Fndrich, "The aggregation kinetics of Alzheimers β-amyloid peptide is controlled by stochastic nucleation", *Protein Science*, **14(7)**. 1.2, 1.2.1, 1.3, 3.1, 3.2

[126] S. I. Cohen, S. Linse, L. M. Luheshi, E. Hellstrand, D. A. White, L. Rajah, D. E. Otzen, M. Vendruscolo, C. M. Dobson and T. P. Knowles, "Proliferation of amyloid-β42 aggregates occurs through a secondary nucleation mechanism", *Proceedings of the National Academy of Sciences*, **110(24)** (2013), 9758. 1.2, 1.2.1, 1.3

[127] S. J. W.P., *Nucleation Theory and Applications*, Wiley-VCH (2005). 1.2.1

[128] E. T. Powers and D. L. Powers, "The kinetics of nucleated polymerizations at high concentrations: amyloid fibril formation near and above the supercritical concentration", *Biophysical journal*, **91(1)** (2006), 122. 1.2.1

[129] F. Oosawa and M. Kasai, "A theory of linear and helical aggregations of macromolecules", *Journal of molecular biology*, **4(1)** (1962), 10. 1.2.1, 1.5

[130] H. Flyvbjerg, E. Jobs and S. Leibler, "Kinetics of self-assembling microtubules: an" inverse problem" in biochemistry", *Proceedings of the National Academy of Sciences*, **93(12)** (1996), 5975. 1.2.1, 1.5

[131] A. Wegner and P. Savko, "Fragmentation of actin filaments", *Biochemistry*, **21(8)** (1982), 1909. 1.2.1

[132] S. I. Cohen, M. Vendruscolo, C. M. Dobson and T. P. Knowles, "Nucleated polymerization with secondary pathways. II. Determination of self-consistent solutions to growth processes described by non-linear master equations", *The Journal of chemical physics*, **135(6)** (2011), 065106. 1.2.1

[133] S. I. Cohen, M. Vendruscolo, C. M. Dobson and T. P. Knowles, "Nucleated polymerization with secondary pathways. III. Equilibrium behavior and oligomer populations", *The Journal of chemical physics*, **135(6)** (2011), 065107. 1.2.1

[134] S. I. Cohen, M. Vendruscolo, C. M. Dobson and T. P. Knowles, "Nucleated polymerisation in the presence of pre-formed seed filaments", *International journal of molecular sciences*, **12(9)** (2011), 5844. 1.6, 1.2.1, 1.2.1, 3.1, 3.1, 3.1, 3.1

[135] V. Foderà, M. Groenning, V. Vetri, F. Librizzi, S. Spagnolo, C. Cornett, L. Olsen, M. van de Weert and M. Leone, "Thioflavin T Hydroxylation at Basic pH and its Effect on Amyloid Fibril Detection", *J. Phys. Chem. B*, **112** (2008), 15174. 1.2.1, 2.1.1

[136] P. Arosio, R. Cukalevski, B. Frohm, T. P. Knowles and S. Linse, "Quantification of the Concentration of Aβ42 Propagons during the Lag Phase by an Amyloid Chain Reaction Assay", *Journal of the American Chemical Society*, **136(1)** (2013), 219. 1.2.1

[137] A. T. Petkova, W.-M. Yau and R. Tycko, "Experimental constraints on quaternary structure in Alzheimer's β-amyloid fibrils", *Biochemistry*, **45(2)** (2006), 498. 1.2.2

[138] L. Breydo, J. W. Wu and V. N. Uversky, "A-synuclein misfolding and Parkinson's disease", *Biochimica et Biophysica Acta (BBA)-Molecular Basis of Disease*, **1822(2)** (2012), 261. 1.2.2

[139] E. M. Jones and W. K. Surewicz, "Fibril conformation as the basis of species-and strain-dependent seeding specificity of mammalian prion amyloids", *Cell*, **121(1)** (2005), 63. 1.2.2

[140] M. R. Krebs, C. E. MacPhee, A. F. Miller, I. E. Dunlop, C. M. Dobson and A. M. Donald, "The formation of spherulites by amyloid fibrils of bovine insulin", *Proceedings of the National Academy of Sciences of the United States of America*, **101(40)** (2004), 14420. 1.2.2

[141] K. R. Domike and A. M. Donald, "Thermal dependence of thermally induced protein spherulite formation and growth: kinetics of β-lactoglobulin and insulin", *Biomacromolecules*, **8(12)** (2007), 3930. 1.2.2, 4.1.3

[142] C. Exley, E. House, J. F. Collingwood, M. R. Davidson, D. Cannon and A. M. Donald, "Spherulites of Amyloid-β {42} In Vitro and in Alzheimer's Disease", *Journal of Alzheimer's Disease*, **20(4)** (2010), 1159. 1.2.2

[143] M. J. Roberti, J. Fölling, M. S. Celej, M. Bossi, T. M. Jovin and E. A. Jares-Erijman, "Imaging Nanometer-Sized¡ i¿ α¡/i¿-Synuclein Aggregates by Superresolution Fluorescence Localization Microscopy", *Biophysical journal*, **102(7)** (2012), 1598. 1.2.2, 4.1.3, 4.2

[144] A. Lomakin, D. S. Chung, G. B. Benedek, D. A. Kirschner and D. B. Teplow, "On the nucleation and growth of amyloid β-protein fibrils: detection of nuclei and quantitation of rate constants", *Proceedings of the National Academy of Sciences*, **93(3)** (1996), 1125. 1.3

[145] T. Steckmann, Z. Awan, B. S. Gerstman and P. P. Chapagain, "Kinetics of peptide secondary structure conversion during amyloid β-protein fibrillogenesis", *Journal of theoretical biology*, **301** (2012), 95. 1.3

[146] Y.-h. Sung and D. Eliezer, "Residual structure, backbone dynamics, and interactions within the synuclein family", *Journal of molecular biology*, **372(3)** (2007), 689. 1.4

[147] L. S. Forno, "Neuropathology of Parkinson's disease", *Journal of Neuropathology & Experimental Neurology*, **55(3)** (1996), 259. 1.4

[148] E. Masliah, E. Rockenstein, A. Adame, M. Alford, L. Crews, M. Hashimoto, P. Seubert, M. Lee, J. Goldstein, T. Chilcote *et al*, "Effects of α-synuclein immunization in a mouse model of Parkinsons disease", *Neuron*, **46(6)** (2005), 857. 1.4

[149] V. N. Uversky and A. Fink, "Amino acid determinants of a-synuclein aggregation: putting together pieces of the puzzle", *FEBS Letters*, **522**. 1.4, 1.10

[150] T. Bartels, J. G. Choi and D. J. Selkoe, "[agr]-Synuclein occurs physiologically as a helically folded tetramer that resists aggregation", *Nature*, **477(7362)** (2011), 107. 1.4

[151] W. Wang, I. Perovic, J. Chittuluru, A. Kaganovich, L. T. Nguyen, J. Liao, J. R. Auclair, D. Johnson, A. Landeru, A. K. Simorellis *et al*, "A soluble α-synuclein construct forms a dynamic tetramer", *Proceedings of the National Academy of Sciences*, **108(43)** (2011), 17797. 1.4

[152] C. A. Waudby, C. Camilloni, A. W. Fitzpatrick, L. D. Cabrita, C. M. Dobson, M. Vendruscolo and J. Christodoulou, "In-cell NMR characterization of the secondary structure populations of a disordered conformation of α-synuclein within E. coli cells", *PloS one*, **8(8)** (2013), e72286. 1.4

[153] G. Fusco, A. De Simone, T. Gopinath, V. Vostrikov, M. Vendruscolo, C. M. Dobson and G. Veglia, "Direct observation of the three regions in α-synuclein that determine its membrane-bound behaviour", *Nature communications*, **5**. 1.4

[154] I. G. Zigoneanu, Y. J. Yang, A. S. Krois, M. E. Haque and G. J. Pielak, "Interaction of α-synuclein with vesicles that mimic mitochondrial membranes", *Biochimica et Biophysica Acta (BBA)-Biomembranes*, **1818(3)** (2012), 512. 1.4

[155] M. Zhu and A. L. Fink, "Lipid binding inhibits α-synuclein fibril formation", *Journal of Biological Chemistry*, **278(19)** (2003), 16873. 1.4

[156] I. Dikiy and D. Eliezer, "Folding and misfolding of alpha-synuclein on membranes", *Biochimica et Biophysica Acta (BBA)-Biomembranes*, **1818(4)** (2012), 1013. 1.4

[157] F. Haque, A. P. Pandey, L. R. Cambrea, J.-C. Rochet and J. S. Hovis, "Adsorption of α-synuclein on lipid bilayers: Modulating the structure and stability of protein assemblies", *The Journal of Physical Chemistry B*, **114(11)** (2010), 4070. 1.4

[158] N. Lorenzen, S. B. Nielsen, A. K. Buell, J. D. Kaspersen, P. Arosio, B. S. Vad, W. Paslawski, G. Christiansen, Z. Valnickova-Hansen, M. Andreasen *et al*, "The role of stable α-synuclein oligomers in the molecular events underlying amyloid formation", *Journal of the American Chemical Society*, **136(10)** (2014), 3859. 1.4

[159] M. J. Volles, S.-J. Lee, J.-C. Rochet, M. D. Shtilerman, T. T. Ding, J. C. Kessler and P. T. Lansbury, "Vesicle permeabilization by protofibrillar α-synuclein: implications for the pathogenesis and treatment of Parkinson's disease", *Biochemistry*, **40(26)** (2001), 7812. 1.4

[160] B. Winner, R. Jappelli, S. K. Maji, P. A. Desplats, L. Boyer, S. Aigner, C. Hetzer, T. Loher, M. Vilar, S. Campioni *et al*, "In vivo demonstration that α-synuclein

oligomers are toxic", *Proceedings of the National Academy of Sciences*, **108(10)** (2011), 4194. 1.4

[161] A. Doerr, "A Fountain of Youth (for Worms)", *Nat. Meth.*, **8** (2011), 376. 2.1.1, 3.1

[162] V. Foderà, "Insulin Fibril Formation: Growth Mechanisms and Fiber Morphologies", *Dipartimento di Scienze Fisiche ed Astronomiche*. 2.1.1, 2.4

[163] A. A. Maskevich, V. I. Stsiapura, V. A. Kuzmitsky, I. M. Kuznetsova, O. I. Povarova, V. N. Uversky and K. K. Turoverov, "Spectral Properties of Thioflavin T in Solvents with Different Dielectric Properties and in a Fibril-Incorporated Form", *Journal of Proteome Research*, **6(4)** (2007), 1392. 2.1.1, 2.1

[164] M. Biancalana and K. Shohei, "Molecular Mechanism of Thioflavin-T Binding to Amyloid Fibrils", *Biochim. Biophys. Acta*, **1804** (2010), 1405. 2.1.1, 3.1, 3.1, 3.1

[165] A. E. Langkilde and B. Vestergaard, "Methods for Structural Characterization of Prefibrillar Intermediates and Amyloid Fibrils", *FEBS L.*, **583(16)** (2009), 2600.

[166] M. Krebs, E. Bromley and A. Donald, "The Binding of Thioflavin-T to Amyloid Fibrils: Localisation and Implications", *J. Struct. Biol.*, **149(1)** (2005), 30. 2.1.1

[167] V. I. Stsiapura, A. A. Maskevich, V. A. Kuzmitsky, V. N. Uversky, I. M. Kuznetsova and K. K. Turoverov, "Thioflavin T as a Molecular Rotor: Fluorescent Properties of Thioflavin T in Solvents with Different Viscosity", *J. Phys. Chem. B*, **112(49)** (2008), 15893. 2.1.1

[168] R. Khurana, C. Coleman, C. Ionescu-Zanetti, S. A. Carter, V. Krishna, R. K. Grover, R. Roy and S. Singh, "Mechanism of Thioflavin T Binding to Amyloid Fibrils", *J. Struct. Biol.*, **151(3)** (2005), 229. 2.1.1

[169] M. Groenning, L. Olsen, M. van de Weert, J. M. Flink, S. Frokjaer and F. S. Jørgensen, "Study on the Binding of Thioflavin T to β-sheet-rich and Non-β-sheet Cavities", *J. Struct. Biol.*, **158(3)** (2007), 358. 2.1.1

[170] M. Groenning, M. Norrman, J. M. Flink, M. van de Weert, J. T. Bukrinsky, G. Schluckebier and S. Frøkjær, "Binding Mode of Thioflavin T in Insulin Amyloid Fibrils", *J. Struct. Biol.*, **159(3)** (2007), 483.

[171] R. Sabatè, I. Lascu and S. J. Saupe, "On the Binding of Thioflavin-T to HET-s Amyloid Fibrils Assembled at pH 2", *J. Struct. Biol.*, **162(3)** (2008), 387 . 2.1.1

[172] C. Wu, Z. Wang, H. Lei, Y. Duan, M. T. Bowers and J.-E. Shea, "The Binding of Thioflavin T and Its Neutral Analog BTA-1 to Protofibrils of the Alzheimer's Disease Aβ16-22 Peptide Probed by Molecular Dynamics Simulations", *J. Mol. Biol.*, **384(3)** (2008), 718. 2.1.1

[173] C. C. Kitts and D. A. V. Bout, "Near-Field Scanning Optical Microscopy Measurements of Fluorescent Molecular Probes Binding to Insulin Amyloid Fibrils", *J. Phys. Chem. B*, **113(35)** (2009), 12090.

[174] V. I. Stsiapura, A. A. Maskevich, S. A. Tikhomirov and O. V. Buganov, "Charge Transfer Process Determines Ultrafast Excited State Deactivation of Thioflavin T in Low-Viscosity Solvents", *J. Phys. Chem. A*, **114(32)** (2010), 8345. 2.1.1, 3.1

[175] H. Kapitza, G. McGregor and K. Jacobson, "Direct measurement of lateral transport in membranes by using time-resolved spatial photometry", *Proceedings of the National Academy of Sciences*, **82(12)** (1985), 4122. 2.1.1, 3.1

[176] S. M. Kelly and N. C. Price, "The use of circular dichroism in the investigation of protein structure and function", *Current protein and peptide science*, **1(4)** (2000), 349. 2.1.2

[177] A. Guinier and G. Fournet, *Small-angle scattering of x-rays, third ed.*, Springer (1955). 2.1.3, 2.2, 2.1.3, 2.3, 2.1.3, 2.1.3

[178] H. D. Mertens and D. I. Svergun, "Structural characterization of proteins and complexes using small-angle X-ray solution scattering", *Journal of structural biology*, **172(1)** (2010), 128. 2.1.3

[179] P. Calmettes, D. Durand, M. Desmadril, P. Minard, V. Receveur and J. Smith, "How random is a highly denatured protein?", *Biophysical chemistry*, **53(1)** (1994), 105. 2.1.3, 2.1.3

[180] J. R. Lakowicz, *Principles of Fluorescence Spectroscopy, third ed.*, Springer (2006). 2.2.1, 3.1

[181] C. E. MacPhee and C. M. Dobson, "Chemical dissection and reassembly of amyloid fibrils formed by a peptide fragment of transthyretin", *Journal of molecular biology*, **297(5)** (2000), 1203. 2.3.1

[182] J. F. Povey, C. M. Smales, S. J. Hassard and M. J. Howard, "Comparison of the effects of 2, 2, 2-trifluoroethanol on peptide and protein structure and function", *Journal of structural biology*, **157(2)** (2007), 329. 2.3.1

[183] M. V. Khan, G. Rabbani, E. Ahmad and R. H. Khan, "Fluoroalcohols-induced modulation and amyloid formation in conalbumin", *International journal of biological macromolecules*, **70** (2014), 606. 2.3.1

[184] Y.-F. Zeng, Z.-R. Lü, L. Yan, S. Oh, J.-M. Yang, J. Lee and Z. M. Ye, "Towards alpha-glucosidase folding induced by trifluoroethanol: Kinetics and computational prediction", *Process Biochemistry*, **47(12)** (2012), 2284. 2.3.1

[185] Z.-R. Lü, L. Shi, J. Wang, D. Park, J. Bhak, J.-M. Yang, Y.-D. Park, H.-W. Zhou and F. Zou, "The effect of trifluoroethanol on tyrosinase activity and conformation: inhibition kinetics and computational simulations", *Applied biochemistry and biotechnology*, **160(7)** (2010), 1896. 2.3.1

[186] Y. Fezoui, D. Hartley, J. Harper, D. Khurana, R. Walsh, M. M. Condron, D. Selkoe, P. T. J. Lansbury, A. Fink and D. B. Teplow, "An Improved Method of Preparing the Amyloid β-protein for Fibrillogenesis and Neurotoxicity Experiments.", *Amyloid*, **7** (2000), 166. 2.3.2

[187] M. D'Amico, M. G. Di Carlo, M. Groenning, V. Militello, V. Vetri and M. Leone, "Thioflavin T promotes Aβ (1–40) amyloid fibrils formation", *The Journal of Physical Chemistry Letters*, **3(12)** (2012), 1596. 2.3.2, 3.1, 3.2, 3.3, 3.4, 3.1

[188] V. Foderà, S. Pagliara, O. Otto, U. F. Keyser and A. M. Donald, "Microfluidics Reveals a Flow-Induced Large-Scale Polymorphism of Protein Aggregates", *The Journal of Physical Chemistry Letters*, **3(19)** (2012), 2803. 2.3.2

[189] B. Hess, C. Kutzner, D. Van Der Spoel and E. Lindahl, "GROMACS 4: Algorithms for highly efficient, load-balanced, and scalable molecular simulation", *Journal of chemical theory and computation*, **4(3)** (2008), 435. 2.3.2

[190] C. Huang, G. Ren, H. Zhou and C.-c. Wang, "A new method for purification of recombinant human α-synuclein in¡ i¿ Escherichia coli¡/i¿", *Protein expression and purification*, **42(1)** (2005), 173. 2.3.3

[191] S. L. Bernstein, D. Liu, T. Wyttenbach, M. T. Bowers, J. C. Lee, H. B. Gray and J. R. Winkler, "α-Synuclein: Stable compact and extended monomeric structures and pH dependence of dimer formation", *Journal of the American Society for Mass Spectrometry*, **15(10)** (2004), 1435. 2.3.3

[192] M. Groenning, "Binding Mode of Thioflavin T and Other Molecular Probes in the Context of Amyloid Fibrils Current Status", *J. Chem. Biol.*, **3** (2010), 1. 2.3.3

[193] S. Nielsen, K. N. Toft, D. Snakenborg, M. G. Jeppesen, J. Jacobsen, B. Vestergaard, J. P. Kutter and L. Arleth, "BioXTAS RAW, a software program for high-throughput automated small-angle X-ray scattering data reduction and preliminary analysis", *Journal of Applied Crystallography*, **42(5)** (2009), 959. 2.3.3

[194] P. Arosio, M. Vendruscolo, C. M. Dobson and T. P. Knowles, "Chemical kinetics for drug discovery to combat protein aggregation diseases", *Trends in pharmacological sciences*, **35(3)** (2014), 127. 3, 3.1, 3.1, 3.1

[195] A. Lorenzo and B. A. Yankner, "Beta-amyloid neurotoxicity requires fibril formation and is inhibited by congo red", *Proceedings of the National Academy of Sciences*, **91(25)** (1994), 12243.

[196] K. Ono, K. Hasegawa, H. Naiki and M. Yamada, "Curcumin has potent anti-amyloidogenic effects for Alzheimer's β-amyloid fibrils in vitro", *Journal of neuroscience research*, **75(6)** (2004), 742. 3

[197] Y. Porat, A. Abramowitz and E. Gazit, "Inhibition of amyloid fibril formation by polyphenols: structural similarity and aromatic interactions as a common inhibition mechanism", *Chemical biology & drug design*, **67(1)** (2006), 27.

[198] A. Sgarbossa, D. Buselli and F. Lenci, "¡ i¿ In vitro¡/i¿ perturbation of aggregation processes in β-amyloid peptides: A spectroscopic study", *FEBS letters*, **582(23)** (2008), 3288. 3

[199] N. Ferreira, S. A. Santos, M. R. M. Domingues, M. J. Saraiva and M. R. Almeida, "Dietary curcumin counteracts extracellular transthyretin deposition: Insights on the mechanism of amyloid inhibition", *Biochimica et Biophysica Acta (BBA)-Molecular Basis of Disease*, **1832(1)** (2013), 39. 3

[200] A. R. A. Ladiwala, J. S. Dordick and P. M. Tessier, "Aromatic small molecules remodel toxic soluble oligomers of amyloid β through three independent pathways", *Journal of Biological Chemistry*, **286(5)** (2011), 3209. 3

[201] A. Abelein, L. Lang, C. Lendel, A. Gräslund and J. Danielsson, "Transient small molecule interactions kinetically modulate amyloid β peptide self-assembly", *FEBS letters*, **586(22)** (2012), 3991. 3

[202] Y. Masuda, M. Fukuchi, T. Yatagawa, M. Tada, K. Takeda, K. Irie, K.-i. Akagi, Y. Monobe, T. Imazawa and K. Takegoshi, "Solid-state NMR analysis of interaction sites of curcumin and 42-residue amyloid β-protein fibrils", *Bioorganic & medicinal chemistry*, **19(20)** (2011), 5967. 3

[203] L. O. Tjernberg, J. Näslund, F. Lindqvist, J. Johansson, A. R. Karlström, J. Thyberg, L. Terenius and C. Nordstedt, "Arrest of-amyloid fibril formation by a pentapeptide ligand", *Journal of Biological Chemistry*, **271(15)** (1996), 8545. 3

[204] M. H. Viet, S. T. Ngo, N. S. Lam and M. S. Li, "Inhibition of aggregation of amyloid peptides by beta-sheet breaker peptides and their binding affinity", *The Journal of Physical Chemistry B*, **115(22)** (2011), 7433. 3

[205] P. Giannozzi, K. Jansen, G. La Penna, V. Minicozzi, S. Morante, G. Rossi and F. Stellato, "Zn induced structural aggregation patterns of β-amyloid peptides by first-principle simulations and XAS measurements", *Metallomics*, **4(2)** (2012), 156. 3

[206] V. Minicozzi, R. Chiaraluce, V. Consalvi, C. Giordano, C. Narcisi, P. Punzi, G. C. Rossi and S. Morante, "Computational and Experimental Studies on β-Sheet Breakers Targeting Aβ1–40 Fibrils", *Journal of Biological Chemistry*, **289(16)** (2014), 11242. 3

[207] B. J. Berne and R. Pecora, *Dynamic light scattering: with applications to chemistry, biology, and physics*, Courier Dover Publications (2000). 3.1

[208] R. F. Pasternack, C. Fleming, S. Herring, P. J. Collings, J. dePaula, G. DeCastro and E. J. Gibbs, "Aggregation kinetics of extended porphyrin and cyanine dye assemblies", *Biophysical journal*, **79(1)** (2000), 550. 3.1

[209] M. B. Borgia, A. A. Nickson, J. Clarke and M. J. Hounslow, "A mechanistic model for amorphous protein aggregation of immunoglobulin-like domains", *Journal of the American Chemical Society*, **135(17)** (2013), 6456. 3.1

[210] I. Morgado and M. Fändrich, "Assembly of Alzheimer's Aβ Peptide into Nanostructured Amyloid Fibrils", *Curr. Opin. Colloid In.*, **16(6)** (2011), 508. 3.1

[211] V. N. Uversky, "Mysterious Oligomerization of the Amyloidogenic Proteins", *FEBS J.*, **277(14)** (2010), 2940. 3.1

[212] J. Bieschke, M. Herbst, T. Wiglenda, R. P. Friedrich, A. Boeddrich, F. Schiele, D. Kleckers, J. M. Lopez del Amo, B. A. Grüning, Q. Wang, M. R. Schmidt, R. Lurz, R. Anwyl, S. Schnoegl, M. Fändrich, R. F. Frank, B. Reif, S. Günther, D. M. Walsh and E. E. Wanker, "Small-molecule Conversion of Toxic Oligomers to Nontoxic β-sheet Rich Amyloid Fibrils", *Nat. Chem. Biol.*, **8** (2012), 93.

[213] I. Horvath, C. F. Weise, E. K. Andersson, E. Chorell, M. Sellstedt, C. Bengtsson, A. Olofsson, S. J. Hultgren, M. Chapman, M. Wolf-Watz and et al., "Mechanisms of Protein Oligomerization: Inhibitor of Functional Amyloids Templates α-Synuclein Fibrillation", *J. Am. Chem. Soc.*, **134(7)** (2012), 3439.

[214] S. Vilasi, R. Sarcina, R. Maritato, A. De Simone, G. Irace and I. Sirangelo, "Heparin Induces Harmless Fibril Formation in Amyloidogenic W7FW14F Apomyoglobin and Amyloid Aggregation in Wild-Type Protein *In Vitro*", *PLoS ONE*, **6(7)** (2011), e22076. 3.1

[215] G. Grelle, A. Otto, M. Lorenz, R. F. Frank, E. E. Wanker and J. Bieschke, "Black Tea Theaflavins Inhibit Formation of Toxic Amyloid-β and α-Synuclein Fibrils", *Biochemistry*, **50(49)** (2011), 10624.

[216] M. D'Amico, S. Raccosta, M. Cannas, V. Martorana and M. Manno, "Existence of Metastable Intermediate Lysozyme Conformation Highlights the Role of Alcohols in Altering Protein Stability", *J. Phys. Chem. B*, **115(14)** (2011), 4078. 3.1

[217] O. Crescenzi, S. Tomaselli, R. Guerrini, S. Salvadori, A. M. D'Ursi, P. A. Temussi and D. Picone, "Solution structure of the Alzheimer amyloid β-peptide (1–42) in an apolar microenvironment", *European Journal of Biochemistry*, **269(22)** (2002), 5642. 3.1

[218] V. N. Maiorov and G. M. Crippen, "Size-independent comparison of protein three-dimensional structures", *Proteins: Structure, Function, and Bioinformatics*, **22(3)** (1995), 273. 3.1, 3.1

[219] J. Khandogin and C. L. Brooks, "Linking folding with aggregation in Alzheimer's β-amyloid peptides", *Proceedings of the National Academy of Sciences*, **104(43)** (2007), 16880. 3.1

[220] R. Azriel and E. Gazit, "Analysis of the structural and functional elements of the minimal active fragment of islet amyloid polypeptide (IAPP)-An experimental support for the key role of the phenylalanine residue in amyloid formation", *Journal of Biological Chemistry*, **276(36)** (2001), 34156. 3.1

[221] W. Kabsch and C. Sander, "Dictionary of protein secondary structure: pattern recognition of hydrogen-bonded and geometrical features", *Biopolymers*, **22(12)** (1983), 2577. 3.1

[222] A. K. Buell, C. Galvagnion, R. Gaspar, E. Sparr, M. Vendruscolo, T. P. Knowles, S. Linse and C. M. Dobson, "Solution conditions determine the relative importance of nucleation and growth processes in α-synuclein aggregation", *Proceedings of the National Academy of Sciences*, **111(21)** (2014), 7671. 4, 4.1.1

[223] K. A. Conway, J. D. Harper and P. T. Lansbury, "Accelerated in vitro fibril formation by a mutant α-synuclein linked to early-onset Parkinson disease", *Nature medicine*, **4(11)** (1998), 1318. 4, 4.1.1

[224] Bockris, J. O'M. and Reddy, A. K. N., *Modern Electrochemistry 1*. 4

[225] V. Foderà and A. Donald, "Tracking the heterogeneous distribution of amyloid spherulites and their population balance with free fibrils", *The European Physical Journal E: Soft Matter and Biological Physics*, **33(4)** (2010), 273. 4.1.3

[226] J.-Y. Li, E. Englund, J. L. Holton, D. Soulet, P. Hagell, A. J. Lees, T. Lashley, N. P. Quinn, S. Rehncrona, A. Björklund *et al*, "Lewy bodies in grafted neurons in subjects with Parkinson's disease suggest host-to-graft disease propagation", *Nature medicine*, **14(5)** (2008), 501. 4.2

Acknowledgments

Many people have contributed to the realization of this PhD research work. Here I would like to spend some words to thank them.

First of all, I wish to express my gratitude to my supervisor Prof. Maurizio Leone for sharing with me his large scientific experience, for useful discussions and for his persistent support. It is also a real pleasure for me to thank Dr. Valeria Vetri for having closely followed my research activity, permitting me to continuously improve my skills while allowing me to progressively develop my autonomy. I would also like to thank all the other members of the Molecular Biophysics and Soft Matter group: Prof. Valeria Militello, Dr. Giovanna Navarra, Dr. Federica Piccirilli, and, in particular, Estella Rao for the support, and Dr. Michele DAmico who has always been exceedingly generous in sharing his time in plenty of stimulating scientific discussions, and whose experimental support has been always at hand. I wish also to thank people at the CNR-IBF (National Council of the Research-Institute of Biophysics) in Palermo, director Dr. Pier Luigi San Biagio, and Dr. Clelia Dispensa and Dr. Maria Antonietta Sabatino, from the University of Palermo, for assistance and for kindly providing access to freeze-drying instrumentation.

I want to express my gratitude to Dr. Vito Foderá, from the Department of Pharmacy, University of Copenhagen, for having closely followed my research activity during the time spent in Copenhagen, for many interesting scientific discussions and human support.

I really thank people of BioSAXS group of the University of Copenhagen. I am really grateful to the group leader, Prof. Bente Vestergaard, who kindly provided the protein α-synuclein. I wish to thank her for kindly hosting me in her laboratories, a really friendly and confortable workplace, for scientific support and for the many important scientific suggestions. Moreover, I wish also to thank her for kindly hosting me in her house and for the human support. Thanks to Martin Nors Pedersen for the help in the laboratory activities carried out during the period spent in Copenhagen.

I wish to thank the Biophysics Group of University of Rome-Tor Vergata, in particular, Prof. Silvia Morante and Dr. Velia Minicozzi, who carried out classical molecular dynamics simulations presented in this work.

Moreover, I really thank Prof. Antonio Emanuele for critical reading of this thesis and for the interesting insights and discussions, and Prof. Ludmilla Morozova-Roche (Umea University) for kindly reviewing this thesis.

I thank Gianluca Napoli and Giacomo Tricomi (University of Palermo), Rico Wellendorph Lehmann and, in particular, Heidi Maria Hasager Peterson (University of Copenhagen) for their careful technical assistance.

Eventually, I wish to express my gratitude to Dr. (in few days) Luisa Spallino and Dr. (in few days) Claudio Guarcello for useful scientific discussions and for their persistent support. I will always be indebted to them.